MC4R ligands: Molecular features, membrane interactions and their potential role in modulation of hormone signaling

Inaugural-Dissertation

zur Erlangung des Doktorgrades
der Mathematisch-Naturwissenschaftlichen Fakultät
der Heinrich-Heine-Universität Düsseldorf

vorgelegt von

Sabine Schriek

aus Warstein

Düsseldorf, Februar 2017

aus dem Institut für Physikalische Biologie
der Heinrich-Heine-Universität Düsseldorf

Gedruckt mit der Genehmigung der
Mathematisch-Naturwissenschaftlichen Fakultät der
Heinrich-Heine-Universität Düsseldorf

Referent: Dr. Manuel Etzkorn
Mentor: Prof. Dr. Groth
Tag der mündlichen Prüfung:

Eidesstattliche Versicherung

Ich versichere an Eides Statt, dass die Dissertation von mir selbstständig und ohne unzulässige fremde Hilfe unter Beachtung der Grundsätze zur Sicherung guter wissenschaftlicher Praxis an der Heinrich-Heine Universität Düsseldorf erstellt worden ist.

Ich versichere, dass die eingereichte schriftliche Fassung der auf dem beigefügten Medium gespeicherten Fassung entspricht.

Neuss, den 28.02.2017

(Sabine Schriek)

Dedicated to my family who gave me their strongest support
all over the years.

Abbreviations

ACTH	adrenocorticotropic hormone
AcN	acetonitrile
AgRP	agouti-related Peptide
AIDS	acquired immuno deficiency syndrom
α-MSH	alpha-melanocyte stimulating hormone
APS	ammonium persulfate
ARC	arcuate nucleus
β-arr	beta-arrestin
CBB	coomassie brilliant blue
cAMP	cyclic adenosine monophosphate
CECF	continuous exchange cell-free expression
CLIP	corticotropin-like intermediate lobe peptide
CNS	central nervous system
C-terminal	carboxy-terminal
DDM	n-Dodecyl β-D-maltoside
DNP	Dynamic Nuclear Polarization
DTT	di-thiothreitol
ECL	extracellular loop
ESI	electrospray ionization
FA	fluorescence anisotropy
FP	fluorescence polarization
GABA	gamma-aminobutyric acid
GDP	guanosine diphosphate
GPCR	G-protein coupled receptor
G-protein	guanine triphosphate binding protein
G-domain	GTPase domain
GRK	G-protein coupled receptor kinase
GTP	guanosine triphosphate
HEK	human embryonic kidney
HIV	human immunodeficiency virus
HSQC	heteronuclear single-quantum coherence
IC	internal conversion
ICL	intracellular loop
IMAC	ion metal affinity chromatography
ISC	intersystem-crossing
MCR	melanocortin Receptor
MC3R	melanocortin receptor 3
MC4R	melanocortin receptor 4
MS	mass spectrometry

MSH	melanocortin stimulation hormone
MP	membrane protein
NCp7	nuclear capsid protein 7
ND	nanodisc
NDP-α-MSH	[Nle 4, D-Phe 7]-α-MSH
Ni-NTA	nickel nitrilotriacetic acid
NMR	nuclear magnetic resonance
N-terminal	amino-terminal
NPY	neuropeptide Y
PDB	protein data bank
PFA	paraformaldehyde
PKA	protein kinase A
PLC	phospholipase C
POMC	proopiomelanocortin
RF	radio-frequency
RP-HPLC	reversed phase high performance liquid chromatography
SDS	sodium-dodecyl-sulfate
SDS-PAGE	sodium-dodecyl-sulfate polyacrylamide gelelectrophoresis
SEC	size exclusion chromatography
SIV	simian immunodeficiency virus
SF	signal FLAG-tag
TCEP	tris(2-carboxyethyl)phosphine
TEMED	tetramethylethylendiamin
TEV	tobacco etch virus
TFA	trifluoroacetic acid
THz	terahertz
Vpr	viral protein R
WT	wilde type

Contents

Zusammenfassung

Fühlen Sie sich hungrig - oder satt? Dieses Gefühl wird vorwiegend durch ein komplexes Wechselspiel zwischen verschiedenen Hormonen und dem Membranprotein Melanocortin Rezeptor 4 (MC4R) in Ihrem Gehirn reguliert. Dieses Membranprotein gehört zu der pharmakologisch extrem wichtigen Klasse der G-Protein gekoppelten Rezeptoren (GPCRs).
Bisher gibt es keine hochaufgelösten Einblicke in die strukturellen und dynamischen Details, die der Liganden-vermittelten MC4R-Aktivierung zugrunde liegen, diese können jedoch zu einer neuen Klasse von GPCR-Medikamenten mit verbesserter Pharmakologie führen.
Das Ziel dieser Arbeit war es, die Eigenschaften der Peptidliganden von MC4R frei in Lösung und in der Gegenwart von synthetischen Lipiddoppelschichten (Nanodiscs) zu studieren, um ein Verständnis der Charakteristika der Hormone unter physiologischen Bedingungen, einschließlich einer Membran nachahmenden Umgebung, zu erhalten.
Deshalb wurde die Expression von Peptidliganden in *E. coli* und von MC4R in HEK 293 Suspensionszellen für den weiteren Gebrauch in NMR-Experimenten und Liganden-Bindungsassays etabliert. Des Weiteren konnten wir einen Fluorophor-konjugierten Peptidliganden herzustellen, welcher in der Lage war, Hormon-Membran Interaktionen in einem Fluoreszenzanisotropie basierten Bindungsassay zu sondieren. Die ligandenvermittelte "Down Stream" Aktivität von MC4R durch rekombinante und Fluorophor konjugierte Liganden wurde erfolgreich in einem cAMP basierten Bioassay getestet.
Unsere NMR-Daten zeigen, dass alle aufgenommenen Liganden generell ungefaltet sind, jedoch zeigen die Hormone ACTH und α-MSH sekundäre Konformationen für mehrere Aminosäuren. Zusätzlich konnten wir ein Modell der Membraninteraktion für ACTH erarbeiten, welches sich durch eine starke Interaktion der N-terminalen Aminosäuren bis zu der Position 14 und eine schwächere Bindung der weiteren Reste mit negativ geladenen Lipiden auszeichnet. Wir konnten ebenfalls zeigen, dass diese Interaktion durch die Zugabe von Calcium moduliert werden kann, was auf einen bisher unbekannten Weg der Hormonsignalmodulierung hindeutet.
Deshalb repräsentiert diese Arbeit nicht nur die Basis für zukünftige NMR-Studien von Melanocortin-Rezeptor Interaktionen und liefert essentielle Informationen und Hilfsmittel für die Optimierung der Probenvorbereitung, sondern sie legt auch nahe, dass Hormon-Membran Interaktionen eine Rolle in physiologischen Signalprozessen spielen könnten.

Abstract

Feeling hungry – or saturated? This feeling is predominantly regulated in your brain by a complex interplay between several hormones and the membrane protein melanocortin receptor 4 (MC4R). This membrane protein belongs to the pharmacologically extremely important class of G-protein coupled receptors (GPCRs).

So far no experimental high-resolution insights into the structural and dynamical details underlying ligand mediated MC4R activation exist but they could give rise to a new class of GPCR-drugs with improved pharmacology.

In this work we aimed to study the features of the peptide ligands of MC4R free in solution and in presence of synthetic lipid bilayers (nanodiscs) to gain understanding of the hormones' characteristics in physiological conditions including membrane mimicking environments.

Therefore, we established the expression of peptide ligands in *E. coli* and of MC4R in human embryonic kidney (HEK) 293 suspension cells for further use in nuclear magnetic resonance (NMR) experiments and ligand binding assays. Furthermore, we were able to produce a fluorophore conjugated peptide ligand that was able to probe hormone-membrane interactions in a fluorescence anisotropy (FA)-based binding assay. Down stream activity of MC4R mediated by recombinant and fluorophore conjugated ligands was successfully tested in a cAMP bioassay.

Our NMR data revealed that all recorded ligands are generally unfolded, but ACTH and alpha-melanocyte stimulating hormone (α-MSH) do show secondary conformations for several amino acids. In addition, we propose a model of a amino-terminal (N-terminal) binding mode of ACTH when interacting with membranes containing negatively charged lipids with strong interactions up to position 14 and weaker binding of the remaining residues. We were able to show that this interaction can be modulated by the addition of calcium, indicating a so far unknown way of hormone signaling modulation. Thus this work does not only represent the basis for future NMR studies of melanocortin-receptor interactions, as well as provide essential information and tools for the optimization of sample preparation, but also suggests that hormone-membrane interactions could play a role in physiological signaling processes.

1

Introduction

Atomic resolution insights into structure and dynamics of protein interactions are important to understand the details underlying these binding events. The main objection of this work is to study the characteristics of hormones known to be ligands of melanocortin receptor 4 (MC4R), a G-protein coupled receptor (GPCR) closely linked to obesity. In addition it be will reported on the cell-free expression of the cytotoxic human immunodeficiency virus (HIV) type 1 viral protein R (Vpr) and the influence of zinc on it's solubility. In the following the two projects will be presented in different sections of each chapter of this work starting with the main project followed by the second project.

1.1 Hormone-Receptor interaction

1.1.1 G-protein coupled Receptors

The central role of human GPCRs in signal transduction is reflected in their high genomic abundance and use as targets for therapeutic agents. About 800 members are found in the human genome rendering them the largest protein family [1], [2], [3]. They play an essential role in the majority of biological processes including external senses (sight, taste, hearing, smell, touch, thermoception) as well as interoceptive senses affecting organs (regulation of blood-pressure, appetite, respiratory rate). As they account for approximately 40 % of the marketed drugs they are also the biggest drug target [3], [4]. One quarter of the 100 top-selling drugs are targeting GPCRs [3]. Therefore, discovery of new ligands stays a major focus in pharmaceutical research to find new or optimized therapeutics. To avoid failures in the late stages of drug development, a careful selection of new potential candidates, through low-cost and high-throughput screens, is essential.
GPCRs transmit signals from the extracellular environment of a cell to the cytosol by binding of specific ligands, such as amines, hormone-like substances as well as

peptides and hormones, resulting in intracellular interaction with guanine triphosphate binding proteins (G-proteins) or arrestins [5]. GPCRs have a large number of diverse natural ligands with different effects on receptor activities including efficacy of downstream regulation. Agonist binding leads to ligand-specific receptor activation by adaption of a conformation [6] enabeling carboxy-terminal (C-terminal) interaction with intracellular interaction partners (G-proteins, arrestins) and signaling through different signal cascades. Antagonists block receptors' responses to agonists. Inverse agonists do not only block responses of non-constitutively active receptors to agonists but are also able to reduce the constitutive activity of the receptors (see also section 1.1.4). The study of GPCR activity modulation by their native ligands provides understanding of structural and physiological features of these processes. Therefore, this data can lead to a new class of GPCR-ligands with improved pharmacology [7].
Two important features characterize GPCRs [1]:
i. transmembrane (TM) seven-helix motif forming a recognition and connection unit;
ii. cytosolic interaction with a G-protein.
These receptors also share a common architecture with an extracellular *N-terminus*, an intracellular *C-terminus*. The seven transmembrane domains (TM1-TM7) are therefore linked by three extracellular loops (ECLs) (ECL1-ECL3) and three intracellular loops (ICLs) (ICL1-ICL3) [2]. Based on sequence homologies, GPCRs are classified into six families (A-F classification system is used):

Class A - rhodopsin-like
Class B - secretin receptor family
Class C - metabotropic glutamate
Class D - fungal mating pheromone receptors
Class E - cyclic AMP receptors
Class F - frizzled / smoothened

Class A (rhodopsin-like receptors) builds the largest class of GPCRs specifically interacting with a wide variety of ligands such as small molecules, neurotransmitters, peptides and hormones. New data, evolving from phylogenetic analysis [1], gave rise to a new family called adhesion like receptors which includes many GPCRs so far classified as secretin-like receptors (Class B). Classes D an E are not found in vertebrates.

1.1.1.1 GPCR Signaling

GPCRs can not only signal through G-protein coupling, as implied by their name, but also through C-terminal interaction with arrestins (biased signaling, see section 1.1.2). G-proteins act like molecular switches for several signaling pathways and are activated when bound to guanine nucleotides. G-proteins can be divided into mono- and heterotrimeric, both classes share a GTPase domain (G-domain).
For heterotrimeric G-proteins the G-domain is located in the Gα subunit, which interacts with the GPCR. This Gα subunit also contains a helical domain and forms a complex with the Gβ and Gγ subunit of the heterotrimeric G-protein.
Guanine nucleotide exchange factors GEF of the Gα subunits are mostly membrane-bound GPCRs. They use an allosteric trigger for activation by exchange of guanosine diphosphate (GDP) to guanosine triphosphate (GTP) instead [8]. In humans 16 genes of Gα with at least 21 isoforms are known. They can be classified by their down-stream regulation activity as follows [9], [10], [11]:

Gα_s - stimulatory for cyclic adenosine monophosphate (cAMP)-cyclase
Gα_i - inhibitory for cAMP-cyclase
Gα_q - activation of phospholipase C phospholipase C (PLC)
G$\alpha_{12/13}$ - acts on the Rho family of GTPases
Gα_v - involved in cell differentiation of aquatic organisms

Activation of heterotrimeric G-proteins with a Gα_s subunit leads to an increase of cAMP, a second messenger that activates signaling cascades such as those connected to protein kinase A (PKA). On the other hand Gβ/Gγ subunits released from the complex activate calcium channels [12]. However, activation of G-proteins with the inhibitory Gα_i subunit leads to the opposite effects, deactivating cAMP-cyclase and closing calcium channels [13].

Desensitization of G-protein coupled GPCR signaling is mediated through GPCR activated G-protein coupled receptor kinases (GRKs). These GRKs phosphorylate the C-terminal domain of the receptor which leads to the recruiting of beta-arrestins to this domain. Arrestin binding shields the G-protein binding site, inhibiting further G-protein activation and acts as a linker to the internalization machinery which regulates receptor endocytosis [14]. Beta-arrestins themselves can act as signal transducers in their function as adaptors and scaffolds, interacting with a variety of signaling molecules [5] Although receptor internalization is thought to be a mechanism for regulation and termination of GPCR signaling by recycling (weak beta-arrestin (β-arr)

interaction of class A GPCRs) or degradation (strong β-arr interaction of class B GPCRs), a sustained signaling was observed for certain GPCRs in endosomes [15].

1.1.2 GPCR Ligand Binding

Ligand Binding by the N-terminal binding pocket of GPCRs takes place in their transmembrane region. Venkatakrishnan et al. described the transmembrane helix (TM3) to be a "structural and functional hub" conserved throughout a large variety of GPCRs, maintaining either structure or functionality of the receptors showing intensive ligand interaction [16]. Overall they found topolgically equivalent residues in the transmembrane helices TM3, TM6 and TM7 of nearly all studied class A GPCRs to be interacting with their divers ligands.
Binding to this "consensus scaffold of the ligand-binding pocket", as it was named by Venkatakrishnan et al., may not be the only important interaction of GPCRs and their ligands [16]. Moreover, an initial ligand-receptor contact by extracellular loops and some transmembrane domains may be part of a first ligand recognition process, as it was described by molecular dynamics simulations for β-adrenergic receptors [17].

Several peptide ligands of GPCRs are described to transition from an unfolded state to a conformation with secondary structure elements upon binding to their targeted receptor [18], [18], [19].
These conformations could be not only mandatory for receptor activation in general ([20], [21]), but also serve as features providing receptor selectivity [22] and biased signaling [23] or - as also postulated for melanocortin receptor 4 (MC4R) - biased G-protein coupling - (for a review on MC4R biased agonists see [24]). Biased signaling describes the activation of either a G-protein or a β-arr coupled pathway by a ligand specific conformational change of the GPCRs cytosolic domain. However, biased G-protein coupling describes the specific coupling of different G-proteins by specific binding of their subunits (e.g. $G\alpha_s$, $G\alpha_i$, $G\alpha_q$, see also section 1.1.1.1) by different ligand mediated conformations of the receptors cytosolic domain.

1.1.3 State of the Art - Membrane Protein Structures

Studies of GPCRs and membrane proteins (MPs) in general are challenging. Sample preparation is problematic due to the need of a suitable membrane mimicking environment and purification protocols to support stability and solubility of the protein maintaining a native and active folded structure [25], [26]. This is reflected in the low

amount of MP structures deposited in the protein data bank (PDB) especially when compared to their high abundance in the genome and their impact on the drug market. Most of the MP structures and almost every GPCR structure available in the PDB was solved by X-ray crystallography. But structural studies in crystallography are limited as they predominantly provide static pictures of the most stable, lowest energetic conformation of GPCRs which are thought to be highly dynamic and to be changing conformation upon ligand binding. Rhodopsin is the only three-dimensional structure solved of a wilde type (WT) GPCR [27]. Other structures could only be obtained from receptors modified for a higher stability during the crystallization process. A commonly used modification is the replacement of the ICL3 with T4 lysozyme ([28], [29]) but also other fusion partners can be used for replacement [30].

To date only few structures of GPCRs in ligand bound conformation, especially true for peptide antagonists and also peptide agonists, have been solved [31] due to instability of active receptor conformations. Nevertheless structural data available for ligand binding pockets of GPCRs differs by shape and electrostatic properties, making further research on an atomic scale essential to understand the dynamics of ligand binding and their discrimination by the receptor [32].

Expression of GPCRs is challenging in terms of low protein yields, folding and receptor functionality. Procaryotic expression systems (*E. coli*) show strong limitations in the expression of membrane proteins. Incorporation rates of receptors into the membrane are low and not incorporated proteins aggregate forming inclusion bodies [33]. These systems can also not provide post translational modifications necessary for the receptors functionality.
However, cell-free expression systems can overcome low protein yields and provide some types of post translational modifications. But proteins precipitate or remain non-functional when expressed in the presence of a membrane mimicking environment, as the cell-free setup lacks chaperons helping the nascent protein to fold correctly.

NMR methodologies and techniques are making considerable progress increasing sensitivity (Dynamic Nuclear Polarization (DNP), see 2.1.1), sample stability (nanodiscs (NDs)), overcoming size limitations enabling measurement of large MPs bound to membrane mimetics [34], and decreasing measurement time by optimized hardware used in higher fields. Increasing yields of isotope labeled MP yields (insect cell culture) [35] and new sample preparation protocols like protein refolding are smoothing the way to new NMR resolved membrane protein structures [36].

1.1.4 Melanocortins and their Receptors

1.1.4.1 The Central Melanocortin System

Energy balance is controlled in the central nervous system (CNS) via the central melanocortin system. Here melanocortin Receptors (MCRs) expressed in the hypothalamus are activated by different hormones (melanocortins) acting as neuropetides. The release of these hormones is regulated by the interplay of two types of neurons of the hypothalamic arcuate nucleus (ARC). Neurons expressing agouti-related Peptide (AgRP) - the inverse agonist for MC4R - and orexigenic neurotransmitter neuropeptide Y (NPY) as well as gamma-aminobutyric acid (GABA) promote weight gain [37] [38]. Increased energy expenditure and decreased food intake leading to the loss of weight [39] is driven by neurons expressing proopiomelanocortin (POMC), a melanocortin precursor protein. POMC expression in the hypothalamus is regulated by several hormones, e.g. leptin - a hormone secreted by liver and adipose cells - binding to co-expressed leptin receptors in ARC^{POMC} neurons [40]. After cleavage of a signal peptide from Pre-Proopiomelanocortin during translation prohormone-convertases are processing the precursor protein in a tissue-specific manner. This gives rise to up to ten different peptides, some of them belonging to the group of melanocortins. POMC derived peptides are ACTH and α- / β- / γ-melanocortin stimulation hormone (MSH) (melanocortins), corticotropin-like intermediate lobe peptide (CLIP), β-lipotropin, β-endorphin) [41] (see figure 1.2).

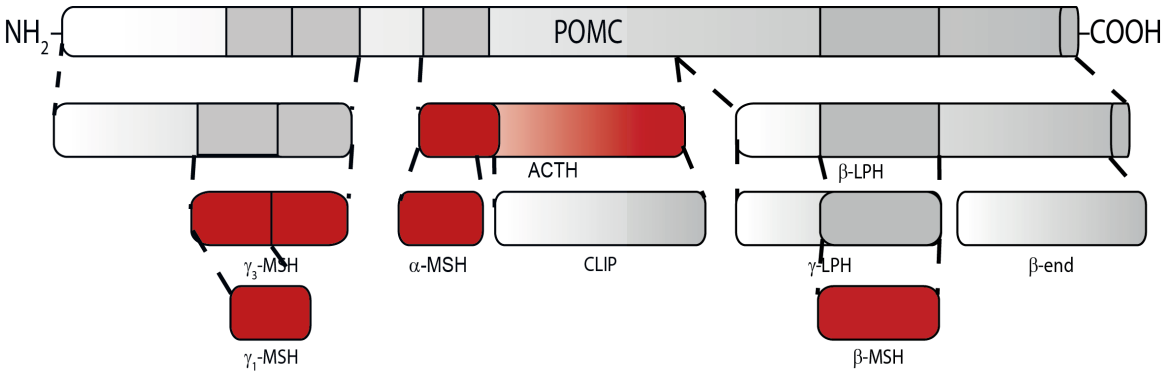

Figure 1.1: Proopiomelanocortin processing to melanocortins. The precursor protein POMC is processed in a tissue specific manner by prohormone-convertases to a variety of peptides including the melanocortins ACTH and α / β and γ-melanocortin stimulating hormone (red) all of which are agonists of the MC4R.

In addition to the hypothalamic ARC, POMC can be found to be synthesized in the pituitary. Peptides processed from the precursor are then secreted to the blood

acting as hormones. The predominant peptide derived from this process is ACTH. It regulates the secretion of glucocorticoids in the adrenal cortex by activation of melanocortin receptor 2 (MC2R), the so called ACTH-receptor. This receptor is the only MCR that can be solely activated by one melanocortin (ACTH).

1.1.4.2 Melanocortin Receptors

MCRs are class A GPCRs which can be divided into five subtypes (Melanocortin receptor 1-5 (MC1-5R)). They are regulating different central and peripheral effects in the human body ranging from pigmentation (MC1R) over adrenal hormone secretion (MC2R) and metabolism (MC3R, MC4R) to exocrine functions (MC5R) (see table 1.1) [42].

Table 1.1: Ligands and functions of melanocortin Receptors [42]

Receptor	Primary Ligands	Function
MC1R	α-MSH	Pigmentation
MC2R	ACTH	Stereoidgenesis
MC3R	ACTH, γ-MSH	Energy homeostasis
MC4R	α-MSH	Energy homeostasis, erectile activity
MC5R	α-MSH, ACTH	Sebaceous gland lipid secretion

Only melanocortin receptor 3 (MC3R) and melanocortin receptor 4 (MC4R) are expressed in the CNS where they are mainly located in the hypothalamus. Melanocortin Receptor 4 is a prototypical GPCR with a molecular weight of 36.9 kDa abundantly expressed in the hypothalamus, regulating energy homeostasis. While MC3R was found to be linked only to food intake, MC4R was found to play a major role in food intake and energy expenditure [43]. Furthermore MC4R was also shown to modulate erectile function, regulate blood pressure and inhibition of inflammation [44], [42]. These effects were first observed in patients suffering from pathological mutations of the MC4R or POMC gene, a precursor of different melanocortins which are ligands of MCRs, leading to sever obesity. These findings were confirmed by studies in *Mc4R* knock-out mice showing sever forms of obesity in homozygous (*Mc4R-/-*) and milder forms in heterozygous (*Mc4R+/-*) mice [45]. Melanocortin receptor 4 deficiency is described to be the most common form of monogenic obesity [46], but also the increase of clinical obesity due to food overconsumption over energy expenditure [47],[48] makes this receptor an important drug target.
melanocortin receptor 4 was shown to be constitutively activated by it's own N-terminus [49]. Therefore MC4R response can not only be driven by agonists like α-MSH and ACTH and blocked by antagonists but also influenced by inverse agonists (AgRP) reducing the constitutive activity of the receptor.

1.1.4.3 Hormone-Receptor Interaction

Binding affinities of melanocortins are varying in the nm-range for all melanocortin Receptor types (for an overview see [50]). Differences of melanocortin binding affinities to MC4R are shown in the following rank order of potency [42]:
α-MSH = ACTH > β-MSH> γ-MSH

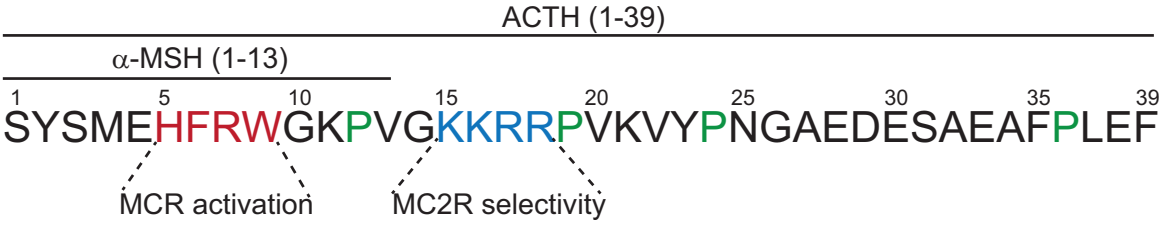

Figure 1.2: ACTH sequence. Peptide sequence of ACTH with its MCR activation site comprising amino acids H6 to W9 (red). The tetrabasic region of ACTH (K15 to R18) was hypothesized to be required for MC2R selectivity (blue). Proline (green) isomerism was intensively studied by Gao et al. [51].

Several studies suggest that all melanocortins share a conserved receptor activation sequence between amino acids H6 to W9, which was named "message" sequence (for a review see [52]). In addition a small N-terminal region of ACTH was discussed to show a tendency to adopt a α-helical structure [53]. Circular dichroism experiments performed in trifluoroethanol (TFE), a solvent know to favore secondary structure elements, showed an α-helical content of ACTH [54]. A structural transition from a flexible unbound to a structured bound form of the hormone upon receptor or lipid interaction was therefore suggested, possibly promoting a kinetically and thermodynamically optimal ligand-binding process (see also [52]. Hormone-receptor interaction was described to involve transmembrane helices TM2, 3, 6 and 7 as well as the extracellular loop ECL2 [55], which mainly corresponds to the GPCR ligand binding models reported in section 1.1.2 [16], [17]. Moreover, Hruby et al. [56] were able to show that a β-turn between amino acids 4-10 is essential for receptor activation. Therefore the tendency of ACTH to form a N-terminal α-helical structure may not be a feature for optimized receptor activation, which seems to be the N-terminal β-turn, but promote other functions. These could be related to either ligand recognition by the receptor and therefore initiation of the binding event, or membrane lipid interaction, as further described in the discussion of this work.

Although all melanocortins were found to share the same message sequence, only ACTH is able to activate MC2R. Studies of either N- or C-terminally truncated forms of ACTH implied that its tetrabasic sequence K15 to R 18 (KKRR) forms an "address" sequence, directing the ligand to MC2R before activation by its "message" sequence.

An overview of the amino acid sequence of ACTH, comprising that of α-MSH, is shown in figure 1.2. The "message" sequence, essential for receptor activation, is displayed in red, the "address" sequence suggested to direct the ligand to MC2R is depicted in blue letters.
The four prolines of ACTH (position 12, 19, 24, 36) are depicted in green. The influence of hormone-detergent interactions on the proline cis- and trans-isomerism in ACTH was intensively studied by Gao et al. [51]. They suggest that this isomerism may play a role in the biological functions of the hormone. Moreover, they describe the hormone-detergent micelle interaction to be mainly based on interactions of the hydrophobic site chains of the peptide (W, Y, F, M).
In structural biology prolines are know to be breaking α-helices and β-sheets as it is disrupting the sterics and hydrogen-bonds of such secondary structure elements.

1.1.4.4 MC4R Down Stream Signaling

Which mediators act in the downstream signaling of MC4R mediated decrease of food intake is not yet well understood. Brain-derived neurotrophic factor (BDNF) is believed to be one of these mediators as it was found to be released by MC4R activation [57], [58]. However, Hohenadel et al. recently reported that "circulating BDNF concentrations were not significantly associated with MC4R functional status"', i.e. loss of function and gain of function variants of MC4R. Therefore they suggest that the bulk of BDNF expression in humans is not mainly regulated by MC4R signaling [59].
Furthermore the corticotropin-releasing hormone (CRH), thyrotropin-releasing hormone (TRH), melanin-concentrating hormone (MCH) and orexin were discussed to mediate effects of the central melanocortin system [60], [61], [62].

1.1.4.5 The Role of Biological Membranes

In the hypothalamus neuropeptides such as melanocortins are translated in the endoplasmatic reticulum (ER), modified in the Golgi apparatus and processed from precursor proteins during their vesicular transport to the synapse. Vesicle fusion is then triggered by calcium influx upon arrival of an action potential at the synapse. This signal leads to the release of neuropeptides as well as neurotransmitters to the synaptic cleft, activating post-synaptic calcium channels and GPCRs such as MC4R by its ligands (figure 1.3).

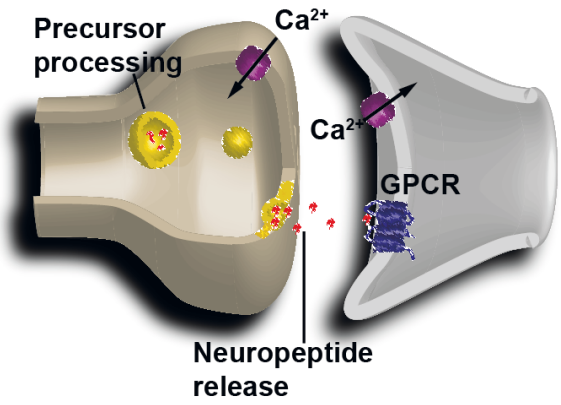

Figure 1.3: Neuropeptide processing and release at the synapse. Neuropeptides, such as melanocortins, are processed from a precursor protein during its vesicular transport from the Golgi apparatus to the synaptic cell membrane. Calcium influx through voltage-gated Ca^{2+} channels triggers neurotransmitter and neuropeptide release upon stimulation by action potentials reaching the synapse. Post synaptic calcium influx is evoked by neurotransmitter signaling, while neuropetides activate GPCRs.

Not only during these processes but even throughout the whole life cycle of a hormone its lipid surrounding changes. It varies within one cell (ER, Golgi apparatus, plasma membrane) and from cell type to cell type [63]. A precise description of a cells biological membrane lipid composition is often not possible.
Several regulatory biological processes are known to involve protein-membrane interactions. Clotting proteins for example show a calcium dependent reversible association with phosphatidylserine (PS) [64]. However, the role of neuropeptide and peptide hormone interaction with membranes is not well understood. Here nanodiscs may provide a suitable tool to study these interactions under well defined conditions such as lipid composition, pH and the influence of other physiological factors like ion concentrations.
NDs are customizable model membranes facilitating the possibility to study membrane proteins and membrane associated proteins in soluble lipid bilayers stabilized by two molecules of a membrane scaffold protein (MSP).

1.2 Human Immunodeficiency Virus Type 1 - Viral protein R

Aquired immunodeficiency syndrom (AIDS) is caused by the lentiviruses HIV type 1 and 2, infecting T helper cells and cells of monocyte-macrophage lineage. These two HIV types derived from cross-species transmissions of simian immunodeficiency virus (SIV) from primates to humans. Viruses resulting from these transmissions did not have high intraspecies transfer rates but HIV-1 group M gave rise to AIDS pandemic. Therefore, HIV-1 is the predominant virus worldwide, commonly referred to as HIV [65].
Treatment of HIV infection is still limited to suppression of the virus replication. Progression of the disease to its latest stage (acquired immuno deficiency syndrom (AIDS)) can only be slowed down. But still antiretroviral therapy (ART) remains challenging. HIV viremia is reported to persist throughout these therapies by building cellular reservoirs (e.g. in resting CD4+ T lymphocytes) [66]. And drug resistance can be observed even though a cocktail of inhibitors targeting key viral enzymes is applied in Highly Active Anti-Retroviral Therapy (HAART) to overcome this fast adaption of HIV due to its high mutation rates [67].
Thus there is a need to find new, effective drug targets to inhibit the viral infection and its spread over different host cells to prevent viral presistence, resistence and the progress of the infection to AIDS.

An increasing number of new HIV infections in the western world (Eastern Mediterranean Region between 2009 and 2013 by 29%; European Region by 6%) was recently reported by the World Health Organisation [68]. In the year 2015 2.1 million people (+ 5.7%) were newly infected world wide, whereof 91,000 life in western and central Europe and North America [69]. Therefore, apart from its devastating role in developing countries, HIV still also imposes a serious threat for the western society.

Because of the infections slow progression and long incubation period HIV was determined to be a lentivirus (lente-, Latin for slow), a member of the retroviridae family. Retroviruses are enveloped viruses replicating their single stranded positive-sense RNA genome in the host cell by use of their own viral reverse transcriptase followed by integration of the transcripted DNA into the host cell genome (provirus). HIV-1 codes for its structural proteins Gag, Pol and Env and also for six auxiliary proteins including Vpr, Vif, Nef (virion associated), Tat, Rev (essential regulatory functions) and Vpu.

1.2.1 HIV-1 Viral protein R (Vpr)

Viral protein R (Vpr) is an accessory protein conserved in all immunodeficiency viruses (HIV type 1 and 2 as well as SIV) [70]. An important role of Vpr during host cell infection is implied by its presence in the mature infectious virion [71].
In addition *in vivo* studies showed that Vpr is also involved in several steps throughout the viral lifecycle. This is including host cell cycle progression and apoptosis, the reverse transcription of HIV-1 and the nuclear import of viral DNA in the host cell [72],[73]. Due to its manifold properties, Vpr represents a promising alternative drug target to treat HIV infections [74].
Figure 1.4 gives an overview of the role of Vpr during HIV infection and replication. In the following Vpr's main functions during these processes are summarized:

(I) G2 arrest: The G2 arrest, i.e. a cell cycle arrest of the host cell in the G2 phase, is predominantly attributed to binding of Vpr to DCAF-1 (previously identified as Vpr binding protein) [74],[75]. The G2 arrest is believed to provide an advantage for HIV by improving viral replication over host cell protein expression.

(II) Apoptosis: Vpr mediates dislocation of anti-apoptotic mitochondrial protein HAX-1, leading to cell death [76]. Apoptosis of the infected cells may mute the host's immune response [77].

(III) Nuclear shuttling: Vpr associates with viral nucleic acids and binds to importin-α to be transferred into the nucleus [78],[79]. This mechanism allows import of viral DNA in non-dividing cells [78]. In addition Vpr's intrinsic nuclear export signal mediates transfer out of the nucleus, making Vpr available for Pr55Gag precursor binding [80].

(IV) Reverse transcription: As a part of the reverse transcription complex Vpr is thought to play a role in the initiation of reverse transcription in the virus particle and to improve reverse transcription accuracy [81].

(V) Budding and virion maturation: Virion incorporation of Vpr is mediated by its interaction with the p6 domain of Pr55Gag [80], the only virion-encoded molecule required for immature virus-like particle assembly (immature framework of virus particle) [82],[83]. Proteolytic cleavage of Pr55Gag leads to association of Vpr with the nuclear capsid protein domain 7 NCp7, which is responsible for Vpr translocation into the core of mature HIV virions.

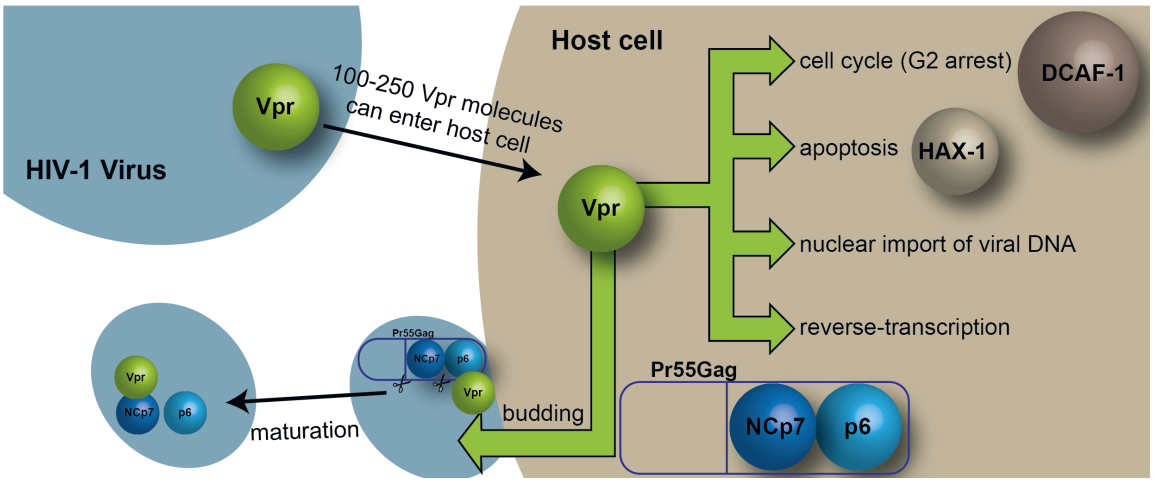

Figure 1.4: Role of Vpr in the HIV-1 infection cycle. HIV viral protein R is already present in the virion and enters the host cell (100-250 Vpr molecules) upon transfection. It is involved in different steps of the viral live cycle including host cell G2 arrest, regulation of apoptosis, nuclear import of DNA and reverse-transcription as well as budding of new virions.

1.2.2 State of the Art of Vpr Research

In general HIV and its proteins were intensively studied in animal and cell culture experiments. However, in particular for Vpr *in vitro* studies, which are crucial to understand the molecular determinants of the interactions between Vpr and viral or host cell proteins, are rare. The reasons for these very limited insights into Vpr function are mostly related to its high cytotoxicity and insolubility, impeding expression and purification of full-length Vpr.

Due to these challenges in HIV-1 Vpr sample preparation for structural studies, only limited information are available. Solution-state NMR experiments carried out so far studied fragments of Vpr as well as the full-length protein in non-physiological conditions [84],[85],[86],[87],[88].

In these studies the limitations of cell toxicity were overcome by producing the Vpr using solid-phase peptide synthesis. While the reported data provide important initial insights, it has to be noted that to enable Vpr solubility buffer conditions with a pH of 2.6 and 30% acetonitrile had to be used for the most 'native' structure [88].

In addition to make the synthesis of the 96 residue Vpr economically feasible for NMR studies only 20 residues were isotope labeled, largely reducing the number of identifiable distance restrains and naturally also reducing the quality of the resulting structure.

A crystallographic structure of DDB1-DCAF1-Vpr-UNG2 under almost physiological conditions was recently published by Wu et al. [89]. For this study a H78C mutation was used and a Nus-A-tag (a 54.8 kDa protein), promoting solubility, was removed by a TEV-protease only after mixing Vpr with its interaction partners, followed by purification anion exchange chromatography. In this structure the hydrophobic core of Vpr is stabilized by its interaction with UNG2.
Recent findings have furthermore shown that the viral protein X, a Vpr homolouge limited to HIV-2 and SIV, is a zinc binding protein. Comparing the sequences of HIV-2 Vpx and HIV-1 Vpr a zinc binding capability of Vpr by the motif "H32, H71, C76, H78" was consequently postulated [90]. In light of these findings the low solubility of Vpr in physiological buffer conditions may be attributed to the absence of zinc in these studies. Comparison of the recent HIV-2 Vpx structure (zinc bound and functional) with the solution-state HIV-1 Vpr structure (zinc-free, pH 2.6, 30% acetonitrile) shows that while the overall fold (three helix bundle) is conserved, structural details, in particular side-chain orientations around the zinc binding side as well as helix packing, are significantly different.
From these data it can be anticipated that a better-defined structure of HIV-1 Vpr is needed to understand its function and to design structure-based treatments.

1.3 Motivations and Objectives

1.3.1 Melanocortin Receptor 4 (MC4R) Hormone Interaction

To date, understanding of molecular details underlying GPCR-ligand interactions is limited and only little data on these processes is available in atomic resolution. Especially ligand binding dynamics, which are important for the design of new therapeutic agents, are poorly understood.
Solution-state NMR spectroscopy is a suitable technique to study the structure of highly dynamic molecules such as GPCRs during a ligand binding event. New techniques enable the investigation of even large membrane proteins using small membrane mimicking environments (nanodiscs) maintaining the proteins stability and function. The GPCR melanocortin receptor 4 is a highly interesting drug target as it is closely linked to energy homeostasis and obesity. Although ligand binding of MC4R was intensively studied, e.g. by site directed mutation, the process itself remains unclear.

The main objective of this work was to establish the expression of both, the ligand ACTH and the receptor MC4R, to enable the setup of ligand binding assays and NMR-based experiments.

Therefore, the following aims were targeted: (I.) Expression of large amounts of different variants of (isotope) labeled hormone peptides
(II.) Establish and optimize expression of MC4R in HEK 293-F cells
(III.) Prove activity of expressed receptor and peptides
(IV.) Design a hormone-fluorophore conjugate suitable for FA-based ligand binding assays
(V.) Characterize structural features of soluble ACTH
(VI.) Study the hormone peptides in physiological conditions mimicking environments

1.3.2 HIV-1 Vpr

The fact that HIV-1 Vpr is not only already present in the mature virion before host cell infection but also connected to a wide variety of processes throughout infection cycle makes viral protein R an important drug target to fight AIDS. Understanding of Vpr function and structure is still limited by low protein expression yields due to high cytotoxicity and poor solubility. Combining the method of cell-free expression and the hypothesis that Vpr has a conserved zinc binding motif, the following work aims to:

(I) produce large amounts of Vpr
(II) establish a sample preparation protocol improving Vpr solubility and structural stability by coordination of zinc
(III) study the function of zinc coordinated Vpr using known interaction partners

2

Theory

Contents

2.1 Fundamentals of Spectroscopy

Spectroscopy is the study of the interaction of electromagnetic radiation and matter giving rise to electronic excitation, molecular vibration or nuclear spin orientation upon excitation of the system. Spectroscopic methods apply radiation to gain data on the structure and properties of matter regarding absorption, emission or diffraction of electromagnetic waves by molecules or single atoms. Absorption of light leads to the transition from unexcited ground state (S_0) to an excited state ($S_1, \ldots, S_n$) were the energetic difference (Δ E) between these states is dependent on the frequency of the electromagnetic wave as given in the following equation:

$$\Delta E = \frac{hc}{\lambda} \tag{2.1}$$

Herein h is the Planck constant, λ is the wave length and c denotes the speed of light.

2.1.1 Fundamentals of NMR Spectroscopy

Nuclear magnet resonance (NMR) spectroscopy is based on a nuclear spin transition upon absorption of electromagnetic radiation at radio-frequency (RF) in a magnetic field (B_0). It can be applied for atoms with a spin quantum number $I \neq 0$ - nuclei with odd numbers of neutrons and / or protons - which is coupled to a magnetic moment μ interacting with the magnetic field. The spin quantum number I can have values ≥ 0 and multiples of 1/2. In the presence of an external magnetic field the magnetic moments of the nuclei experience a torque causing their precession around (B_0). The magnetic moments can precess either parallel or anti-parallel to the magnetic field. This motion called Lamor precession is dependent on the gyromagnetic ratio γ and the strength of B_0 (see equation 2.2). In NMR spectroscopy the gyromagnetic ratio describes the ratio of the magnetic moment of a nucleus to its angular momentum [91].

$$\nu_0 = \frac{\gamma B_0}{2\pi} \tag{2.2}$$

Here ν_0 denotes the precession frequency termed Larmor frequency.
For transitions from S_0 to an excited state an electro-magnetic pulse (usually at RF)

is applied for perturbation of the nuclear spin alignment. Here the resonance condition needs to be met, i.e. the frequency of electromagnetic radiation has to be equal to the Lamor frequency which is is equivalent to the nuclear resonance frequency and dependent on the static magnetic field B_0 and the observed nuclei.

Significant differences to other forms of spectroscopy are that
(i.) generation of ground and excited state requires an external magnetic field (B_0)
(ii.) exited state lifetime is 10^9 times longer than excited electronic states leading to narrow spectral lines

In NMR spectroscopy the electron environment of single atoms and their interaction with other atoms is displayed by the nuclei absorption frequencies and their shifts upon a change of their environment and interactions. Chemical shifts of NMR absorption frequencies are quoted as their difference to the absorption frequencies of a chosen reference compound, with a chemical shift set to 0, and given as parts per million (ppm) as displayed in equation 2.3. This notation is independent from the magnetic field strength, as not only the frequencies at which the NMR absorption of the compound of interest occurs scales with the field strength but also the frequency of the reference compound. Additionally it is normally observed for very small chemical shifts:

$$\delta_{ppm} = 10^6 \frac{\nu - \nu_{ref}}{\nu_{ref}} \tag{2.3}$$

NMR spectroscopy can provide high-resolution insight into protein structure and conformational dynamics on an atomic level. While solid-state NMR is the method of choice for large insoluble proteins, solution NMR is commonly used for small soluble proteins. Solution spectra, when compared to solid-state, show sharp transitions as the fast isotropic tumbling, which is not present in solid-state, averages anisotropic interactions. Those are otherwise leading to broadening of the resonances and therefore to a decrease of resolution.
A common drawback in NMR is the low sensitivity caused by only small magnetic moments of the nuclei (^{1}H, ^{13}C, ^{15}N) leading to a need of high protein concentrations in the mg range and long measurement times causing high costs. A method overcoming these limitations is Dynamic Nuclear Polarization-NMR where spin polarization is transferred from electrons of a paramagnetic polarizing agents (radicals) to the nuclei dramatically increasing signal intensities. DNP experiments are performed at low temperatures (100 K) using terahertz (THz) microwave irradiation for excitation of the electrons. Radicals need to be in a certain distance to the protein of interest to specifically transfer excitation for highest efficacy without quenching effects (in a range from $\approx 8 - 10$ Å to ≈ 50 Å). A specific distance of the radicals to the protein of interest can be achieved for example by their fixation either to spacers on the

protein, to membrane mimetics such as nanodiscs for membrane proteins or to a ligand interacting with the protein (see section 5.1.2).

2.1.1.1 2D NMR Experiments

In the following the correlations or interactions established through commonly used NMR techniques will be shortly summarized [91]:

COSY: Homonuclear (one isotope) correlation spectroscopy (COSY) identifies spins that are coupled over 2- or 3-bonds to each other and displays them as cross-peaks.

TOCSY: Total correlations spectroscopy (TOCSY) is a homonuclear experiment yielding through bond correlations along a continous chain of spins.

HSQC: In heteronuclear (two isotopes: usually ^{1}H-^{15}N or ^{1}H-^{13}C) single quantum coherence spectroscopy (HSQC) the magnetization of a proton is transferred to the second considered nucleus (one-bond).

NOESY: In nuclear Overhauser effect spectroscopy (NOESY) cross peaks display spatially close nuclei (through-space correlations) instead of through-bond coupled nuclei as described for TOCSY. This experimental setup is used to gain structural information.

2.1.2 Fundamentals of Fluorescence Spectroscopy

Fluorescence spectroscopy is based on the absorption of a photon of wavelength λ_{abs} by a molecules electron followed by energy emission in form of fluorescence.

Upon photon absorption the electronic state of a molecule is excited from its ground state S_0 to a higher excited state $S_1, \ldots, S_n$ (figure 2.1) by the energy Δ E (equation 2.1). After excitation of the molecule it looses energy through non-radiative transitions within picoseconds dropping back to the first-excited state S_1. From here the energy can either further dissipate through internal conversion (IC)), intersystem-crossing (ISC) or through emission of a photon with wavelength λ_{em} and energy hν_{em}, referred to as fluorescence emission. Compared to the wavelength of excitation λ_{exc}, λ_{em} is shifted towards higher wavelengths $\Delta\lambda = \lambda_{\text{em}} - \lambda_{\text{exc}} > 0$ (Stokes-shift).
An important parameter in fluorescence spectroscopy is the fluorescence quantum yield

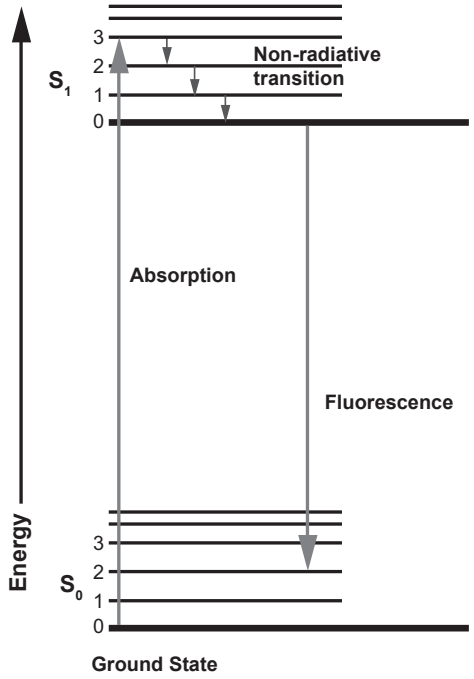

Figure 2.1: Jablonski diagram showing possible electronical transitions. Excitation from singlet ground state (S_0) by photon absorption to the singlet states (S_1 to S_n). The molecules energy levels are denoted by thick lines while thinner ones denote vibrational levels. The molecule absorbs (left grey arrow) a photon of an appropriate wavelength and transits to an excited singlet state. Through non-radiative internal conversion (IC) it relaxes quickly to the first excited singlet state followed by emission of fluorescence while relaxing to the ground state.

(ϕ_f) giving the ratio of emitted photons per absorbed photons, defined in equation 2.4. The quantum yield corresponds to the probability of receiving a fluorescence photon emission after excitation and transition back to S_1, i.e. not a non-radiative transitions from S_1 to ground state S_0 like IC or ISC, and can be used to describe the quality of a dye.

$$\phi_F = \frac{\#\text{ of emitted photons}}{\#\text{ of absorbed photons}} = \frac{k_F}{k_f + k_{ISC} + k_{IC}} \tag{2.4}$$

Herein k_F, k_{ISC} and k_{IC} denote the transition rates from S_1 to S_0 for photon emission, internal conversion or intersystem-crossing. When selecting a dye for fluorescence applications $\phi_F > 90$ % should be chosen for an excellent dye. Another important parameter for the right choice of a good dye, besides solubility, is the fluorescence lifetime. It is given by the factor $\tau_F = \frac{1}{k_F + k_{isc} + k_{ic}}$ (also see equation 2.4). It describes the duration (1-10 nanoseconds) of a molecules exited state till it reaches S_0 again. Therefore it represents the average time an experimenter has to wait for photon emission after excitation.

2.1.2.1 Fluorescence Polarization

Measurements of fluorescence polarization or fluorescence anisotropy (FP or FA) are well established and used in high throughput screenings for drug discovery. It can be used to study protein-protein and ligand binding interactions in solution working with ligand / tracer concentrations down into the low picomolar range.
Fluorescence polarization is based on the fact that excitation of a fluorophore from ground state to S_1 can only take place if polarized light and transition dipole moment of the excitation process are directed in the same way. The orientation of the emission is defined relative to the orientation of the polarized excitation light. $I_{\parallel}$ and $I_{\perp}$ denote emission intensities which are parallel and perpendicular to the polarization of the incoming light, respectively. For small fluorophore-conjugated molecules (ligand / tracer) emitted light is largely depolarized due to a rapid tumbling free in solution. Upon binding of an interaction partner the ligand / tracer tumbles slower and light emission takes place in the same plane (parallel) as the excitation energy increasing the fluorescence polarization (FP) value. The degree of polarization is described by the ratio of fluorescence intensities ($I_{\parallel}$, $I_{\perp}$) of the polarized and not polarized light (see equation 2.5, 2.6) [92]. FP values are independent of the fluorophore concentration, i.e. do not depend on the absolute light emission (equation 2.5). In comparison to FP (see equation 2.5), FA values are directly quantitative to the population of bound and free ligand (see equation

Fluorescence Polarization (FP)

$$FP = \frac{I_{\parallel} - I_{\perp}}{I_{\parallel} + GI_{\perp}} \tag{2.5}$$

Fluorescence Anisotropy (FA)

$$FA = \frac{I_{\parallel} - I_{\perp}}{I_{\parallel} + 2GI_{\perp}} \tag{2.6}$$

Possible values for FP are low (-0.33 to 0.5) but measurements can be performed very precisely (± 0.002). Due to the low values it is often described in mP (P/1000) or mA (A/1000) respectively.
A grating factor (G-factor; G) can be introduced (equations 2.5, 2.6) to correct a possible instrumental bias in light detection sensitivities on the parallel or perpendicular plane.

Fluorescence anisotropy is related to the rotational relaxation time (ρ), a parameter describing the time-dependence of the tumbling of a molecular entity in a solvent (equation 2.7), of the dye conjugated ligand. Therefore, it is essential to choose a fluorophore with a life time meeting the requirements given by the rotational relaxation time of the ligand free in solution and bound to its interaction partner. The shorter the life time of a fluorophore is, the less it can rotate during its excited state, thus the higher is the polarization of the emitted light [93].

$$\rho = \frac{3\eta V}{RT} \tag{2.7}$$

Here V denotes the volume of the rotating molecule, R is the universal gas constant and T is the absolute temperature while η is the solvent viscosity.

The FP value is directly affected by changes in the degree of depolarization of plane polarized light caused by alterations in the size of fluorescent molecules due to dissociation or binding events. This means that FA increases when a fast tumbling fluorescent molecule, such as a dye-conjugated small ligand, binds to a large interaction partner, for example a receptor, decreasing the speed of rotation and vice versa.

2.2 Further Biochemical and Biophysical Methods

2.2.1 Continuous Exchange Cell-Free Expression

Continuous exchange cell-free expression CECF is a flexible and open system for protein expression. It can be based on different translation systems by the choice of the cell extract providing the translational and transcriptional machinery and easily expanded by further reaction components promoting solubility of the expressed protein. In CECF a compartment containing the reaction mixture with all high-molecular-weight compounds is separated by a permeable membrane from a compartment containing the feeding mixture with low-molecular-weight precursors (figure 2.2) [94].

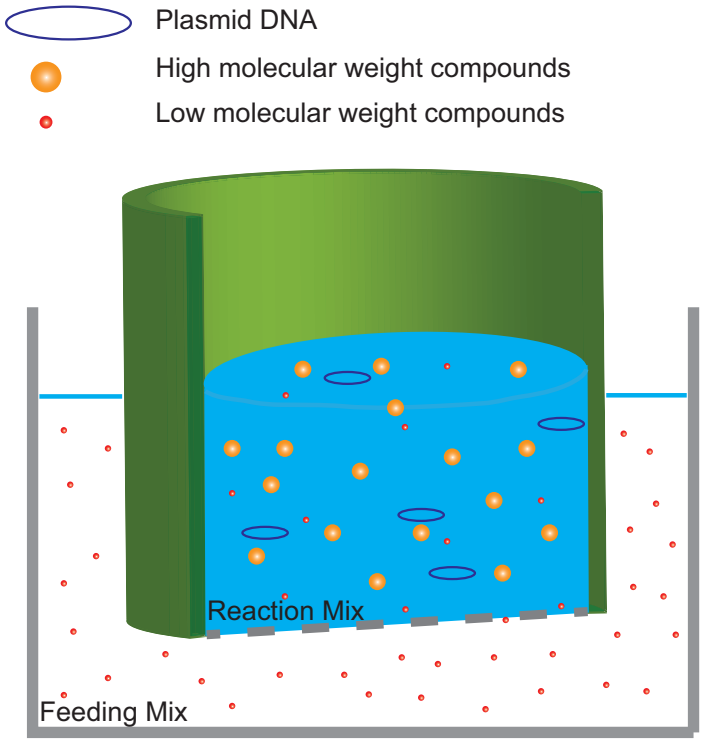

Figure 2.2: Cell-free expression setup. In CECF the reaction mixture containing all high-molecular-weight compounds is separated by a permeable membrane from the feeding mixture containing low-molecular-weight compounds.

2.2.2 Immobilized Metal Affinity Chromatography(IMAC)

Immobilized Metal Affinity Chromatography is based on the covalent binding of amino acids (e.g. histidine) to metals (e.g. nickel) immobilized with a chelating agent on a solid phase (e.g. agarose or sepharose). In this work a six-fold histidine-tag of the analyte in the mobile phase was used for covalent binding to the nickel immobilized on the solid phase (sepharose or agarose) via nitrilotriacetic acid (NTA) as a chelating agent.

2.2.3 Size-Exclusion Chromatography (SEC)

Size-exclusion chromatography (SEC) is a chromatographic method used to separate molecules according to their frictional coefficient [95]. Here the analyte does not adsorb to the solid phase (beads) but has access to its pores of a defined size. While bigger molecules which can not access the pores pass the column rapidly in the void volume (volume between the packed particles), elution of smaller molecules is retarded in the measure of their ability to access these cavities in the spherical beads [96]. Selection of the correct pore size is therefore essential for resolution. Molecules with high molecular weight (e.g. proteins) elute earlier than those with low molecular weight (e.g. salts). The mobile phase consists of a buffer which is compatible with the analyte and minimizes its electrostatic and hydrophobic interactions with the column resin by using an adequate salt concentration (>0.1 M - <0.5 M).

2.2.4 RP-HPLC

Reversed phase high performance liquid chromatography (RP-HPLC) is based on the analytes interaction with a hydrophobic stationary phase and the use of a hydrophilic organic solvent for elution. To increase the interaction of charged groups of the analyte and the hydrophobic stationary phase, ion-pairing agents such as trifluoroacetic acid (TFA) are used. For analyte elution the polarity of the mobile phase is reduced in a gradient that needs to be adapted experimentally for optimal separation of salts and other compounds from the analyte.

When analytes are applied to the column, two effects dominate the chromatographic process. On the one hand, adsorption of analytes occurs at the mobile phase / stationary phase interface. On the other hand, dispersion of analytes occurs between those two phases which can be described by Nernst's law. Each compartment of the column at which a concentration equilibrium occurs between analytes in the mobile and in the stationary phase is called a theoretical plate. The equilibrium constant depends, among other things, on the chemical nature of the analyte, as well as on the chemical nature of stationary and mobile phase. Thus, it can, for example, be influenced by changes in the composition of the mobile phase.
This method is commonly used to analyse protein purity but not for purification, as the strong hydrophobic interactions and the use of organic solvents can lead to denaturation of the sample. In this work a silica based column resin with bonded C_{18} hydrocarbon chains was used for peptide purification, as the analyte is unfolded and therefore not influenced by the harsh conditions using a acetonitrile (AcN) gradient as mobile phase.

2.2.5 Discontinuous SDS-PAGE Analysis

Sodium-Dodecyl-Sulfate Polyacrylamide Gelelectrophoresis (SDS-PAGE) by Laemmli [97] is a method based on a polyacrylamide gel for separation of macromolecules (e.g. proteins) by their molecular mass in an electric field using the negative charge of the denaturating anionic detergent sodium-dodecyl-sulfate (SDS). This detergent is bound by polypeptides in proportion to their molecular mass. As mobility of denaturated proteins / peptides in the gel depends not only on their molecular weight but also on their charge, SDS is used to compensate unequal charge distributions of molecules applying a uniform negative charge.
The discontinuous SDS-PAGE is a common form of polyacrylamide gelelectrophoresis in which a stacking gel on top of the separation gel is used to concentrate proteins in diluted samples and to separate proteins from the stack of unbound SDS by differences in pore size, ionic strength and pH. The content of acrylamide monomers can be adapted to the size of the protein to gain the appropriate pore size for stacking and separation. Therefore gels are commonly characterized by the total amount of acrylamide monomers - acrylamide and the cross-linker bisacrylamide - denoted as %T and the percentage concentration of the cross-linker determined as %C. Pore size decreases with increasing %T and also with a $\%C \neq 5$. In glycine-SDS-PAGE, performed in a tris-glycine buffer system containing SDS, a neutral pH (pH 6.8) is used for the stacking and a basic pH (pH 8.3-9) for separating gel. Here the small chloride cations run in front of the proteins (leading ions) and larger glycinate ions run behind the proteins (trailing ions) in the neutral stacking gel while in the basic

separation gel both ions behave as leading ions. As disulfide bond formation is favored in the basic separating gel which can not be avoided by reducing agent in the not co-migrating sample buffer. Therefore new buffering technologies were established to enable separation of proteins at a low pH (below the pKa of cysteine) maintaining a reducing environment in the gel at the same time.
Another discontinuous system used to separate proteins in the range of 1 to 100 kDa is Tricine-SDS-PAGE. Comparing Tricine to glycine-SDS-PAGE [97] especially proteins in the range of 5 to 20 kDa can be separated with a higher resolution while using less acrylamide and no urea [98] (for an update on this method see [99]). This is achieved by an improved destacking of the small range proteins from the bulk of SDS which was observed to be not sufficient in glycine-SDS-PAGE, resulting in streaking of the proteins in higher acrylamide concentrations. The difference in separation characteristics of these two methods are dedicated to the strongly differing pK values of the functional groups of glycine and Tricine influencing the electrophoretic mobilities of these trailing ions relative to the electrophoretic mobilities of proteins. In Tricine-SDS-PAGE the separation gel has the same pH as the stacking gel but a smaller pore size and a lower acrylamide content.

3

Materials

Contents

3.1 Chemicals

Ampicillin di-sodium salt, Sigma Aldrich
Anti His-Tag (27E8) Mouse mAb, Cell Signaling Technology
cOmplete Protease Inhibitor Cocktail Tablets, Roche
Coomassie Blue G250, Serva
Di-Sodium hydrogen phosphate dihydrate p.a., AppliChem
1,4-Dithiothreitol (DTT), Carl Roth
4-(2-Hydroxyethyl)piperazine-1-ethanesulfonic acid (HEPES), Applichem
Hydrochloride, Sigma Aldrich
Imidazole, Sigma Aldrich
Luria Bertani (Lennox), PanReac Applichem
2-Mercaptoethanol, Roth
o-phosphoric acid, Grüssing
Sodium dihydrogen phosphate monohydrate p.a., AppliChem
Sodiumchloride (NaCl), Applichem
Sodiumazide (NaN_3), Janssen Chimica
Tryptone (technical Bacto for media), BD
Yeast extract (technical Bacto for media), BD

Adrenocorticotropic Hormone

Acetonitrile HiPerSolv Chromanorm, HPLC grade, VWR
Atto 647, Atto-Tech GmbH
Cy3B maleimide, GE Healthcare
Glucose monohydrate pH.EUR.8.0, Caelo
Luria Bertani
Trifluoroacetic acid 99 %, Roth
Tris(2-carboxyethyl)phosphin (TCEP), Sigma Aldrich

Peptides ACTH (C-term. amide), Peptide and Elephants
ACTH, AnaSpec
ACTH(1-23)C (C-term. amide), Peptide and Elephants
ac-α-MSH, Abbiotec
SHU 9119, Tocris
MC4R(1-26) (C-term. amide), Peptide and Elephants

Melanocortin Receptor 4

Dulbelcco's Modified Eagle Medium high glucose (11965084), Gibco / Life Technologies
Free Style Medium, Gibco / Life Technologies
Geniticin selective antibiotic (G418, 10131027), Gibco / Life Technologies
HEK 293 cells, Gibco / Life Technologies
HEK 293-F cells, Gibco / Life Technologies
Methyl-sulfoxide (DMSO), Acros Organics
Penicillin-Streptomycin (15070063), Gibco / Life Technologies
Pluronic F-68, Gibco / Life Technologies

HIV-1 vpr

Acetyl phosphate lithium potassium salt, Sigma Aldrich
Adenosine-5-triphosphate disodium salt trihydrate, Roche Diagnostics
Amino acids, Carl Roth
Cytidine-5-triphosphate disodium salt hydrate, Carl Roth
Dipotassium phosphate (K_2HPO_4), Carl Roth
Folinic acid calcium salt, Sigma Aldrich
Glucose monohydrate, Caleo
Guanosine-5-triphosphate disodium salt hydrate,
KH_2PO_4, Carl Roth
Lipids: E. coli total mixture (Avanti Polar Lipids)
Magnesium acetate (Mg^{2+} acetate)tetrahydrate, Carl Roth
Phosphoenol pyruvic acid (PEP) monopotassium salt, Carl Roth
PEG 8000, Carl Roth
Potassium acetate (K^+ acetate), Carl Roth
Potassium chloride (KCl), Carl Roth
Primary antibody: HIV-1 Vpr antibody vN-20, Santa Cruz
Pyruvate kinase, Roche
Ribolock, Thermo Fisher
Secondary antibody: Anti-Goat IgG (whole molecule)-Peroxidase (A5420), Sigma Aldrich
Tris-(hydroxymethyl)-aminomethane, Carl Roth
tRNA *E. coli* total, Roche
Uridine-5-triphosphate trisodium salt dihydrate, Carl Roth
Zinc acetate dihydrate, Merck

3.2 Buffers and Media

100 mM Sodium phosphate buffer pH 7.0 (NaPi)

0.06 M $NaH_2PO_4 \cdot H_2O$
0.94 M $Na_2HPO_4 \cdot 2H_2O$

HEPES buffer pH 7.4

pH adjusted by mixing 1 M HEPES salt (MW:260.29 g/mol) and HEPES acid (MW: 238.3 g/mol).

Luria Bertani

10 g Tryptone
5 g Yeast extract
10 g NaCl
ad 1 l

Tris-Glycine SDS-PAGE buffers

Stacking gel buffer 0.5 M Tris/HCl pH 6.8
0.4% SDS

Separating gel buffer1.5 M Tris/HCl pH 8.8
0.4% SDS

Tris-glycine buffer
25 mM Tris / HCl pH8.3
192 mM glycine
0.1% SDS

Stacking gel
266 µl bis-/acrylamide (37.5:1)
500 µl stacking gel buffer
1234 µl H_2O

1.6 µl tetramethylethylendiamin (TEMED)
16 µl ammonium persulfate (APS)

Separating gel 15% / 12%
2000 / 1600 µl bis-/acrylamide (37.5:1)
1000 µl separating gel buffer
200 µl glycerol
800 / 1200 µl H_20
2 µl TEMED
20 µl 10% APS

Tris-Tricine SDS-PAGE buffers

Gel buffer
3 M Tris/HCl pH 8.45
0.3% SDS (w/v)

Stacking gel
400 µl bis-/acrylamide (37.5:1)
750 µl gel buffer
1850 µl H_2O
2.4 µl TEMED
24 µl APS

Separating gel
3000 µl bis-/acrylamide (37.5:1)
2000 µl gelbuffer
500 µl glycerol
500 µl H_20
3 µl TEMED
30 µl 10% APS

Anode buffer
0.2 M Tris/HCl pH 8.9

Kathode buffer
0.1 M Tricine
0.1 M Tris

0.1% SDS (w/v)

Coomassie Brilliant Blue

10% ammonium sulfate
0.1% Coomassie G-250
3% ortho-phosphoric acid
20% ethanol
H_2O ad 1 L

Sample buffer (4x)

200 mM Tris/HCl pH 6.8
48% glycerol (w/v)
16% SDS (w/v)
0.04% bromphenol blue
8% β-mercaptoethanol (for reducing buffer)

3.3 Kits

cAMP-Glo Assay, Promega
NucleoSpin Plasmid Mini-Prep Kit, Macherey-Nagel
Super Signal West Pico, Thermo Fisher
Super Signal West Dura extended duration substrate, Thermo Fisher

3.4 Instruments and Materials

Äkta Pure, GE Healthcare
Cell disruptor: One Shot system, Constant Systems Ltd.
cOmplete His-Tag purification resin, Roche
cOmplete His-Tag purification column (1 ml, 5 ml) Roche
Hamilton syringes (100 µl / 250 µl), Hamilton
Heating Block Ori-Block 3, Techne

Laser Scanning Microscope (LMS), Zeiss
Mini-PROTEAN Tetra cell system, Bio Rad
Nanodrop 200, Peq Lab
Regenerated cellulose filter 0.2 µm, GE
Research Plus Pipettes, Eppendorf
Roll mixer RM5 CAT, M. Zipperer GmbH
Spectrophotometer V-650, Jasco
Tecan Spark, Tecan ThermoMixer compact / comfort, Eppendorf
Trans Blot Turbo system, Bio Rad
2.2 ml 96-well Deep-well plates, VWR

Adrenocorticotropic Hormone

Avanti J-20, Beckman Coulter
Centrifuge 5415 R, Eppendorf (max. 16,100xg)
WellChrom HPLC system, Knauer
Agilent 1260 Infinity HPLC, Agilent
Optima L-100XP Preparative Ultracentrifuge, Beckman Coulter
SpeedVac (AVC 2-18) with cold-trap LT-105, Christ
Superdex 16_300 pg, GE Healthcare
384-well plate (black) non-binding, Corning Zorbax-C8 semi-preparative column, Agilent
Zorbax-C8 stable bond analytical column, Agilent

Melanocortin Receptor 4

Baffled Erlenmeyer flask with vent caps (431405), Corning
Cell culture flasks T-25 / T-75, Sarstedt and Cell Star
Celltron orbital shaker with steel flask clamps, INFORS
CO_2 Incubator ATP.line C150 (E2), Binder
Cryo tube vial, Thermo Fisher
Plate Reader Infinite m1000, Tecan
pureGrade S 384-well plate (white), BrandTech Scientific Inc. Tissue culture dish 100x20 mm, BD Falcon

HIV-1 vpr

FOC 120 cooled incubator, VELP Scientifica
Scientific

Shaker: RS-OS 5, Phoenix Instruments
Slide-A-Lyzer MINI devices (7/10K MWCO) 0.1 ml (69560), Thermo Fisher

3.5 Software

CARA 1.9.1.7
Cyana 2.1
Marvin JS (ChemAxon)
OriginPro 9.0G, OriginLab
Pymol, DeLano Scientific
Sparky
TopSpin 3.2

4

Methods

Contents

4.1 General Methods

4.1.1 SDS-PAGE

Sodium dodecyl sulfate-polyacrylamide gel electrophoresis (SDS-PAGE) is a method for rapid assessment of protein purity and can be expanded by the use of blotting methods to also verify protein identity. It is based on the separation of proteins by size, enabling determination of their relative molecular mass in a certain range. Sample preparation can be performed with a reducing agent and / or denaturating by SDS and heat or without these steps for non-reducing or native gels. In this work two different gel systems, Tris-glycine and Tris-tricine, with varying acrylamide concentrations (%T) were used according to the protein size. While MC4R with a mass of 35 kDa was separated by a 12 % Tris-glycine PAGE, 6xHis-GB1-ACTH fusion proteins (12.6-14.4 kDa) and hormones were displayed by a 15 % Tris-glycine PAGE and 15 % Tris-tricine gels were used for hormone peptides as well as for HIV viral proteins like Vpr (11.2-13.9 kDa). A 4-fold reducing sample buffer was used for MC4R, ACTH and HIV-1 p6 after purification, non-reducing buffer was used for HIV-1 Vpr and for HIV-1 p6 after pulldown experiments.

4.1.2 Western Blot

Western blot was used to identify the protein of interest during establishment of the expression and purification protocol. For the "Signal-Flag tag-MC4R (6xHis tag)" construct detection was performed by an anti-Flag tag antibody (Cell Signaling Technologies) while 6xHis-GB1-ACTH, viral proteins 6xHis-p6 and 6xHis-Ncp7 were detected by a anti-Histidine Tag antibody (Cell Signaling Technologies). HIV1 viral protein R was specifically detected using the antibody vN-20 (Santa Cruz) which is directed against the N-terminus of the protein.

4.2 Adrenocorticotropic Hormone

To obtain isotope labeled adrenocorticotropic hormone for structure analysis, the peptide was expressed as a fusion protein. This is comprised of a six-fold histidine-tag (His-tag) and a B1 immunoglobulin-binding domain of streptococcal protein G (GB1) followed by a tobacco etch virus (TEV) protease recognition site at the N-terminus of the hormone. While the His-Tag facilitates the use of nickel nitrilotriacetic acid (Ni-NTA) affinity-chromatography (ion metal affinity chromatography (IMAC)), the GB1 domain provides solubility. The rather large fusion protein is less vulnerable for degradation than the small peptide during bacterial expression. By TEV protease cleavage (Q|S) the peptide can be released from the fusion protein without any artificial amino acid remaining at the N-terminus of the hormone. The mixture of cleaved fusion tag and peptide was subjected to size exclusion chromatography (SEC) for separation. Subsequently the peptide was applied to an AcN / water gradient in reversed phase high performance liquid chromatography (RP-HPLC) for further purification and desalting followed by lyophilization. The protocol for hormone expression and purification established in this work is shown in figure 4.1 and described in detail in the following sections.

The addition of a C-terminal Cysteine to the ACTH sequence, which natively does not contain any Cysteine, was used to provide a specific labeling site for maleimide reactions. In this way fluorophors and other labels could easily be attached to the peptide. As binding of ACTH to Melanocortin Receptors is known to be limited to the N-terminal amino acids 1-20 ACTH(1-23) was found to be a suitable short form for Fluorescence Polarization experiments,avoiding negative effects of the flexible C-terminus given in the full length ACTH(1-39).

4.2.1 Recombinant Expression of ACTH

E.coli BL21 was used for expression of fusion proteins 6xHis-GB1-ACTH(1-39)/C and 6xHis-GB1-ACTH(1-23)C. Expression was performed in Luria Bertani medium with 100 µg/ml ampicillin at 37 °C shaking at 120 - 180 rpm in 2 - 5 L baffled flasks. Expression cultures were inoculated with an over night pre-culture to an optical density (OD) at 600 nm of 0.1 and grown to an OD of 0.6 - 0.8 until induction with 1 mM Isopropyl-β-D-thiogalactopyranosid (IPTG). Cells were harvested 2 - 3 h after induction by centrifugation at 3000 - 5000 rpm (Avanti J-20, Beckman Coulter) and stored at -20 °C until disruption.

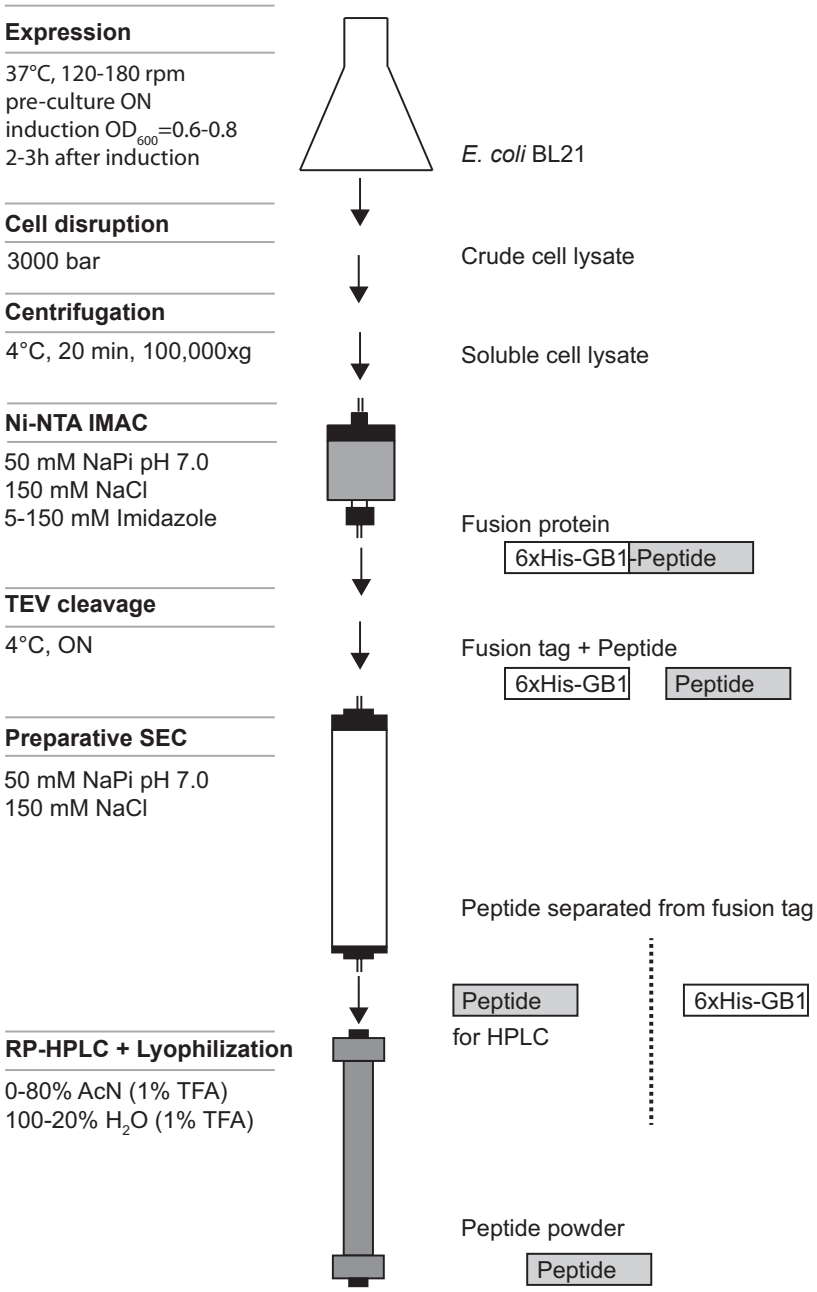

Figure 4.1: Purification protocol for peptide hormones To obtain isotope labeled peptide in amounts sufficient for NMR, a protocol for expression and purification of melanocortins was established. After expression in *E. coli* Bl21 cells were lysed and the soluble lysate fraction was subjected to Ni-NTA affinity chromatography before TEV cleavage of the fusion protein. Fusion partners were separated by SEC before further purification via RP-HPLC and subsequent lyophilization to obtain salt free peptide powder which can be prepared for NMR experiments.

4.2.2 Peptide Purification

To separate the proteins and peptides of interest, fusionproteins and peptide hormones were purified step wise by using different chromatographic methods. Chromatography is the process of separation of substances solved in a mobile phase by interaction of the analytes with a stationary phase. Therefor different forms of analyte-stationary phase interactions are used for different chromatographic methods such as in size-exclusion and affinity chromatography or in reverse-phase high-performance liquid chromatography (rp-HPLC), which is based on differences in hydrophobicity.

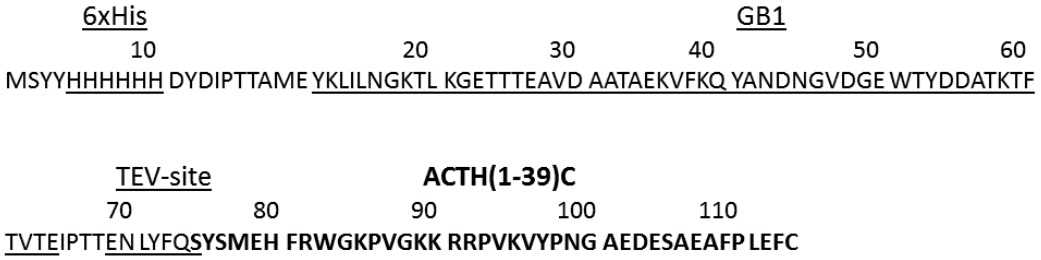

Figure 4.2: Amino acid sequence of the 6xHis-GB1-ACTH(1-39)Cys fusion protein. His-Tag, TEV-recognition site and IgG B1 domain are underlined, ACTH is highlighted in bolt.

4.2.2.1 Immobilized Metal Affinity Chromatography(IMAC)

Immobilized Metal Affinity Chromatography is based on the covalent binding of amino acids, (e.g. Histidine) to metals (e.g. nickel) immobilized with a chelating agent on a solid phase, mostly (e.g. sepharose). For purification of ACTH fusion proteins Nickel-NTA Sepharose was used for IMAC. Here the six-fold Histidine-Tag of the analyte in the mobile phase covalently binds to the nickel immobilized on the solid phase (sepharose) via nitrilotriacetic acid (NTA) as a chelating agent.
Cell lysate for IMAC was gained by cell disruption with a One Shot system from Constant Systems Ltd. using 3000 bar. Disruption was performed up to two times after resuspending the defrosted cells in 50 mM NaPi pH 7.0, 150 mM sodium chloride and cOmplete protease inhibitor (1 tablet/ 50 ml), for cysteine variants at least 2 mM di-thiothreitol (DTT) were added to the lysis buffer. Crude cell lysate as clarified by ultra centrifugation at 100,000xg at 4 °C for 25 min before ist was applied to the equilibrated Ni-NTA resin. IMAC was performed as described in the following protocol using 50 mM NaPi pH 7.0, 150 mM NaCl buffer (+2 mM DTT):

IMAC protocol

Fill 1 ml Ni-NTA sepharose beads (Macherey & Nagel) into a 20 ml Econo-Pac column (Bio Rad). Let resin settle, open the column, let ethanole run through. Was the resin with at least three column volumes (CV) of Milli Q (MQ) water before equilibration with at least 3xCV of the buffer desired for purification. Close column bottom and add the cleared lysate containing the analyte. Seal column top and bottom an incubate Ni-NTA beads and sample for at least 1 h rotating on a roll mixer at 4 °C. The following steps can be performed at room temperature using buffers chilled to 4 °C. Let resin settle and lysate run through, collecting the flow through. Wash the resin with 3x 1 CV buffer and 3x 1 CV buffer with 5 mM imidazole to elute *E.coli* proteins unspecifically bound to the beads. Then elute the purified analyte with buffer containing 150 mM imidazole. Finally clean the column with 2xCV 2 M imidazole, intensively rinse it with water and store it in 20% ethanole.

4.2.2.2 Size-Exclusion Chromatography (SEC)

A Superdex column (GE Healthcare) was used for SEC to separate ACTH from its fusion partner after cleavage with TEV protease. SEC was run at a flow rate of 1 ml/min for Superdex 16_600 30 pg at 4°C column and buffer temperature, elution profile was recorder at 280 nm. For the mobile phase a 50 mM NaPi, 150 mM sodium chloride buffer (pH 7.0) was used for elution, 2 mM DTT was added for ACTH variants with C-terminal Cysteines. Buffer were filtered through a 0.1 μm filter and subsequently degased stirring in an exicator for at least 30 min. Column equilibration was performed with at least two column volumes (2x121 ml) of elution buffer before sample application and elution.

4.2.2.3 RP-HPLC

Reversed phase high performance liquid chromatography (RP-HPLC) is commonly used for analysis of molecules. It is based on the analytes interaction with a hydrophobic stationary phase and the use of a hydrophilic organic solvent for elution. To obtain highly concentrated ACTH after dilution due to size-exclusion chromatography (SEC), rp-HPLC was used for further purification gaining concentrated peptide in a highly volatile solvent. As other methods commonly used for increasing peptide concentration, such as centrifugal concentrators and PD10 desalting columns followed by lyophilization, lead to a high loss of peptide, RP-HPLC was used for desalting followed by lyophilization in this work.

Table 4.1: RP-HPLC gradient time table. Peptides were purified in a acetonitrile (AcN) / H_2O gradient with 0.1 % trifluoroacetic acid (TFA) as indicated.

Time [min]	% H_2O	% AcN
0	100	0
5	75	25
30	50	50
35	0	100
40	100	0

ACTH was purified at room temperature with a Knauer WellChrom HPLC system applying a gradient of acetonitrile (AcN) / H_2O with 0.1 % TFA described in the following table:

Peptide elution was observed at 280 nm. An Agilent Zorbax-C8 stable bound semi-preparative column was used. The time point of ACTH elution was determined by comparison of test runs with 6xHis-GB1 and ACTH fractions from SEC as well as the SEC buffer. In this way peaks according to buffer contents or impurities consisting of the fusion tag could be differed from peaks according to ACTH. This outcome was also confirmed by SDS-PAGE analytics and MALDI TOF mass spectrometry.

4.2.3 Assembly of Nanodiscs

Expression of the membrane scaffold protein (MSP) 1D1 and nanodisc (ND) assembly were performed according to established protocols [100]. NDs were assembeled with different lipids differing in the size of headgroups, length and saturation of fatty acid chains and phase transition temperatures (T_m). The following lipids incorporated into NDs were purchased from Avanti Polar Lipids Inc.:

POPS: Palmitoyloleoylphosphatidylserine; T_m = -2 °C
POPC: Palmitoyloleoylphosphatidylcholine; T_m = 14 °C
DMPG: 1,2-dimyristoyl-sn-glycero-3-phosphoglycerol; T_m = 23 °C
DMPC: 1,2-dimyristoyl-sn-glycero-3-phosphocholine; T_m = 24 °C

A buffer exchange from 20 mM NaPi pH 7.4 to 10 mM HEPES pH 7.0 containing 50 mM NaCl was performed for NDs when used in buffer containing calcium chloride.

4.2.4 NMR Data Acquisition and Assignment

In this work NMR spectra were acquired in either a 600 MHz or 700 MHz Bruker AvanceIII spectrometer (Bruker, Wissembourg, France) equipped with a 5 mm inverse detection triple-resonance z-gradient cryogenic probehead (CP TCI). All data was processed in Bruker TopSpin3.5 (Bruker). The backbone and sidechain assignment of ACTH(1-39)C was performed following a standard triple resonance-based protocol [101], [102]. Hormones were prepared in a 20 mM NaPi pH 7.0, 50 mM NaCl buffer containing 10 % D_2O (v/v) or 10 M HEPES pH 7.4, 50 mM NaCl for experiments with calcium. Two-dimensional ^{15}N,^{13}C-edited heteronuclear single-quantum coherence (HSQC) and three-dimensional HNCO, HN(CA)CO, HN(CO)CACB and HNCACB experiments were performed to obtain the chemical-shift assignments of the backbone atoms. Additional 3D (H)CCHTOCSY, ^{15}N-TOCSY-HSQC (mixing time 80 ms) and ^{15}N-NOESY-HSQC (mixing time 300 ms), were acquired for complete side chain resonance assignment and NOE measurements (see supplement 8.1 table 8.1 for details on acquisition parameters). Assignment of the ^{1}H, ^{13}C, and ^{15}N signals in spectra was performed in CARA1.9.1.7 [103]. Peak volumes were calculated with CARA 1.9.1.7.

4.2.5 Maleimide Conjugation of Reactants to ACTH-Cys

The C-terminal cysteine in the ACTH-Cys variants were used to specifically attach reactants such as fluorophores - Cy3B maleimide dye (GE Healthcare) or Atto 647 maleimide (Atto Tech)- or a biradical - TOTAPOL maleimide (Vlado Gelev)- to the peptide. The labeling reaction (see figure 4.3) was performed in 50 mM NaPi containing 150 mM sodiumchloride (pH 7.0-7.4). The reactant was added in tenfold molar excess compared to the peptide. In order to keep the thiol groups in a reduced state or to reduce preexisting disulfid-bridged dimers, a 1:1 molar ratio of Tris(2-carboxyethyl)phosphin (TCEP) was added ahead of the actual reaction. This low ratio was chosen to avoid degradation of the radical by TCEP. The reaction was performed at 4 °C overnight. For Cy3B maleimide a tenfold TCEP excess and incubation at room temperature over night was performed. Afterwards, the reaction mixture was applied to RP-HPLC to separate ACTH conjugates from non-bound dye or radical.
The peptide fraction was dried under vacuum and the aliquot was subsequently stored at -20°C until further use.

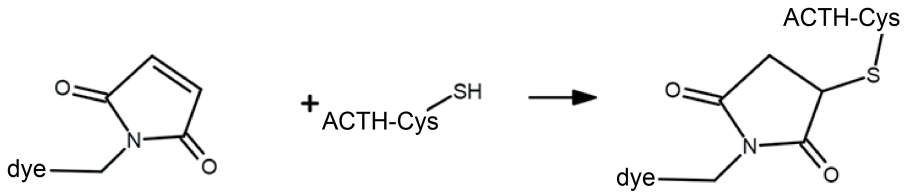

Figure 4.3: Maleimide reaction of reactants and protein. Reactants with a maleimide group can be conjugated to the thiol group of a protein's cysteine residue. The reaction scheme was prepared with Marvin JS (ChemAxon).

4.2.6 Fluorescence Anisotropy

Fluorescence polarization measurements were performed in a Tecan Spark using filters for excitation of fluorophores and a monochromator for fluorescence detection. Measurements were performed in 384-well non-binding plate (Corning) with a working volume of 40 μl. A grating factor of 1.7 was determined by stepwise adjustment to obtain low values for free dye (Ctrl.). Detection with a monochromator instead of a filter can lead, due to limited or fixed band width, to a loss of sensitivity and a higher variation of the recorded values. Therefore, we averaged FP values of ten measurements per sample. Subsequently FP values were transformed to FA values, using the equation 2.6 shown in section 2.1.2.1.

4.3 Melanocortin Receptor 4

4.3.1 Expression in HEK 293 Cells

For expression of melanocortin receptor 4 (MC4R) HEK cells were chosen as a eukaryotic expression system to provide typical post translational modifications. Two different expression strategies were used for MC4R expression. Semi-adherent HEK 293 cells stably transfected with the following constructs under control of a cytomegalovirus (CMV) promoter were kindly provided by Baran Ersoy [49]:

I. N-terminal signal peptide (prolactin) for membrane incorporation, followed by a FLAG-tag MC4R

II. N-terminal signal peptide (prolactin), FLAG-Tag Δ(1-24)MC4R (no maintained basal activity)

III. WT MC4R

To increase the protein expression yield of MC4R HEK 293-F cells, optimized for growth in cell suspensions, were stably transfected with a MC4R construct flanked by a N-terminal signal peptide prolactin followed by a FLAG-tag for detection in western blot. A six-fold His-tag was added to the *C-terminus* of the protein to enable protein purification by affinity Ni-NTA chromatography. The expression vector was changed from pcDNA3.1 to a pHL-IRES under the control of a more moderate promoter, chicken β-actin (CBA), than before, (CMV) as described above, (kindly provided by James Yu, HMS). The idea of this was to avoid degradation of overexpressed protein due to too strong expression.
The so called Free Style system (Gibco) enables cultivation of HEK 293 cells in suspension using shaker flasks or spinner flasks with culture volumes ranging from 15 ml up to 36 l.

4.3.2 cAMP Down-Stream Assay

Ligand mediated activation of MC4R was tested with a cAMP-based bioassay from Promega (cAMP-Glo). For a scheme of the luminescence assay see figure 5.18.
The assay was performed according to the manufacturers protocoll with cell numbers of 10,000 or 24,000 (if indicated) cell / well.

4.3.3 PFA Fixation

HEK 293-F cells were grown semi-adherent with medium containing 10% fetal bovine serum (FBS) on a poly-lysine coated cover slip. They were rinsed two times with phosphate buffer saline (PBS) with 1 mM $CaCl_2$ and incubated with $\sim$ 200 nM ACTH(1-39)C-Cy3B for 45 min at 37 °C, 5% CO_2. After two more washing steps cells were fixated with 4% paraformaldehyde (PFA) for 34 min at room temperature (RT) and

washed again before incubation with 1% glycine in PBS for 20 min at RT. A further washing step was performed previous to blocking with 3% bovine serum albumine (BSA) in PBS for 1 h at RT. Cells were again washed two times for 5 min at RT and mounted on a slide with mounting medium before letting dry for 12 h in the dark at RT.

4.3.4 Membrane Preparation of Tnao38 Cells

A membrane preparation of Tnao38 insect cells (kindly provided by the lab of Prof. Dr. Reza Ahmadian) expressing SF-MC4R-6xHis was prepared by Marcel Falke (HHU, Düsseldorf) as follows:

Resuspend cells harvested from 1 l Tnao38 cell culture in 100 ml 50 mM HEPES/ NaOH pH 7.4, 150 mM NaCl, 2 mM DTT + protease inhibitor.
Lyse cells by nitrogen cavitation (Parr 4635 Cell Disruptor Vessell) at 500 psi (1psi = 6.9 kPa) and 4 °C for 15 min.
Separate the soluble membrane fraction from remaining cell debris by centrifugation at 500xg for 20 min at 4 °C.
Transfer the supernatant to a fresh tube and centrifuge at 40,000 rpm and 4 °C in a Beckman Coulter Optima XL 100 with a Ti55.2 rotor.
Transfer the membrane pellet to a dounce tissue grinder, resuspended in $\sim$ 50 ml 50 mM HEPES/ NaOH pH 7.4, 150 mM NaCl, 2 mM DTT + protease inhibitor to a final concentration of 10 mg/ml, for homogenization.

For FA experiments $\sim$ 60 μl membrane preparation were further diluted to meet a concentration according to a previous concentration of 60,000000 cells / well (40 μl)

4.4 HIV-1 Vpr

Continuous exchange cell-free expression (CECF) is a flexible and open system for protein expression. It can be based on different translational systems by the choice of the cell extract used and easily expanded by further reaction components promoting folding and solubility of the protein expressed. In CECF a compartment containing the reaction mixture with all high-molecular-weight compounds is separated by a permeable compartment with the feeding mixture containing low-molecular-weight

precursors. CECF can be run in different modes: precipitate-based (P-CF), detergent-based (D-CF) or lipid-based (L-CF) cell-free expression.
In this work CECF expression was used to produce high amounts of human immunodeficiency virus type 1 (HIV-1) viral protein R (Vpr), overcoming its cytotoxic effects, and to provide zinc for incorporation during protein expression.
An *E. coli*-based CECF was run in precipitate-based mode (i.e. without detergents or other compounds promoting protein solubility) or with addition of zinc salts for incorporation into HIV-1 Vpr.
Expression was carried out in Slide-A-Lyzer MINI dialysis devices (Thermo Fisher Scientific) with a molecular weight cut off (MWCO) of 7,000 kDa (or 10,000 kDa for expression of control reactions with larger proteins) in 50 μM reaction mixture and 500 μM feeding mixture using 96-well plates. It was incubated at 27 °C, shaking for at least 18 h. Reaction and feeding mixtures were prepared according to the protocol of Schwarz et al. [94].

5

Results and Discussion

5.1 Hormone Expression and Characterization

5.1.1 Expression and Purification

To study structure and dynamics of hormone-receptor interaction a protocol for the expression and purification of isotope labeled hormone peptides had to be established. Peptides ACTH(1-39), ACTH(1-39)C and ACTH(1-23)C were expressed using a 6xHis-GB1 fusion tag with a TEV recognition site (ENLYFQ|S - cut between Q|S) for stable expression and easy purification before cleavage at the *N-terminus* of the hormone.

The fusion protein was purified via Ni-NTA affinity chromatography, shown for ^{15}N 6xHis-GB1-ACTH(1-39)C in figure 5.1.

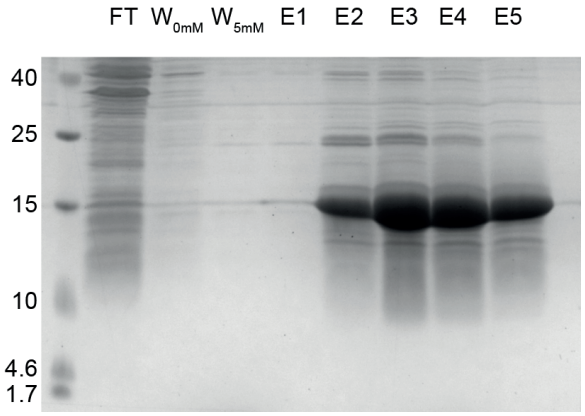

Figure 5.1: Purification of ^{15}N-labeled 6xHis-GB1-ACTH(1-39)C by IMAC. Intense bands of ^{15}N-6xHis-GB1-ACTH(1-39)C are found in the elution fractions E2-4 (15 kDa). Host cell proteins can mainly be found in the flowthrough (FT). The background could be reduced by several washing steps (only the last steps of washing with 0 mM and 5 mM imidazole are shown: W_{0mM}, W_{5mM}).

After protein overexpression and cell disruption, a high amount of fusion protein (15 kDa) was purified by Ni-NTA IMAC from the soluble cell lysate. The elution fractions in figure 5.1 (E2-E5) contain only a low background of *E. coli* proteins when compared to the intensity of the 15 kDa band. The native peptide sequence was cleaved from the fusion protein by TEV protease (figure 5.4). Subsequently, the peptide hormones were separated by SEC from the remaining fusion tag and TEV protease (figure 5.2, figure 5.4).

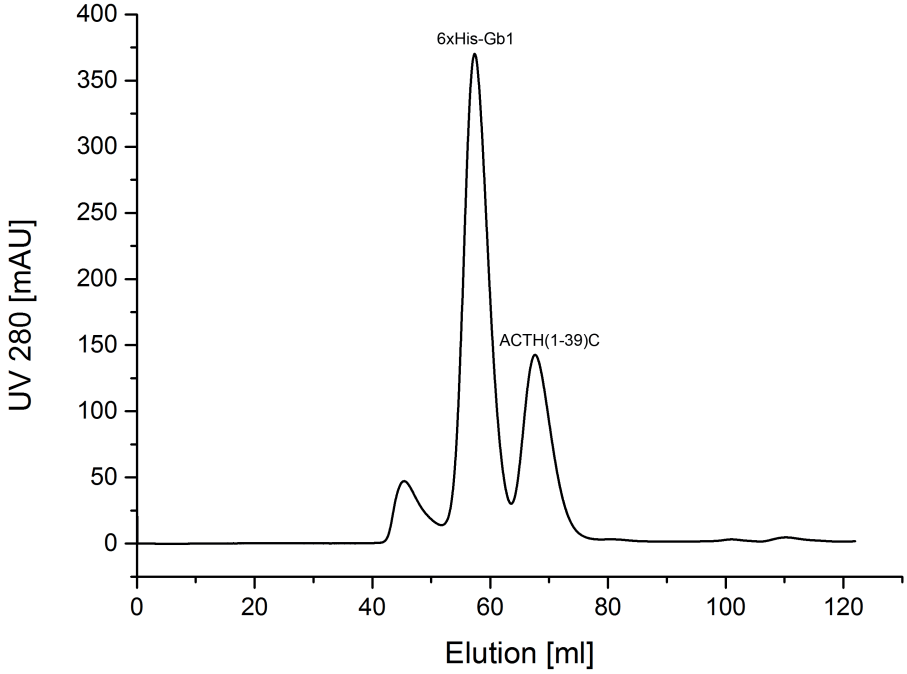

Figure 5.2: SEC of ^{15}N-ACTH(1-39)C after TEV protease cleavage. ^{15}N 6xHis-GB1 (55-65 ml) and ^{15}N-ACTH(1-39)C (65-75 ml) are separated by SEC after TEV protease mediated fusion protein cleavage. The void volume containing host cell proteins and TEV protease elutes after 43 ml. A Superdex 16/600 30 pg column (GE) was used for size exclusion chromatography.

In the SEC chromatogram in figure 5.2 ACTH is found to be successfully separated from remaining host cell proteins and TEV protease which elute in the void volume (43 ml). The fusion tag 6xHis-GB1 can be found in the elution volume of 55-65 ml and ^{15}N-ACTH(1-39)C elutes after 75 ml. SEC elution peaks were fractionated in 2 ml steps and samples of the fractions with the highest protein content were further analyzed by SDS-PAGE (figure 5.4) before combining all fractions of one peak.

To obtain peptide concentrations sufficient for NMR spectroscopic studies, it was necessary to concentrate the peptide solution after SEC. The use of centrifugal concentrators led to a high loss of protein using different membrane types - regenerated cellulose (Centricon, Merck Millipore) or polyethersulfone (Vivaspin, Sartorius) - due to unspecific interaction of the peptide with the membranes.

Therefore, a second strategy to concentrate the peptide for further measurements was applied using lyophilization of the peptide. As salt present in the SEC buffer would also be concentrated by this step, a desalting step had to be performed previously. But the use of a PD10 desalting column also lead to a high loss of peptide. As before, this is thought to be a consequence of unspecific binding of the hormone to the column resin further enhanced by the absence of salts.
However, peptides were successfully subjected to RP-HPLC using a water / acetonitrile gradient as mobile phase. After lyophilization peptide powder was dissolved in buffers with a moderate and specific salt content for NMR experiments or further modification.

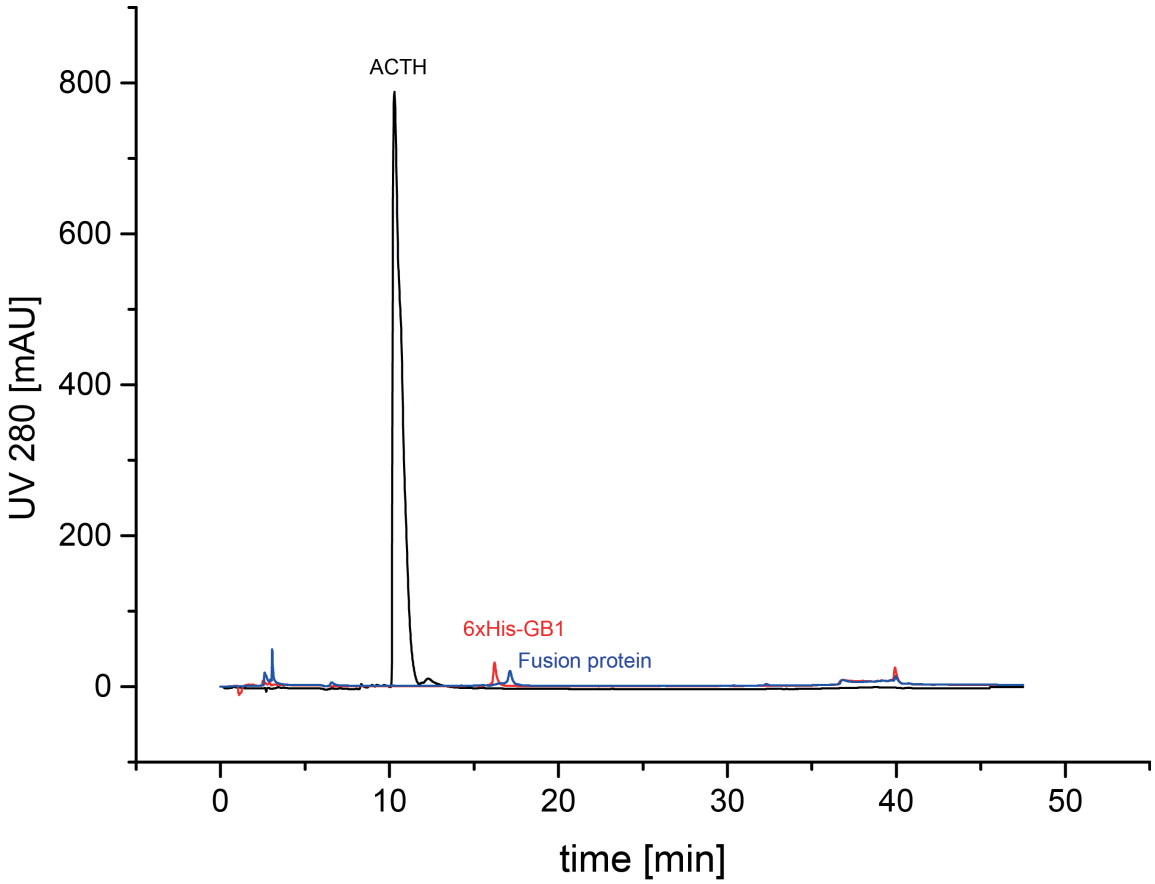

Figure 5.3: ACTH desalting by RP-HPLC. ^{15}N ACTH was purified and desalted in an AcN / water gradient by RP-HPLC for subsequent lyophilization. ACTH(1-39) (black) elution (10 min) is compared to RP-HPLC runs with fusion protein (blue) and 6xHis-GB1 (red) purified by SEC to identify the pure peptide.

Comparison of spectra recorded of ACTH(1-39)C concentrated with and without RP-HPLC (e.g. with centrifugal concentrator) showed that the peptide is unfolded in both cases.

Therefore, the following data on recombinantly expressed peptides was recorded of hormones purified and concentrated by RP-HPLC with subsequent lyophilization.

Figure 5.3 shows the chromatogram of ACTH(1-39) (black), fusion protein (blue) and 6xHis-GB1 (red) at 280 nm in an AcN / water gradient. While fusion protein and 6xHis-GB1 elutes before 8 min and after 15 min respectively, ACTH(1-39) elutes at 10 min. Although SEC is already sufficient to separate the peptide from its fusion tag and possible remaining uncleaved fusion protein, RP-HPLC facilitates to further purification separating even the small content of *E. coli* proteins of the same size as the peptide. Moreover, peptide dimers were found to be separated from monomers by RP-HPLC (data not shown) but dimer formation could generally be avoided by using reducing agents such as DTT or tris(2-carboxyethyl)phosphine (TCEP) during previous purification steps (see Supplement 8, figure 8.1).

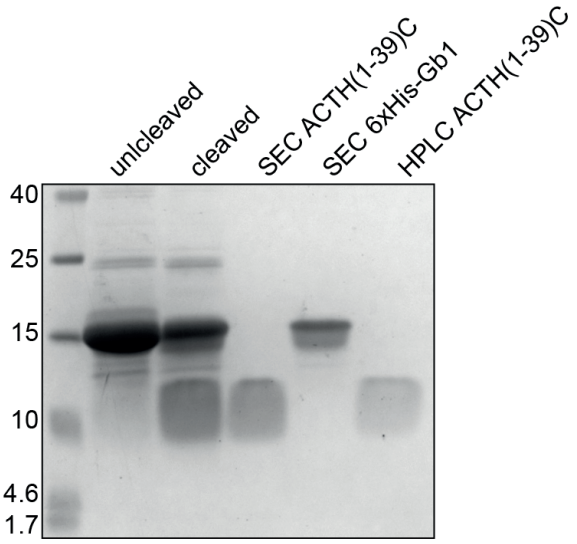

Figure 5.4: Fusion partners after TEV cleavage purified by SEC and RP-HPLC. SDS-PAGE analytics of 6xHis-GB1-ACTH(1-39)C before and after TEV cleavage (lane 1 / 2), SEC fractions containing 6xHis-GB1 or ACTH(1-39)C (lane 3 / 4) and ACTH(1-39)C after reversed RP-HPLC. 6xHis-GB1 remains at the height of 15 kDa while peptides run at 10-12 kDa.

A SDS-PAGE of the purification steps confirms the findings of SEC and RP-HPLC chromatograms (figure 5.4). Fusion protein was efficiently cleaved by TEV protease (figure 5.4, lane 1 / 2) which is visible in a second band running lower than that of the fusion protein. Interestingly 6xGB1 was found to stay at the same height (15 kDa) even after cleavage. In figure 5.4 the free peptide band is very broad, possibly due to insufficient separation from the bulk of SDS (see section 2.2.5). In other gels more defined bands of the 4.6 kDa peptide ACTH(1-39)C could be achieved with a band at the height of ca. 10 kDa (see figures 5.5, 5.7 8.1).

Hormones expressed and purified as shown above were used for NMR experiments (section 5.1.3) or ligand binding assays (section 5.3.1) as well as conjugation with different labels such as fluorophores and a biradical (TOTAPOL) (section 5.1.2). The molecular mass of purified ACTH(1-23)C and (1-39)C was additionally verified by electrospray ionization (ESI) mass spectrometry (MS) (Supplement: chapter 8, 8.2) to verify the molecular mass.

5.1.1.1 Peptide truncation during expression

Overexpression of the protein of interest was accompanied by overexpression of proteins running at a different height in SDS-PAGE analytics several times. This was possibly caused by mutation of the plasmid or degradation of the protein. SDS-PAGE analysis of the purified ^{13}C-, ^{15}N-labeled fusion protein after TEV cleavage (figure 5.5) shows that besides remains of uncleaved fusionprotein and 6x-GB1 peptides running at 12 and 9 kDa were released. While normally not desired, we used these additional peptides to study the influence of C-terminal truncations on the peptides structural features (see section 5.1.3).

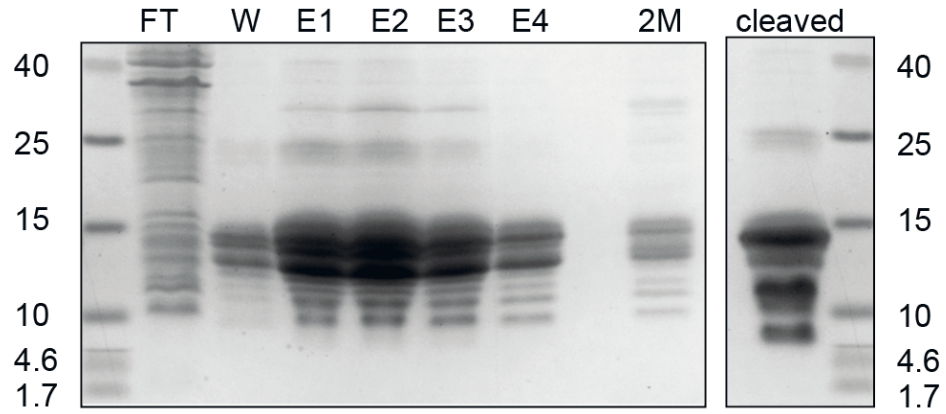

Figure 5.5: Purification of ^{13}C, ^{15}N labeled 6xHis-GB1-ACTH(1-39)C by IMAC. A double band of overexpressed protein was observed during all washing and elution (E1-5) steps of IMAC purification implying that more than the fusionprotein 6xHis-GB1-ACTH(1-39)C was overexpressed. SDS-PAGE analytics of TEV cleaved ^{13}C, ^{15}N labeled 6xHis-GB1-ACTH(1-39)C shows more than the expected bands for 6x-GB1 (15 kDa) and ACTH(1-39)C (ca. 10 kDa). Another band below 10 kDa was detected with CBB staining.

Fusion protein was subjected to SEC after cleavage with TEV protease. The elution profile shown in figure 5.6 reveals an additional peptide peak (78-83 ml) according to a smaller size than that of ACTH(1-39)C (ACTH(1-28); see figure 5.7). Furthermore using RP-HPLC two peptides were detected in the SEC peak eluting at 63-70 ml (ACTH(1-39)C and ACTH(1-39); see figure 5.6).

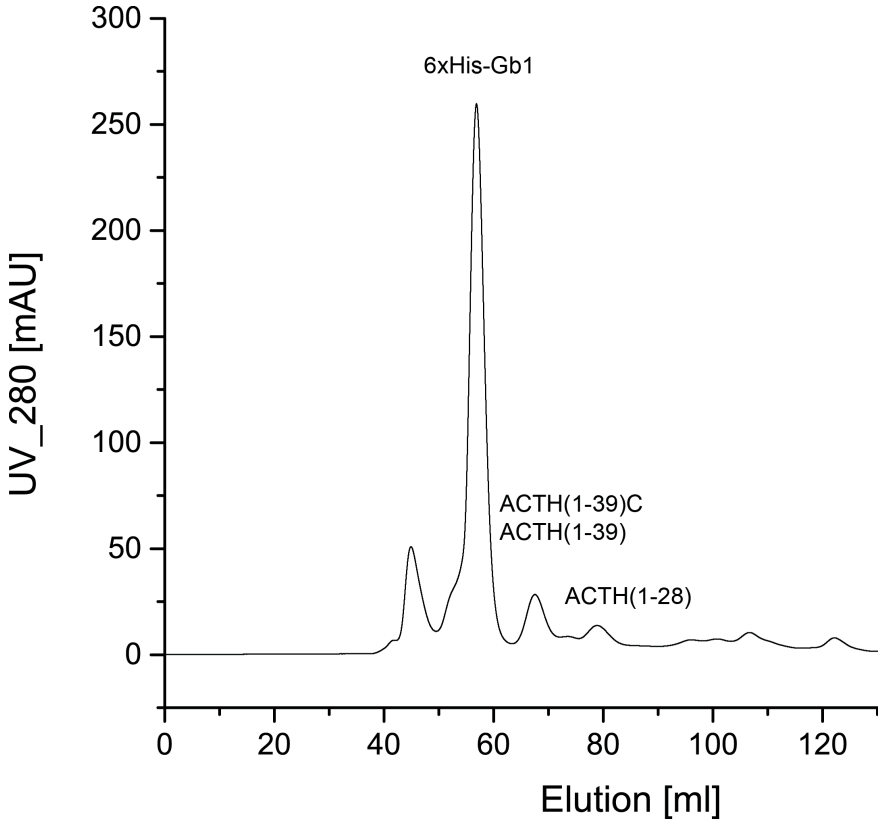

Figure 5.6: SEC purification of ACTH(1-39)C reveals another smaller peptide. Additionally to ACTH(1-39)C a smaller peptide was purified by SEC (78-83 ml) later on determined to be ACTH(1-28). In a further RP-HPLC run the peptide peak eluting at 63-70 ml was found to contain ACTH(1-39)C and ACTH(1-39).

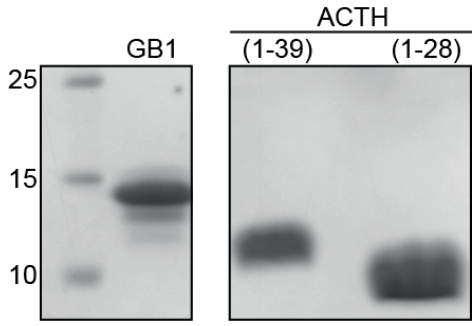

Figure 5.7: Smaller peptides than ACTH(1-39)C in SDS-PAGE. Besides ACTH-(1-39)C smaller peptides (ACTH 1-39 and ca. 1-28) were purified by SEC and RP-HPLC subsequently. Peptide size was confirmed by MS.

Purified peptides of all sizes were subjected to ESI MS (Supplement: chapter 8, section 8.2) and NMR spectroscopy (see section 5.1.3, figures 5.13, 5.14) to determine molecular mass and identity. In this way it was confirmed that besides ACTH(1-39)C also ACTH(1-39) and ACTH(1-28) were expressed and purified in concentrations sufficient for acquisition of NMR spectra (figures 5.13, 5.14). It is not clear whether these truncations are caused by protease activity or codon mutations. The cysteine at position 40 could have been transformed to a stop codon by a point mutation (TGC to TGA), while a single nucleotide exchange could not transform the codon of aspartic acid (GAC) to a stop codon (TAA, TAG, TGA). Neither the codons used for cysteine (TGC) nor that used for aspartic acid (GAC) are rare codons in *E.coli* that could probably lead to mixed protein populations by termination of the translation process. However, digestion by proteases seems unlikely as protein truncations were not observed for every expression performed.

5.1.2 Hormone-Conjugates

5.1.2.1 Fluorophore Conjugated ACTH

Ligand binding assays based on fluorescence anisotropy (FA) / fluorescence polarization (FP) can be used with low amounts of receptor and fluorophore conjugated ligand. They can be run in a high-throughput format for an easy component screening to find new potential pharmacological hits. In this work fluorophore conjugated ligands were tested for their ability to be used for FA measurements with the receptor exposed on cell surfaces and stabilized in membrane fragments or membrane mimetics.

Maleimide Conjugation

For conjugation of different labels to the hormones, an additional cysteine at the C-terminus of the peptides ACTH(1-23) and ACTH(1-39) was introduced. This cysteine - unique in the peptide sequence - enables the site specific conjugation of modified labels via a maleimide reaction (see section 4.2.5, figure 4.3). In this way different fluorophores (Cy3B, Atto 647) and also the biradical TOTAPOL for use in fluorescence assays and DNP NMR, respectively, were added to the C-terminus of the hormones.

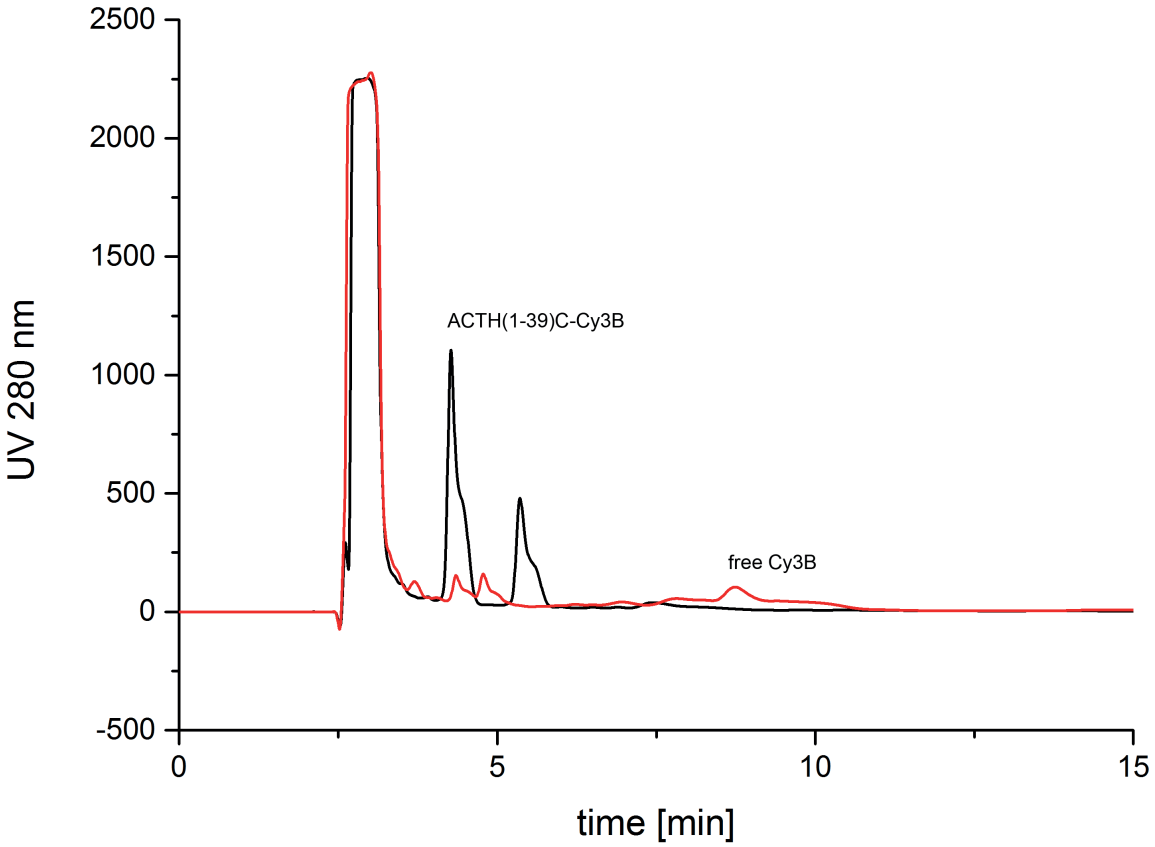

Figure 5.8: ACTH(1-39)C-Cy3B purification via RP-HPLC. ACTH(1-39)C-Cy3B conjugate (black) and free dye as control (red) were applied to RP-HPLC for purification of the conjugate. The conjugate elutes after 4 minutes before free dye elutes at 8 minutes.

ACTH(1-39)C was conjugated to Cy3B (GE Healthcare) and applied to MC4R expressing HEK cells for fluorescence imaging using paraformaldehyde cell fixation (see section 5.3.1, figure 5.20). Figure 5.8 shows the elution profile of the peptide-dye reaction mixture at 280 nm (black) in an AcN / water gradient compared to that of free Cy3B (red). ACTH(1-39)C-Cy3B conjugate ($\sim$ 4.5 min) is separated from free dye ($\sim$ 9 min) that was applied in excess over the peptide.

ACTH for Fluorescence Polarization

To find a suitable dye for FA based ligand binding assays with MC4R exposed on cell membranes a screening for autofluorescence of HEK 293-F cells was performed. The aim was to determine an excitation wavelength with a low fluorescent background. Therefore all filters available in the instrument were tested.

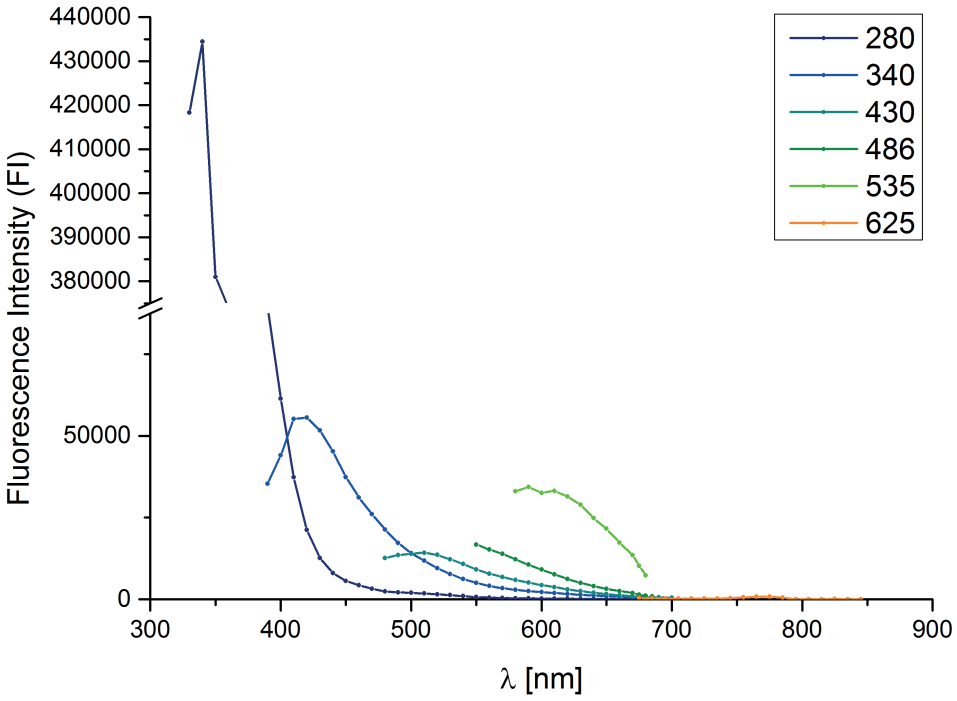

Figure 5.9: HEK 293-F autofluorescence. All filters available for excitation were tested for autofluorescence of HEK cells. The excitation wave length 62 nm was determined to be the one with lowest fluorescent background.

Excitation of a HEK cell suspension with wave lengths of 280, 340 and 535 nm shows high fluorescent background, excitation with 430 and 486 nm filters leads to a decrease of fluorescent background. However, an excitation wave length of 625 nm is found to cause an even lower signal level by HEK cells. Therefore Atto 647, a dye described to be highly hydrophilic, was chosen for further FA ligand design.

As an increase of FA is caused due to a slower tumbling of the fluorophore, ligands need to be designed accordingly (see section 2.1.2.1). The amino acid sequence 1-24 of ACTH is highly conserved in mammals [104] implying an important role in physiological activity. However amino acids 25-39 are hypothesized to have a protective function avoiding enzymatic degradation of the hormone. Furthermore high *in vivo* corticotropic activity compared to full-length ACTH (100%) was described for peptide truncations 1-24 (50%) down to 1-19 (20%) while smaller peptides showed a strongly decreased activity [52]. N-terminal binding of ACTH to its receptor could possibly leave the *C-terminus* flexible. This can lead to decreased anisotropy values and a not sufficient difference of the FA values for bound and free ligand. Therefore we used a truncated ACTH, i.e. the first 23 amino acids, and added a C-temrinal cysteine at position 24 for maleimide conjugation of a modified fluorophore.

Purification of the peptide conjugate ACTH(1-23)C-Atto 647 by RP-HPLC is shown in figure 5.10. The same AcN / water gradient as used for peptide purification shown in figure 5.3 and 5.11 was applied. To determine the elution peak of the conjugate, RP-HPLC chromatograms (280 nm) of free peptide (blue) and dye (red) were compared to the elution profile of the reaction mixture (black).

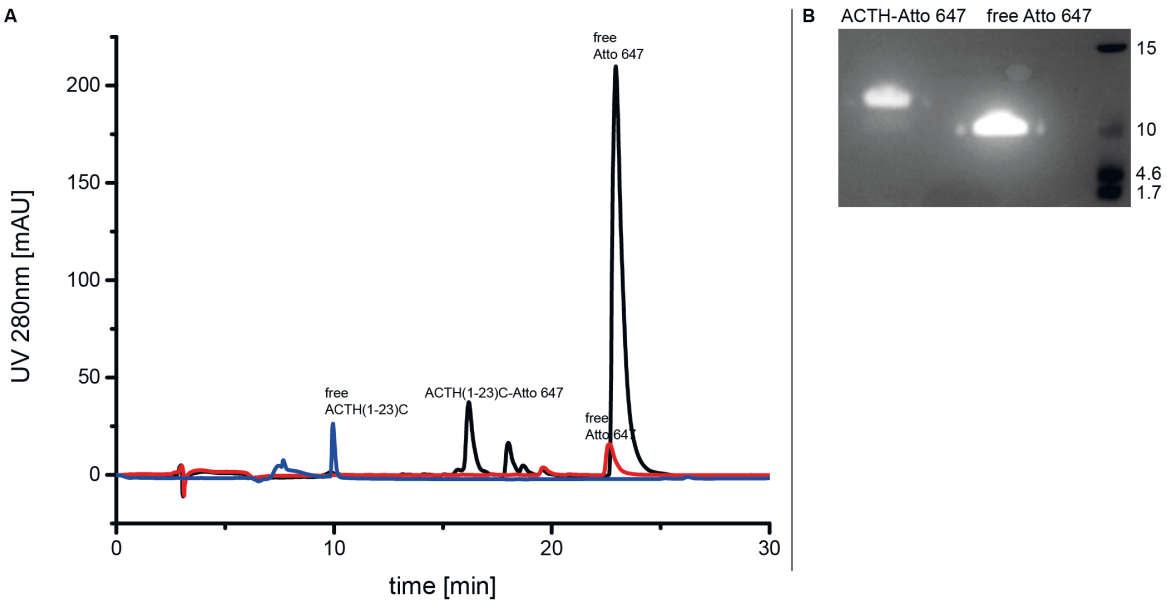

Figure 5.10: ACTH(1-23)C-Atto 647 purification via RP-HPLC. (A) Overlay of ACTH(1-23)C-Atto 647 conjugation mix (black), free ACTH(1-23)C (blue) and free dye (red) RP-HPLC chromatograms. Free ACTH(1-23)C elutes after 10 min before the peptide conjugate (ACTH(1-23)C-Atto647) elutes after 16 min and free dye (Atto-647) elutes after 22.5 min. **(B)** The second elution peak gained from RP-HPLC shows ACTH(1-23)C-Atto647 conjugate (black) which runs higher than the separated free dye (red).

Free peptide elutes at 10 min followed by ACTH(1-23)C-Atto 647 at 16 min and free dye (Cy3B) at $\sim$23 min (figure 5.10 **(A)**). SDS-PAGE analysis of RP-HPLC elution fractions shows that the content of the peak at 16 min (ACTH(1-23)C-Atto647) runs higher than that of the peak at 22.5 min (free dye) (figure 5.10 **(B)**; excited at 639 nm) confirming ACTH(1-23)C-Atto 647 (furthermore referred to as ACTH(1-23)C-647) and free dye.

5.1.2.2 ACTH(1-23)C-TOTAPOL

In general, an increase of NMR sensitivity can be achieved by the use of Dynamic Nuclear Polarization (DNP)-NMR (see 2.1.1). To avoid quenching effects or loss of excitation due to high distances between the radical and protein of interest, TOTAPOL was conjugated to the ligand. By this the radical can be brought close to the GPCR leading to a specific transfer of magnetization to the protein of interest.

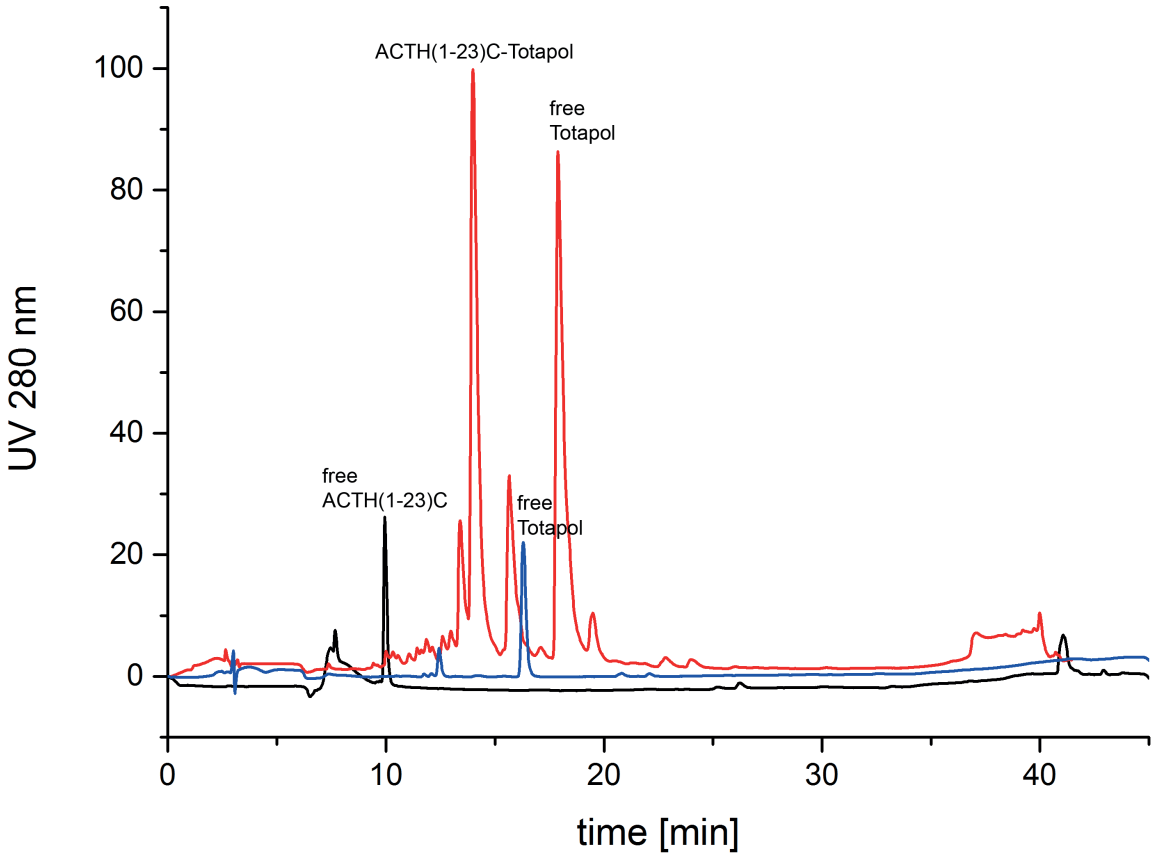

Figure 5.11: ACTH(1-23)C-TOTAPOL purification by RP-HPLC. After conjugation ACTH(1-23)C-TOTAPOL (red) was purified in an AcN / water gradient - eluting at 14-15 min - by RP-HPLC. To distinguish the conjugate from the free peptide and radical, samples of free ACTH(1-23)C (black) and free TOTAPOL (blue) were also subjected to RP-HPLC.

The radical TOTAPOL was conjugated to ACTH(1-23)C (see section 5.1.2.1) and purified by RP-HPLC (figure 5.11) followed by lyophilization. Conjugation was confirmed to be successful by MS (Supplement: chapter 8, section 8.2).

5.1.3 Peptide Characterization

Detection of chemical shift perturbations by NMR can provide information on dynamics of ligand binding processes as well as conformational changes. Peptide ligands of several GPCRs have been found transition from a random coil arrangement to a defined structure upon binding to their receptor [18], [18], [19]. Such structural changes can be observed by comparison of spectra recorded from peptides free in solution to those recorded in their bound conformation. In the following NMR spectra of (isotope labeled) hormones expressed and purified as previously described (4.2) recorded free in solution are reported. These spectra can also serve as a reference for later studies of the hormone-receptor interactions.

Data was recorded for hormones with different length (full length ACTH (1-39) / truncated ACTH (1-23 / 28) and ACTH with an additional cysteine at the *C-terminus* (1-39)C / (1-28)C used for fluorophore conjugation).

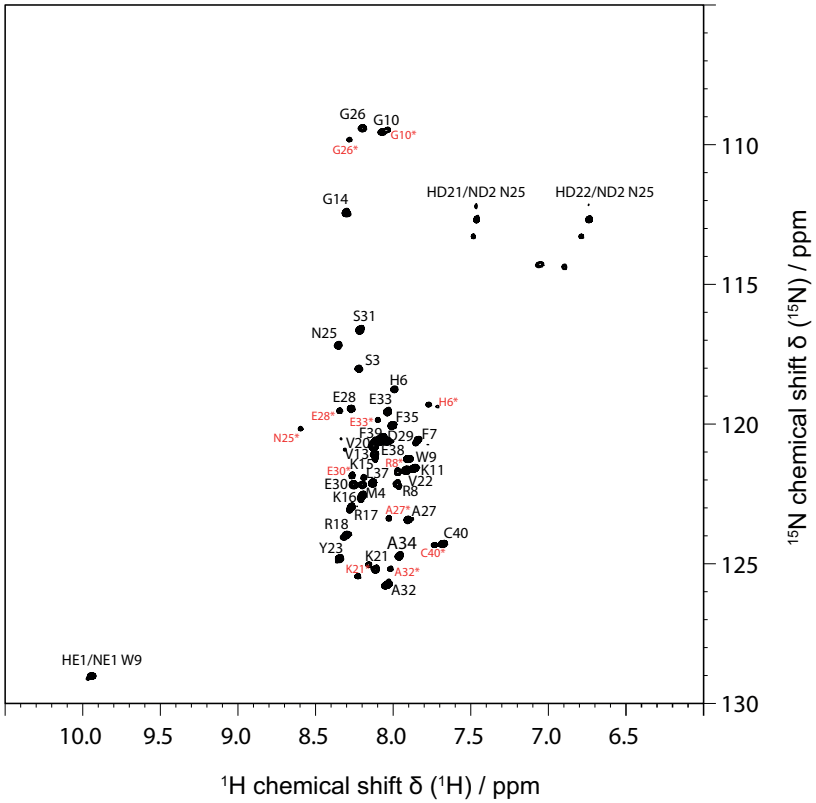

Figure 5.12: Free ACTH(1-39)C. Fully assigned (black) ^{1}H- ^{15}N-HSQC spectrum of 100 µM ACTH(1-39)C at 10 °C in 20 mM NaPi pH 7.0, 50 mM NaCl (Spectrometer: B600-M). Secondary conformations are visible for several residues (red). One cause of these conformations could be the cis- / trans- isomerism of proline (positions 12, 19, 24, 36).

ACTH(1-39)C could be fully assigned (figure 5.12) in a ^{15}N-nitrogen based HSQC. This spectrum shows secondary conformations which for some peaks are possibly resulting from cis and trans isomers of proline (Pro 12,19,24,36) already studied by Gao et al. [51]. The HSCQ spectrum shows that ACTH(1-39)C is unfolded as it displays only a very narrow dispersion of chemical shifts.

The truncated forms of ACTH obtained during an expression of ACTH(1-39)C, i.e. WT ACTH(1-39) and ACTH(1-28) (see section 5.1.1.1), were used to validate if structural features of ACTH vary due to the addition of a C-terminal cysteine (figure 5.13) or truncation (figure 5.14). In the following picture an overlay of ^{13}C-carbon based HSQC spectra comparing ACTH(1-39)C and full-length ACTH, i.e. wilde type (WT)-ACTH, is shown (figure 5.13).

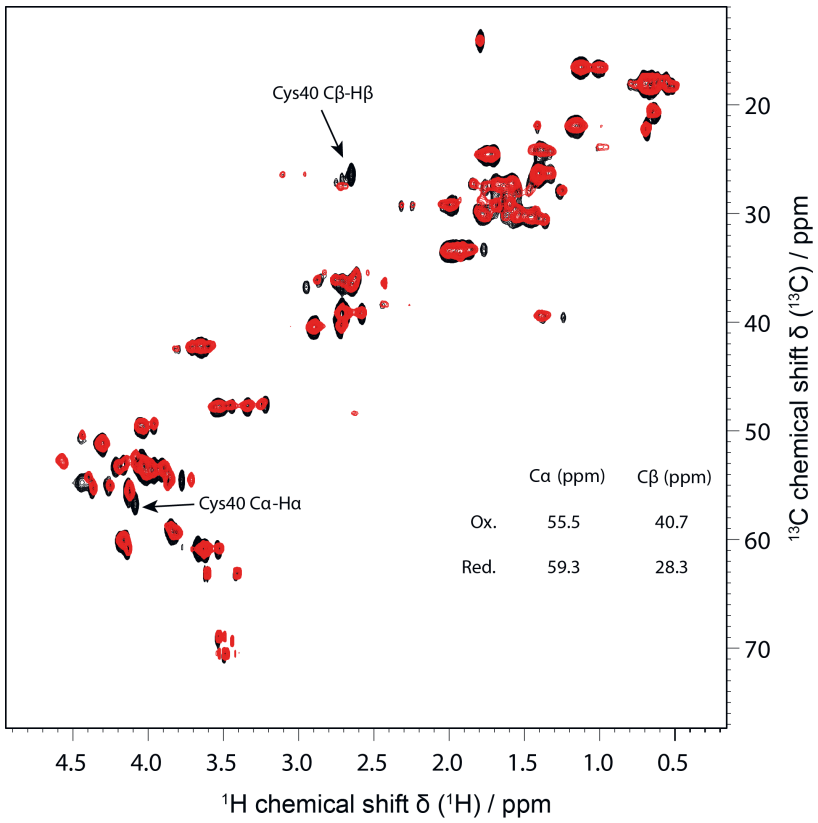

Figure 5.13: Comparison of free ACTH(1-39)C and ACTH(1-39). Overlay of ^{1}H, ^{13}C carbon based spectra of 309 M ACTH(1-39)C (black) and 70 µM ACTH(1-39) (red) recorded at 10 °C in 20 mM NaPi pH 7.0 50 mM NaCl (Spectrometer: B600-M). As indicated by the conserved chemical shifts, structural features of ACTH did not change by addition of a cysteine at position 40. The cysteine was reduced by the use of DTT as seen from the Cβ chemical shift when compared to literature values (for literature values see figure). Size of the molecule was confirmed by MS.

Comparing the spectra of ACTH with and without an additional C-terminal cysteine, no essential changes of structural features are observed. Therefore the ACTH(1-39)C peptide is expected to show no different behavior than ACTH in further ligand binding studies with MC4R. The C-terminal cysteine of ACTH(1-39)C was found to be reduced by DTT as seen from the typical chemical shift of the cysteines (literature values of reduced cysteine: Cα = 59.3 ppm Cβ = 28.3 ppm) showing that no intermolecular dimers were formed under the tested conditions.

An overlay of ACTH(1-39)C (black) and **(A)** the truncated form named ACTH(1-28) (red) or **(B)** ACTH(1-23)C is shown in figure 5.14. As described before (section 5.1.2.1) we produced ACTH truncated to amino acids 1-23 with an additional cysteine at the C-terminus to facilitate a ligand suitable for FA assays when conjugated to a fluorophore.

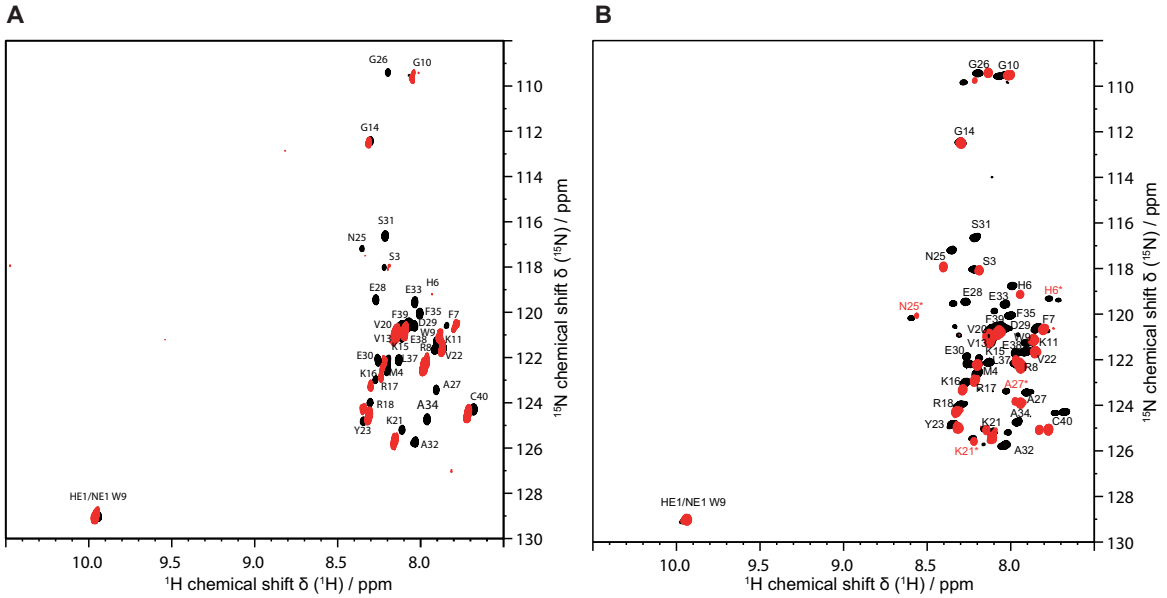

Figure 5.14: Comparison of free ACTH(1-39)C to ACTH(1-28) and ACTH(1-23)C. Overlay of ^{1}H-, ^{15}N-HSQC spectra of **(A)** 309 µM ACTH(1-39)C (black) and ACTH(1-28) (red) and **(B)** 309 µM ACTH(1-39)C (black) and 100 µM ACTH(1-23)C (red). Truncation of ACTH does not lead to essential alterations of its structural features implying that no long range interactions exist in the full-length peptide.

Peaks for amino acids 1 to 28 (figure 5.14, **(A)**) could be assigned by direct comparison to the data from ACTH(1-39)C, confirming the length of the truncated peptide to be ACTH(1-28) (see section 5.1.1.1). This truncation may have been caused by a termination of the translation at position 29 due to a Codon mutation or by enzymatic degradation.

In figure 5.14 peaks of ACTH(1-39)C are displayed in black. Peaks according to the truncated forms ACTH(1-28) and ACTH(1-23)C, depicted in red, show only minor shifts to the comparable amino acids in the sequence of ACTH(1-39)C. This shows that no long range interactions are present in the full-length peptide, which would be indicative for a tertiary structure of the peptide. The observed changes of chemical shifts are caused by the truncated length of the peptides and the C-terminal addition / subtraction of a cysteine, respectively. These modifications slightly change the environment of the amino acids amide groups leading to marginal conformational changes of the hormones.
The rather low shift seen for cysteine after the truncation of the peptide from 40 to 24 amino acids can be explained by the properties of its foregoing amino acids. In both sequences the next to the cysteine possess aromatic side chains (F39 / Y 23) building a comparable environment for the amide group of cysteine.

Furthermore, a 3D structure calculation based on NOE distances (see section 2.1.1.1) did not converge into an ordered structure due to the absence of NOE restrains (see Supplement 8.1, figure 8.5), which is in line with an unfolded peptide.

5.1.3.1 NMR Spectra of Commercial Neuropeptides

To compare structural features of recombinantly expressed peptides to chemically synthesized hormones, NMR data of commercially purchased peptides α-MSH and ACTH were recorded (figure 5.15). In addition the N-terminal amino acid sequence 1-26 of MC4R - shown to maintain the receptors basal activity - was subjected to NMR spectroscopy (Supplement: 8, figure 8.3).
Data obtained from α-MSH and ACTH (figure 5.15) was used for chemical shift comparison to ACTH(1-39)C in the following section 5.1.3.2 (figure 5.16) and in the supplement (figures 8.7 - 8.9).

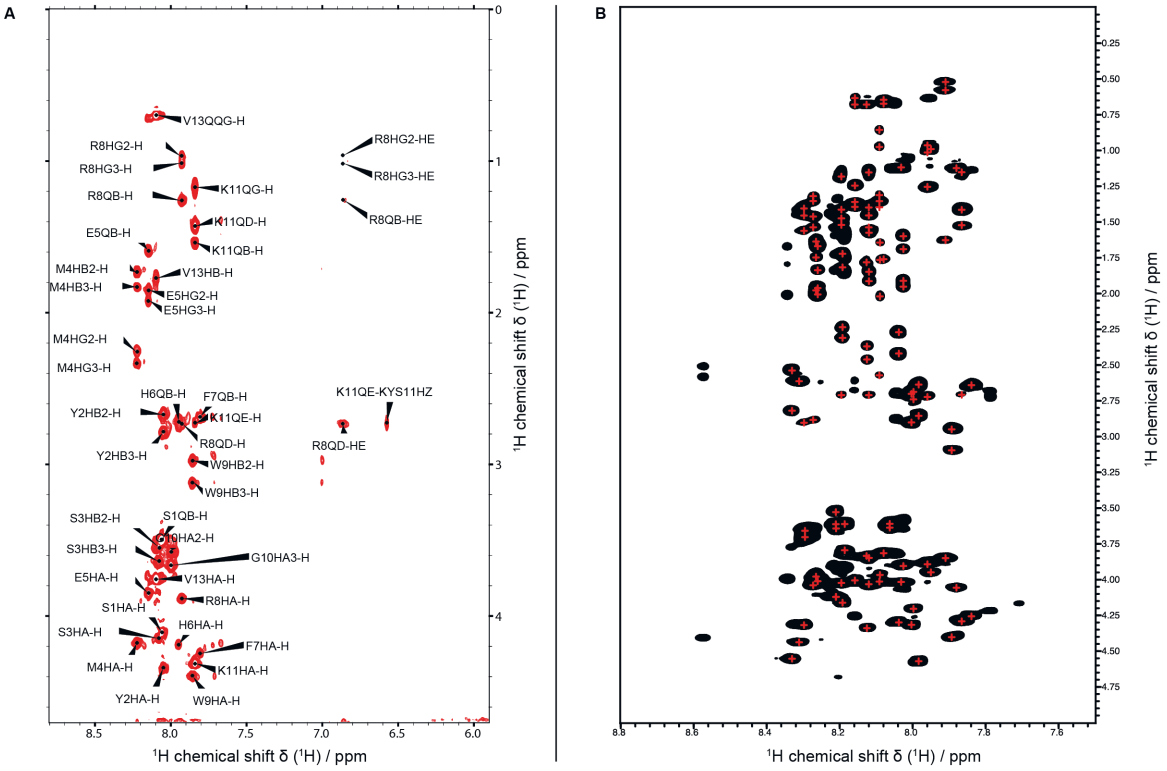

Figure 5.15: Fully assigned TOCSY spectra of commercial α-MSH and ACTH. TOCSY spectra of **(A)** 100 µM α-MSH and **(B)** of 1.1 mM full-length ACTH(1-39) (for proton chemical shifts of marked / assigned peaks see supplement (figures 8.7 - 8.9)). α-MSH was ordered acetylated at the *N-terminus* (Tocris). Peaks of ACTH (AnaSpec) that were not marked belong to secondary conformations of the amino acids

5.1.3.2 Comparison of H^{α} chemical shifts of neuropeptides

In order to verify if structural features of full-length ACTH vary from those of ACTH after addition of a C-terminal cysteine and that of N-terminally acetylated α-MSH, H^{α} chemical shifts for these peptides were compared (figure 5.16).

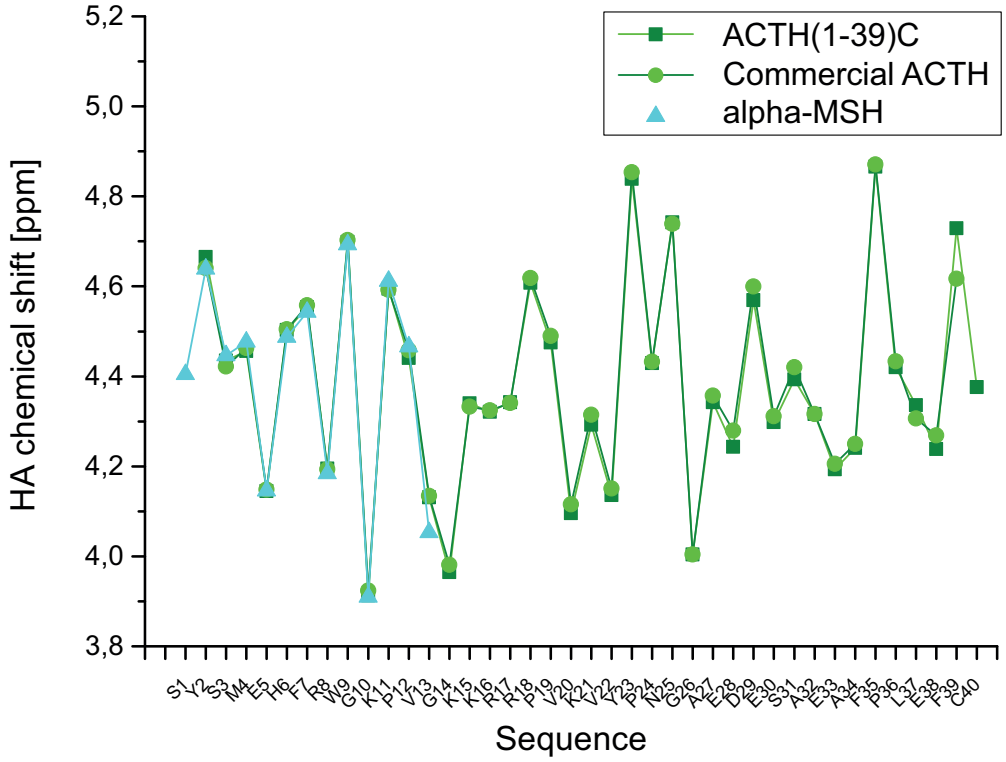

Figure 5.16: Comparison of ACTH(1-39)/Cys and α-MSH chemical shifts. Overlay of H^{α} chemical shifts of ACTH(1-39) and acetylated α-MSH (Tocris) to ACTH(1-39)C.

The data shows that there are essentially no differences between the H^{α} chemical shifts recorded for ACTH (AnaSpec), ACTH(1-39)C and ac-α-MSH (Tocris) (figure 5.16). This shows that the structural features of chemically synthesized WT-ACTH (AnaSpec) and ac-α-MSH (Tocris) - corresponding to ACTH(1-13) - are comparable to those of recombinantly expressed ACTH(1-39)C. Moreover, the data shows that the addition of cysteine to the *N-terminus* of ACTH does not have significant effects on the peptides structural features.

5.2 Melanocortin Receptor 4 Expression

Expression of GPCRs is challenging, as expression systems such as *E. coli* and cell-free expression are limited in the yield of natively folded and functional receptor and in providing post translational modifications. Eukaryotic expression systems such as human embryonic kidney (HEK) cells can provide these modifications. However, HEK 293 cells , when adherently grown, achieve only low protein yields in relation to the incubation space and volume of medium needed.
Therefore, we aimed to establish a stably transfected cell line of HEK 293-F cells. These suspension cells have the advantage of convenient upscaling, thus enabling the production of larger amounts of functional receptor.
Human embryonic kidney HEKs 293 cells were grown semi-adherent (HEKs 293) as well as in suspension (HEKs 293-F) with volumes ranging from 10 ml (petri dish), over 30 ml (shaker flask) to 500 ml (spin flask).
Baran Ersoy (Harvard Medical School) kindly provided MC4R constructs, some of them with a N-terminal signal peptide (prolactin) for optimal membrane incorporation followed by a FLAG-tag for antibody detection in bloting experiments (from here on referred to as SF-MC4R). These constructs were provided on a pcDNA3.1 vector and were previously used for *in-vivo* assays [49].
To increase the protein yield a new MC4R construct was designed by addition of a C-terminal 6-fold histidine tag and the transfer to a pHL-IRES vector. The new vector provides a more moderate promotor thought to increase the receptors membrane incorporation rate while decreasing degradation.
In figure 5.17 protein yields of the expression vectors pcDNA3.1 and pHL-IRES (optimized for GPCR expression) in adherent and suspension cells are compared in a Western Blot normalized by cell number. The pHL-IRES vector was coding for a signal FLAG-tag (SF)-MC4R-6xHis fusion protein while pcDNA 3.1 vector was used for expression of signal FLAG-tag (SF)-MC4R, SF-MC4R(Δ1-24) and MC4R WT (see section 4.3).

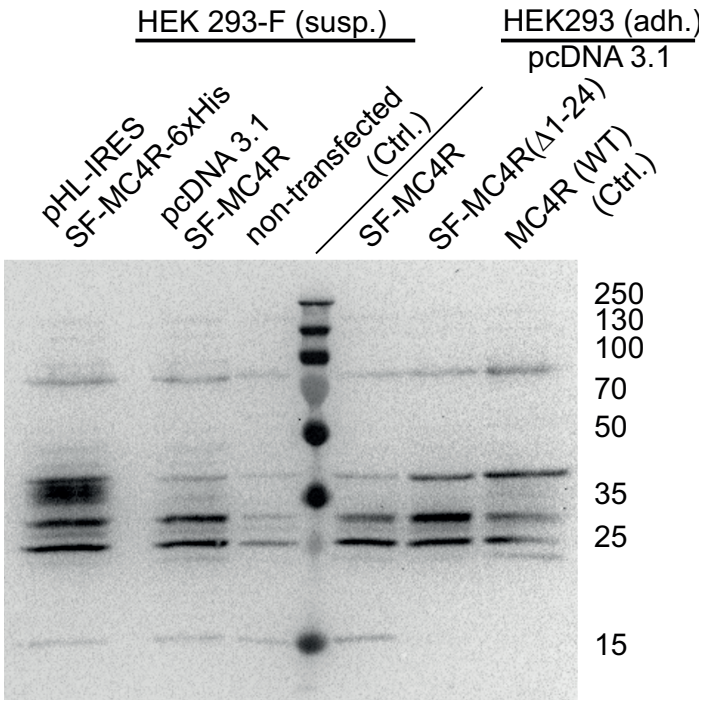

Figure 5.17: Increase of MC4R expression yield by use of pHL-IRES vector. Comparison of expression levels of pHL-IRES-SF-MC4R-6xHis and pcDNA-3.1-SF-MC4R as well as different MC4R constructs (SF-MC4R, SF-MC4R(Δ1-24), MC4R(WT)) shows that only pHL-IRES yields expression levels that can be detected in Western Blot. For detection of the fusion protein an anti-FLAG-tag antibody (Cell Signaling Technologies) was applied as a primary antibody.

While protein concentration was too low for detection in Western Blot when expressed with the pcDNA3.1 vector, the MC4R fusion protein expressed with a pHL-IRES could be detected.

5.2.1 MC4R Activity

Function of a GPCR can be defined, in contrast to ligand binding, by its biological activity, i.e. a conformational change upon ligand binding and C-terminal interaction with G-proteins or arrestins (see 1.1.1.1).
In this work we applied a cyclic-adenosine monophosphate (cAMP) based bioassay (see figure 5.18) to test the activity of the recombinantly expressed receptor and peptides.

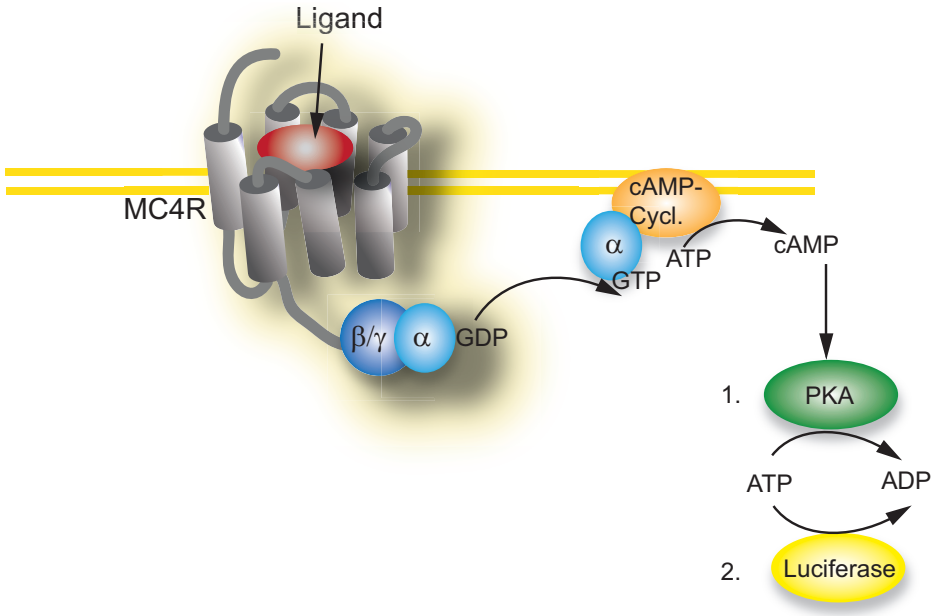

Figure 5.18: cAMP based bioassay. A cAMP based assay was applied to detect down stream activation of MC4R in living, stably transfected HEK 293-F cells, upon ligand binding. Activation of MC4R leads to cAMP-cyclase activity. Accumulated cAMP activates an ATP-dependent protein kinase A (PKA) that is added after cell lysis to the cell lysate. sSubsequently, fter a fixed incubation time, a ATP-dependent luciferase is added. When the GPCR was successfully activated, cAMP mediated activation leads to a decrease of ATP and therefore to a decrease of luminescence.

Upon activation of MC4R, the membrane associated cAMP cyclase is activated by the α-subunit of the GPCR. Stably transfected HEK 293-F cells expressing MC4R were incubated with the ligand previously to cell lysis and addition of protein kinase A (PKA). When the receptor was successfully activated, cAMP is accumulated and activates the ATP-dependent PKA, decreasing the total ATP concentration in the lysate. Finally luciferase, an enzyme generating bioluminescene in the presence of ATP, was added to the mixture. The read out of this assay is the relative luminescence of the luciferase. Therefore, the receptor activity mediated cAMP increase is detected by a decreased luminescence of the luciferase competing for ATP with a cAMP activated protein kinase A (PKA).

To prove down stream activity of recombinantly expressed MC4R, HEK cells were incubated with a serial dilution of commercial α-MSH (figure 5.19).
Biological activity of SF-MC4R-6xHis expressed in HEK293-F suspension cells using a pHL-IRES vector was successfully tested with commercial ligands. The sigmoidal decrease of luminescence in figure 5.19 is dependent on the increasing ligand concentration. The EC_{50} of 0.0039 ± 0.05 nM calculated for α-MSH is unusually low, when compared to literature values (e.g. EC_{50} of α-MSH with MC4R WT ~ 5.67 nM [105]).

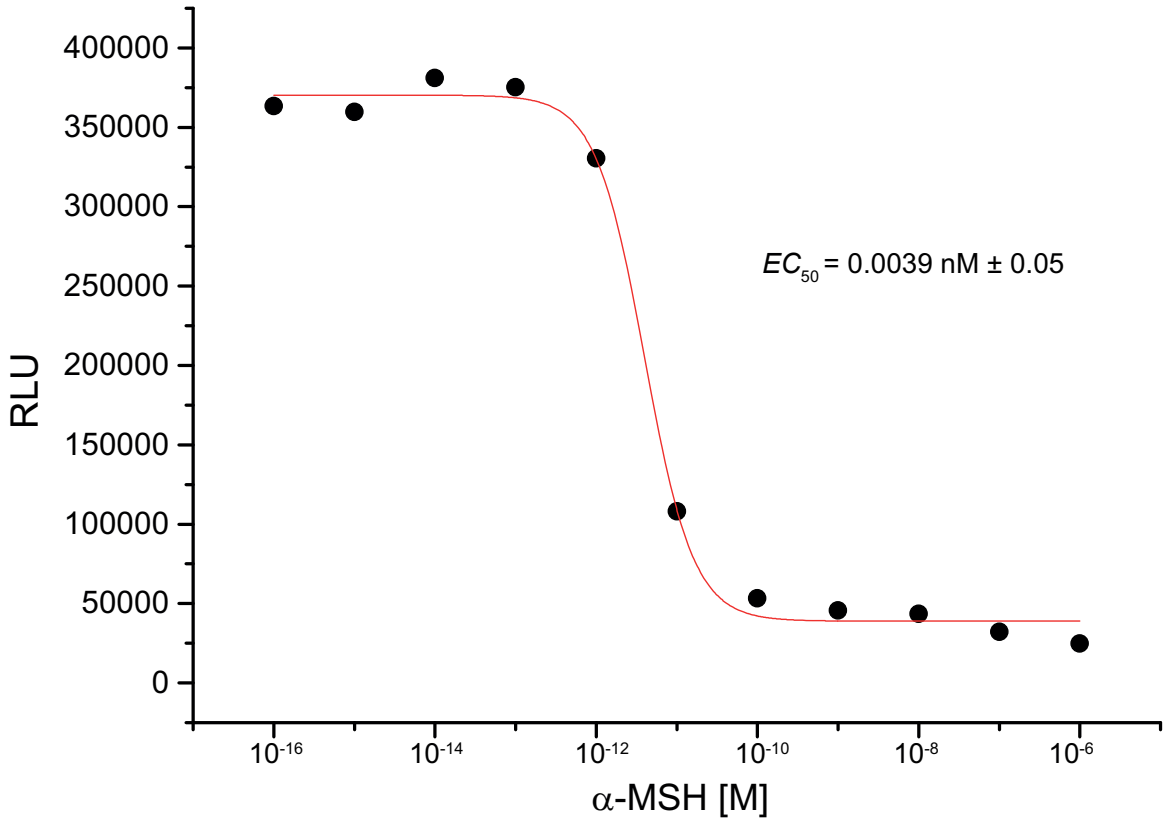

Figure 5.19: Activation of MC4R by α-MSH. Down stream activation of MC4R was recorded in a cAMP-bioassay after incubation of SF-MC4R-6xHis transfected HEK 293-F cells (24,000 / well) with an increasing concentration of α-MSH (ABBIOTEC). An EC_{50} = 0.0039 ± 0.05 nM was calculated (data represent the mean ± standard deviation of n=2). RLU values for the described conditions are displayed as black squares, the corresponding curve fit is shown as a red curve.

In general, the data obtained from this cAMP assay shows large variations in the calculated EC_{50} values (see also Supplement 8, figure 8.19). This can be caused by different factors in the long process of sample preparation and assay performance, but optimization of cell number, cell separation, ligand dilution and ligand incubation times did not lead to a better performance of the assay.
Although calculation of EC_{50} values did not obtain results fully comparable to literature, our data clearly shows that active MC4R was expressed and incorporated into the cell membrane with its ligand binding pocket accessible for the ligand outside the cell.

5.3 Hormone Signaling

5.3.1 Hormone-Receptor Interactions

Ligand binding and receptor exposition in HEK 293-F cells was visualized by fluorescence imaging with ACTH(1-39)C-Cy3B in cell fixation. Cells were incubated with the ligand and washed before fixation with paraformaldehyde (PFA). For Laser Scanning Microscopy (LSM) a laser with a wavelength of 561 nm was used for excitation.

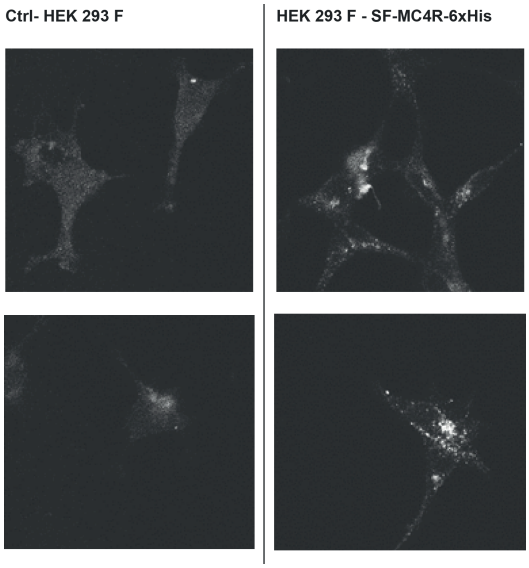

Figure 5.20: Imaging of ACTH(1-39)C-Cy3B bound to MC4R expressing cells. SF-MC4R-6xHis expressing HEK 293-F cells show specific fluorescence in fluorescence imaging after incubation with ACTH(1-39)C-Cy3B. A specific signal of the ligand is observed for transfected cells, non-transfected cells (Ctrl) show only a general fluorescent background. HEK 293F cells were grown semi-adherent on cover slips using serum in the cell medium. Imaging was performed using a 561 nM laser for excitation, HEK 293-F cells were transfected with pHL-IRES-SF-MC4R-6xHis.

Figure 5.20 shows specific binding of the dye conjugated ligand for HEK 293-F cells transfected with pHL-IRES-SF-MC4R-6xHis, a pHL-IRES vector coding for a MC4R fusion protein with a N-terminal prolactin (signalpeptide) / FLAG-tag and a C-terminal 6xHistidine-tag. Non-transfected cells were also treated with the ligand as negative control and do not show any specific fluorescence of ACTH(1-39)C-Cy3B. This implies, that the receptor was accessible for ACTH(1-39)C-Cy3B and that the

binding pocket was therefore exposed on the outer cell membrane. The images do not allow to determine the concrete localization of the peptide, they how ever would be consistent with a partial localization at the cell membrane and a partial internalized after receptor activation.

To validate the activity of peptides expressed, purified and modified as described in chapter 4 and section 5.1.2 we also tested them in a cAMP based assay (figure 5.21, for a scheme of the assay see figure 5.18). Additionally the commercial ligands NDP-α-MSH (Tocris) and α-MSH-Rhodamine (Phoenix Pharmaceuticals INC.) were subjected to this assay.

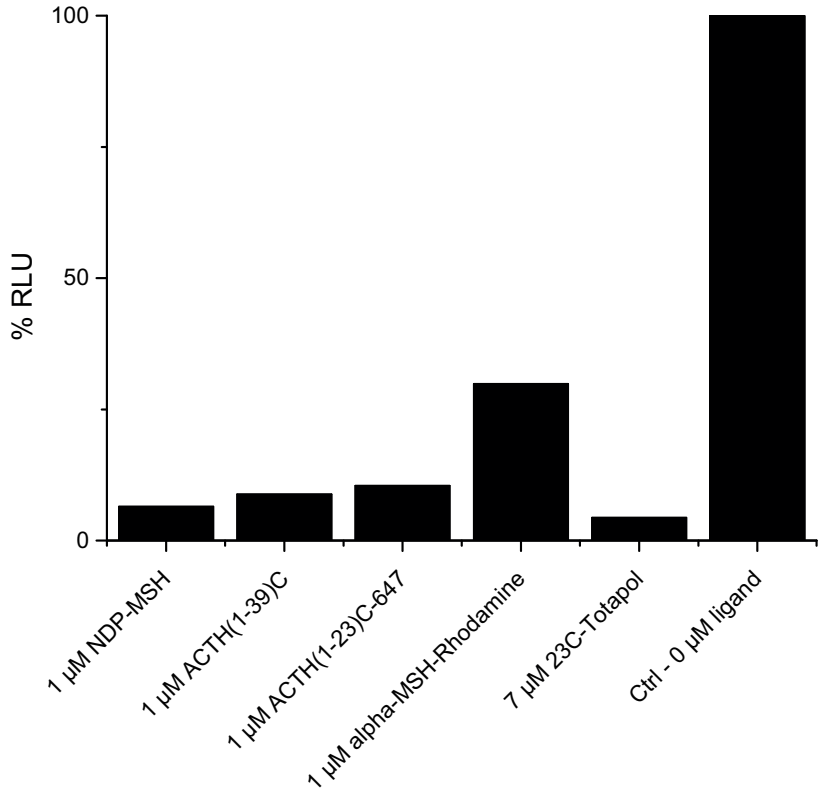

Figure 5.21: Peptide mediated activation of MC4R. Commercial - NDP-α-MSH, α-MSH-Rhodamine - and recombinantly expressed ACTH(1-39)C, as well as modified synthesized ACTH(1-23)C (Atto 647 / TOTAPOL) were tested for activation of MC4R. Receptor activity is displayed by the decrease of relative luminescence (RLU) in % (100% = 0 µM ligand (Ctrl.), e.g. no activation).

Activation of MC4R is observed for all peptides as seen by the decrease of luminescence (figure 5.21). Receptor activity is displayed in percentage of relative luminescence (RLU) with values normalized to the basal level of luminescence of non-treated cells (100% = no ligand (Ctrl.)). Hormone activity was not inhibited, neither by addition of cysteine to the C-terminus of ACTH nor by conjugation of Atto 647 to ACTH(1-23)C. All tested ligands were able to drive receptor activity in a way comparable to the

commercial ligand NDP-α-MSH, which is often used for MC4R ligand binding studies in literature and hence serves as a positive control.
Furthermore, ACTH mediated MC4R activity is strongly decreased in the presence of a 10-fold excess of SHU 9119, a synthetic antagonist of MC4R (see Supplement 8.3, figure 8.20). To exclude an unspecific decrease of luminescence, i.e. not mediated by specific MC4R activation, possibly caused by incubation of the cells with peptide ligands, non-transfected HEK 293-F cell were also treated with 1 muM ligand (ACTH, [Nle 4, D-Phe 7]-α-MSH (NDP-α-MSH)). A decrease of the relative luminescence is only observed for MC4R expressing cells after treatment with ligands (see Supplement 8.3, figure 8.21).

5.3.2 Hormone-Membrane Interaction

To study structure and dynamics of hormone-receptor interactions in NMR, it is essential to find suitable membrane mimetics. On the one hand they need to sufficiently stabilize the GPCR and on the other hand they should represent the most native physiological condition that can be mimicked *in vitro*. For NMR-based structural studies the environment of a membrane protein should not only maintain its native structure and activity but also meet the requirements of the experimental setup, e.g. size restrictions in solution-state NMR. Often detergents are used for membrane mimicking in GPCR purification, especially n-Dodecyl β-D-maltoside (DDM) is commonly applied [106], [18], [23]. However, the performance of ligand binding studies can be disturbed by unspecific interaction of the hormone with the membrane mimetic and binding of ACTH to SDS and DPC micelles was already reported before [107], [51].

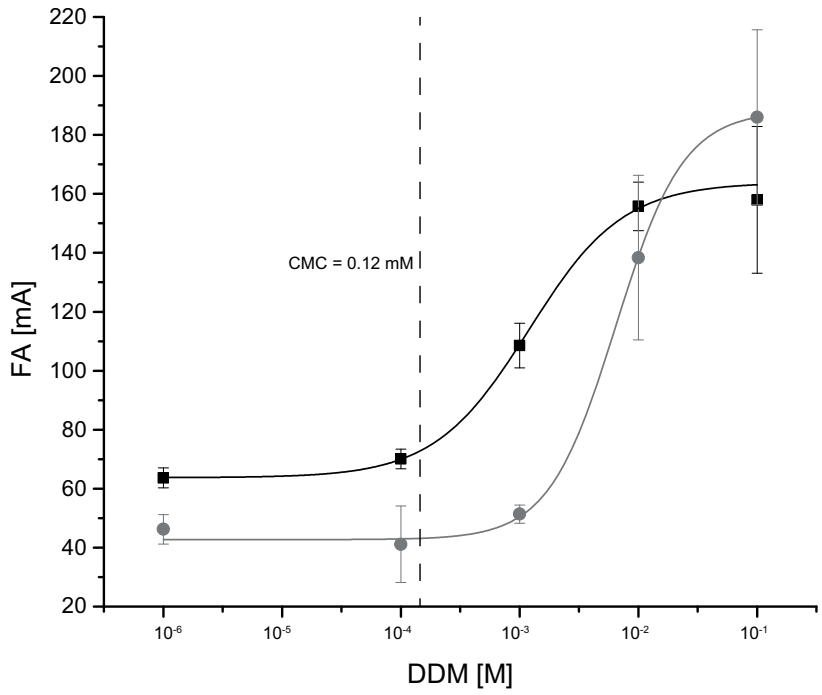

Figure 5.22: Peptide interaction with DDM micelles. FA values and fits for the interaction of 40 nM ACTH(1-23)C-647 (28 °C) and 40 nM α-MSH-Rhodamine (26 °C) with 100 to 0.001 mM DDM are displayed in black / gray. An increase of FA is observed when exceeding the CMC of DDM indicated by the dashed line (0.12-0.17 mM). A K_d = 1.19 ± 0.13 mM for ACTH(1-23)C-647 and a K_d = 6.5 ± 1.5 mM for α-MSH-Rhodamine was calculated (data represent the mean ± standard deviation of n=3).

To test whether this is also the case for DDM α-MSH and ACTH(1-23)C-647 as well as ^{15}N labeled ACTH(1-39)C were studied in presence of DDM micelles using a FA based ligand binding assay and NMR spectroscopy (figure 5.22, 5.23).
These fluorescene anisotropy experiments (figure 5.22) show interaction of ACTH(1-23)C-647 and α-MSH-Rhodamine (Phoenix Peptides INC.) with DDM micelles. The increase of FA values is observed after exceeding the critical micelle concentration (CMC) (0.12-0.17 mM). A K_d = 1.19 ± 0.13 mM for ACTH(1-23)C-647 and a K_d = 6.5 ± 1.5 mM for α-MSH-Rhodamine was calculated (data represent the mean ± standard deviation of n=3).
This data suggests that the use of DDM for receptor purification and stabilization may be problematic for the setup of FA-based ligand binding assays.

To exclude artifacts probably caused by unspecific interaction of the dye with detergent micelles NMR spectroscopy was performed with ^{15}N-labeled ACTH(1-39)C in presence of 150 mM DDM. By this we also aimed to obtain residue specific information and to decipher the binding mode of ACTH(1-39)C-micelle interaction.
Figure 5.23 displays the residue specific volume ratio of all resolved peaks in a ^{1}H-,^{15}N-HSQC NMR spectrum, of detergent micelle interacting ^{15}N-ACTH and free peptide.

Ligand interaction leads to a line broadening, i.e. a decrease of detectable peak volumes. The ratio of peak volumes from bound (decreased volume) to free peptide (reference volume) can therefore be used as a measure for ligand interaction giving residue specific information. Data of ^{15}N-ACTH in the presence of DDM micelles reveals a N- and C-terminal interaction of ACTH with DDM micelles.

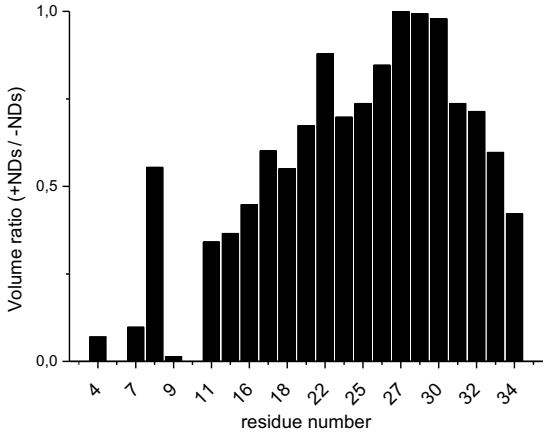

Figure 5.23: ^{15}N ACTH interaction with DDM micelles. The volume ratio of 40 µM bound to free ^{15}N ACTH(1-39)C shows N- and C-terminal interaction with DDM micelles (150 mM DDM).

Furthermore, hormone-detergent interaction may not only interfere with ligand binding studies, but also cause artificial conformational changes of the peptide due to the round shape of detergent micelles, strongly differing from the planar surface of cell membranes.
To understand the native environment of the neuropeptide, it makes sense to have a look at the peptides natural life cycle. In general neuropeptides are processed from precursor proteins. These precursors are translated at the endoplasmatic reticulum before post translational modifications are performed in the Golgi apparatus. Finally tissue specific convertases process the precursor protein POMC during its vesicular transport to the synapse where neuropeptide release is triggered by an arriving action potential, leading to calcium influx (see section 1.1.4.5). During this process membrane environments surrounding the peptides vary by their lipid composition. In addition the lipid composition of the post synaptic membrane hosting the receptor may also have an impact on the stability of the receptor and possibly on ligand binding.

Nanodiscs become more and more popular providing a lipid bilayer with a natural surface shape and a native-like lipid composition. ND lipid content can be varied to meet physiological conditions for example by the lipid type or the ratio of charged and neutral lipids incorporated.
To study the impact of different lipid compositions on ACTH, FA measurements were performed with NDs comprised of an increasing amount of negative charged lipids. For ND assembly membrane scaffold protein (MSP1D1) was mixed with neutral charged lipids - Palmitoyloleoylphosphatidylcholine (POPC) - and lipids carrying a negative net charge - 1-Palmitoyl-2-oleoylphosphatidylserine 1-Palmitoyl-2-oleoylphosphatidylserine (POPS). Figure 5.24 shows FA values of ACTH(1-23)C-647 in presence of NDs comprising 100% POPC, 30% POPS / 70% POPC and 50% POPS / 50% POPC.

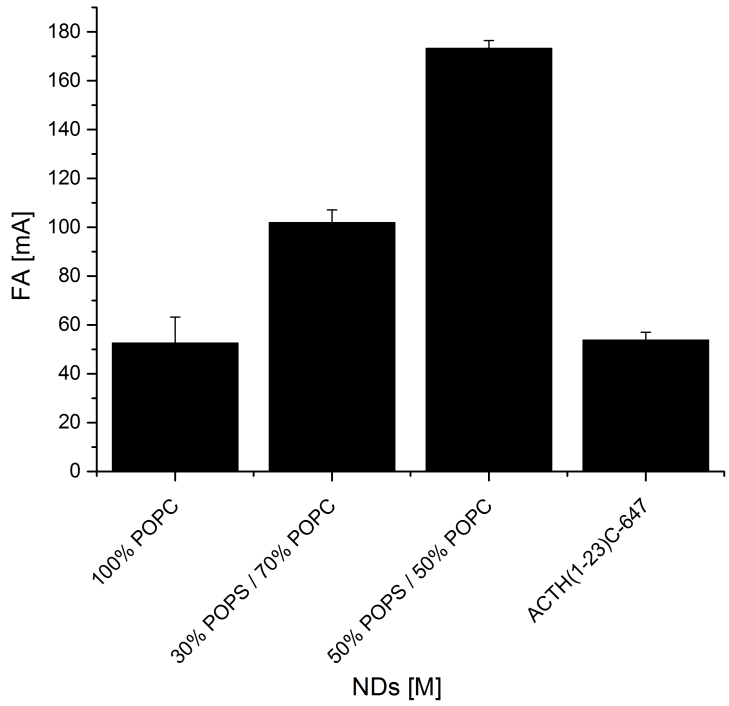

Figure 5.24: Charge driven interaction of ACTH(1-23)C-647 to NDs. FA values of 40 nM ACTH(1-23)C-647 at 29 °C in the presence of 400 nM NDs comprised of the indicated lipid compositions.

Fluorescence anisotropy values of ACTH(1-23)C-647 in presence of 100% neutral charged lipids (POPC) are in the range of the free peptide. Polarization is higher for NDs with 50% POPS than with 30%, showing that peptide binding affinities correlate with the percentage of negative charged lipids. Our data clearly shows that the interaction of ACTH(1-23)C-647 with NDs is driven by the negative charge the lipids. And no binding can be detected for NDs without negative charge. The latter

also confirms that the ligand does not interact with the membrane scaffold protein of the NDs.

To further study hormone association in more detail, data on hormone-membrane interaction was recorded by NMR. Figure 5.3.2 shows the volume ratio of ^{15}N-ACTH(1-39)C peaks in presence of NDs to free ACTH. NDs with an increasing negative charge and different types of lipids (POPS / POPC; DMPG / DMPC) were studied. The anionic 1,2-dimyristoyl-sn-glycero-3-phosphoglycerol (DMPG) and the neutral charged 1,2-Dimyristoyl-sn-glycero-3-phosphocholine (DMPC) alter from POPS / POPC by a smaller headgroup, smaller chain length, the absence of an unsaturation in the fatty acids and a higher temperature of phase transition. ND comprising DMPC and DMPG are commonly used in the field of NMR spectroscopy, but to increase the physiological relevance of our studies we decided to additionally use NDs comprised of two of the major structural lipids in eukaryotic membranes, i.e. POPC and POPS.
For a better comparison also the data on peptide detergent interaction as discussed above (figure 5.22) is displayed again **(D)**. Note that the reference spectrum of free ACTH and the data of ACTH in the presence of POPS / POPC NDs was recorded at the Bruker 600 MHz. Data on NDs comprised of DMPG / DMPC lipids was recorded a 700 MHz spectrometer. Therefore no quantitative conclusions about the difference of the interaction strength of POPS / POC compared to DPMG / DMPC NDs can be drawn from these data.

Data is displayed as normalized volume ratio of bound to free ACTH. While almost no interaction can be observed for ACTH with only neutral head groups (A), amino acids around 1-13 show interaction when 30% negatively charged lipids are present (B + E). An increasing interaction surface is found when 50% of the lipids have a negative head group, showing strong binding for N-terminal residues (roughly 1-16) and weaker binding for amino acids up to position 27.

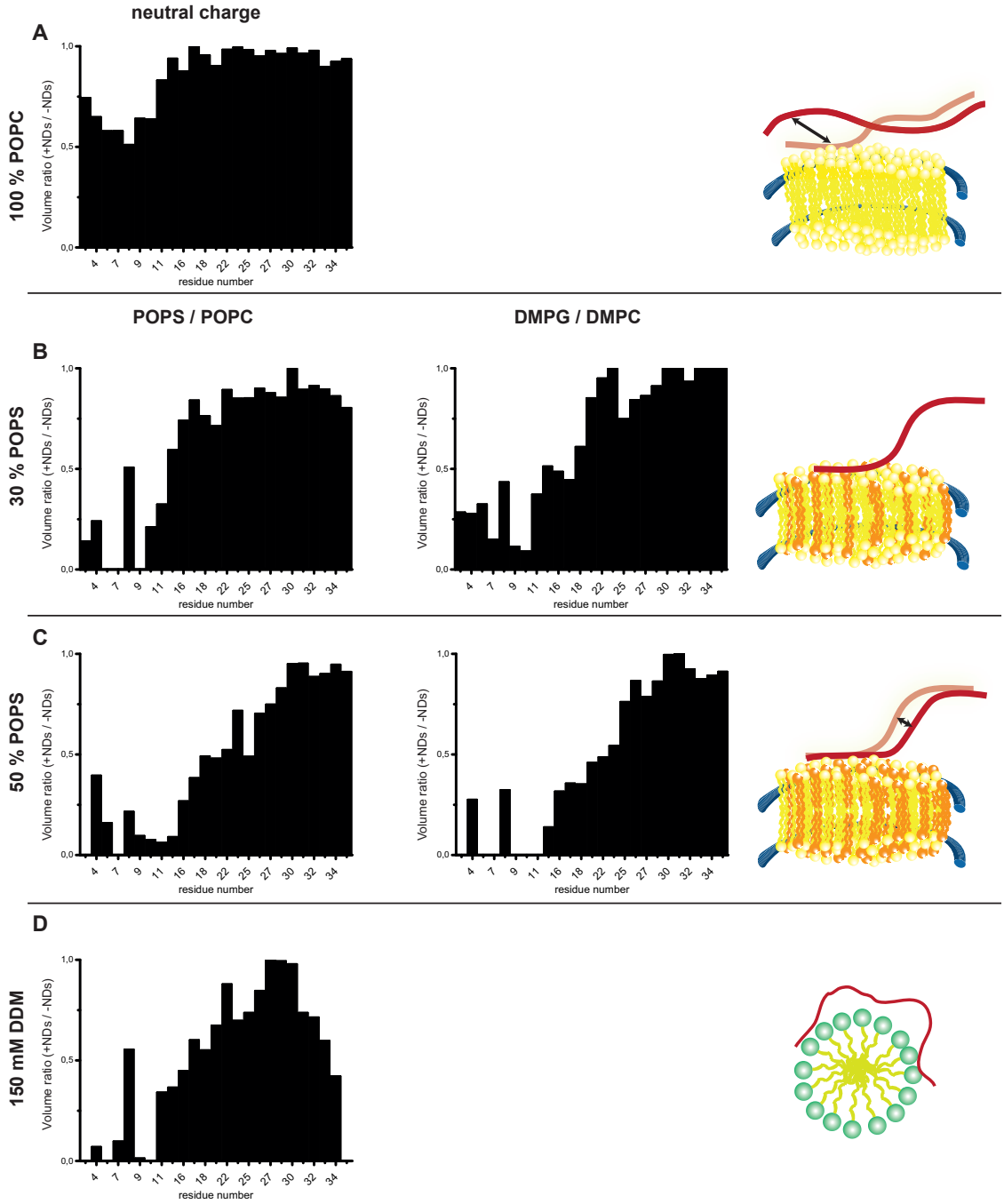

Figure 5.25: ACTH interacts with membrane mimetics. 20 µM nanodiscs with (A) 100% POPC, (B) 70% POPC / 30% POPS and 50% POPC / 50% POPS, (C) 70% DMPC / 30% DMPG and 50% DMPC / 50% DMPG or (D) 150 mM DDM with 40 µM ^{15}N-ACTH(1-39)C in 20 mM NaPi pH 7.0, 50 mM NaCl. Spectra were recorded at 10 °C using a Bruker 600 MHz spectrometer for free ACTH and with POS / POC NDs or a 700 MHz spectrometer for DMPG / DMPC NDs.

This data also implies that the dye conjugated ligand designed for FA-based assays, applied in figure 5.24, is suitable for its purpose, when the peptides *N-terminus* strongly

interacts with its binding partner, while its core and C-terminal region shows a weaker or no binding affinity.

Over all these findings suggest, that NMR studies of MC4R ligand binding could be performed using NDs with neutral head groups. In this way interactions of the hormones with membrane mimetics causing increased background noise can be avoided. However usage of lipids with only neutral head groups is not fully comparable to physiological conditions. In particular the charged lipid phosphatidylserine (PS) is often found in eukaryotic membranes [63].

Due to the disappearance of NMR signals of bound peptide residues no structural insights could be obtained for the lipid-bound conformation. Data recorded on α-synuclein [108] showed a conformational change of the proteins N-terminus from random coiled to α-helical upon lipid interaction. A small region at the N-terminus of ACTH was discussed to show a tendency to adopt a α-helical structure [53] and it was found to adopt this structure in the presence of trifluoroethanol (TFE) [54]. These findings raised the discussion if a α-helical structure of the *N-terminus* of ACTH could also be induced by the hormones interaction with receptors or membrane lipids (for a review see [52]. Further NMR based studies as presented above could possibly reveal if this is true for the interaction with anionic lipids.
A structural transition of the N-terminal sequence could be part of the hormones binding process to its receptor, adopting a conformation for optimal thermodynamic and kinetic binding conditions and activation [22], [109].
Nevertheless, cyclization of α-melanotropins fragment analouges between position 4-10 was shown to produce a hexapeptide with prolonged and increased agonist activity (90-100 times more potent) [20], [21], implying that a β-turn between these position is essential for receptor activation [56]. Thus adaption of a N-terminal α-helical structure would not be conclusive in terms of hormone-receptor interaction. For better understanding of details underlying hormone-membrane interactions further experiments need to be performed with varying parameters such as pH, type of ions and lipids or ionic strength.

5.3.2.1 Hormone-Membrane Interaction in the Presence of Calcium

Noteworthy, our findings could suggest that ACTH in native lipid composition is not released from the membrane after fusion of the transport vesicle at the synaptic cleft. The fusion of neuropeptide vesicles is triggered by influx of calcium upon an action potential reaching the synapse. Excitation at the post-synaptic membrane by neurotransmitters and neuropeptides furthermore leads to an opening of calcium channels. Therefore the extracellular and intracellular calcium concentrations are frequently changing. Since our data point to a charge driven interaction of ACTH with membrane mimetics, we studied these with respect to the role of varying calcium concentrations.

As high concentrations of calcium chloride in phosphate buffers lead to precipitation of calcium phosphate, NaPi buffer had to be exchanged for the following experiments. To ensure that changing 20 mM NaPi pH 7.0 to 20 mM HEPES with a physiologcal pH (pH 7.4) does not influence structural features of the peptide or hormone-membrane interaction further NMR and FA data was recorded.
Comparison of 40 µM ^{15}N-ACTH(1-39)C in 20 mM NaPi pH 7.0, 50 mM NaCl and ^{15}N-ACTH 30 µM 10 mM HEPES pH 7.4, 50 mM NaCl (figure 5.27) does not show essential changes of ACTH structural features. However, peaks of S3, F7, G10 can not be detected in HEPES buffer pH 7.4 and K16, R17, R18 show only low intensities. This is in line with an increased ^{1}H-exchange caused by the pH shift from pH 7.0 in NaPi to pH 7.4 in HEPES. Therefore the data has only limited information content on the N-terminal peptide sequence 1-18 binding to NDs. However high sensitivity can be seen for amino acids 21 and higher. The loss in peak intensities is caused by an increased exchange rate of amide protons with water due to the higher pH. This exchange runs on the time scale of the NMR experiment leading to a decreased signal intensity.

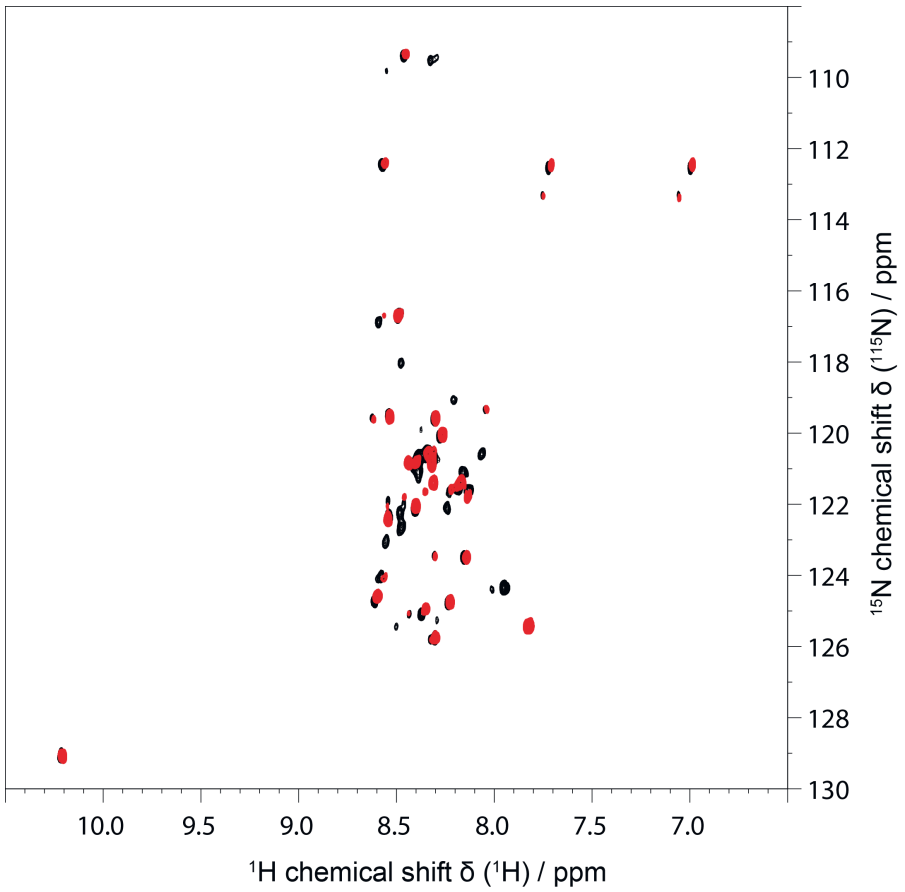

Figure 5.26: Higher pH of HEPES buffer effects ACTH N-terminal residues. Overlay of ^{1}H-, ^{15}N-HSQC spectra of 40 µM ^{15}N ACTH(1-39)C in 20 mM NaPi pH 7.0, 50 mM NaCl (black) and 40 µM ^{15}N ACTH in 10 mM HEPES pH 7.4, 50 mM NaCl red at 10 °C. Spectra do not show essential differences in the structural features of the peptide. But as a result of increased ^{1}H-exchange rates at high pH residues S3, F7, G10 can not be detected and K16, R17, R18 show only low intensities in HEPES buffer.

FA measurements comparing peptide-ND interaction in NaPi and HEPES buffer were performed with 100 nM ACTH(1-23)C-647 in presence of decreasing 30% POPS / 70% POPC or 50% POPS / 50% POPC ND concentrations (figure 5.27).
Comparison of hormone-membrane binding in the different buffers shows even stronger binding of ACTH(1-23)C-647 to NDs with negative charged lipids when using HEPES pH 7.4. K_d-values for ACTH interaction with 50% POPC NDs dropped from 104 ± 6 nM to 52 ± 1 nM and with 30% POPS NDs from 360 ± 18.7 nM to 150 ± 7.6 nM. Note that the calculated K_d values represent the dissociation constant of the hormone interaction with NDs and not with single lipids (i.e. ∼ 132 lipids in total with 30% or 50% charged lipids).

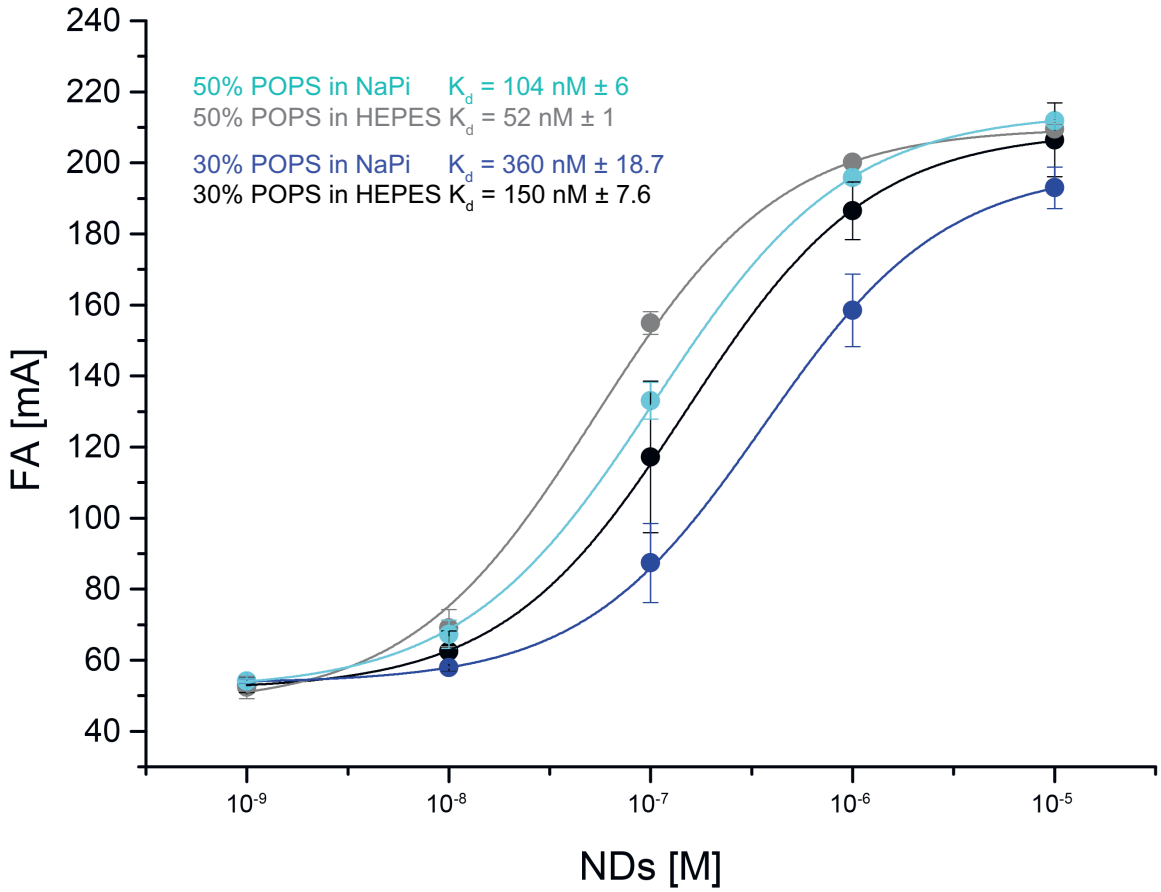

Figure 5.27: ACTH interaction with NDs in NaPi vs. HEPES buffer. FA values and fits for the interaction of 100 nM ACTH(1-23)C-647 with 10 to 0.001 µM M nanodiscs with 30% POPS / 70% POPC black / blue) and POPC 50% POPS / 50% POPC (gray / cyan) respectively in 20 mM NaPi pH 7.0, 50 mM NaCl (blue / cyan) compared to 20 mM HEPES pH 7.4, 50 mM NaCl (black / gray) at 26 °C are displayed as indicated. K_ds of 104 ± 6 nM / 52 ± 1 nM for 50% POPS and of 360 ± 18.2 nM / 150 ± 7.6 nM for 30% POPS NDs in NaPi / HEPES buffer were calculated (data represent the mean ± standard deviation of n=3).

To test whether the used dye (Atto 647) interacts with the lipids ACTH(1-23)C-647 and Atto-647 dye (each 40 nM) were studied by FA using increasing ND concentrations (figure 5.28).

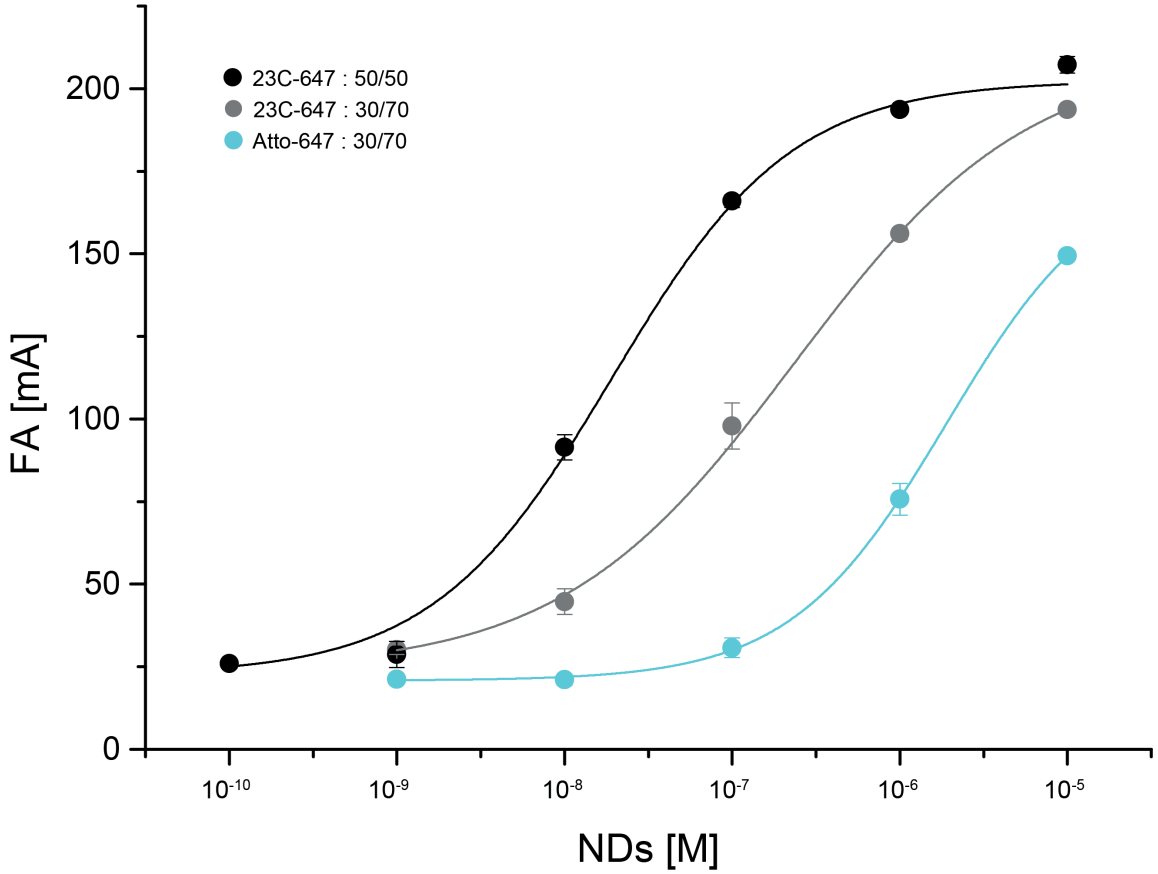

Figure 5.28: Weak interaction of Atto 647 to NDs. FA values and fits comparing the interaction of ACTH(1-23)C-647 (40 nM) in 10 mM HEPES pH 7.4, 50 mM NaCl with increasing concentrations of NDs comprised of POPC 50% POPS / 50% POPC (black) or 30% POPS / 70% POPC (gray) to that of Atto-647 dye (cyan) with 30% POPS / 70% POPC NDs at 26 °C are displayed as indicated. A weak interaction of the dye is observed.

While strong interactions in the middle nM-range are found for ACTH(1-23)C-647 with negatively charged NDs (30% POPS / 70% POPC, POPC 50% POPS / 50% POPC) a weak interaction of Atto 647 dye and NDs with 30% negative charge (30% POPS / 70% POPC) in the µM-range is observed. This implies that unspecific interaction of ACTH(1-23)C-647 can be partly but not completely driven by the conjugated dye.

The impact of varying calcium concentrations on the peptide-membrane interaction was studied by FA. Figure 5.29 displays 100 nM ACTH(1-23)C-647 in presence of increasing calcium concentrations with and without NDs (30% POPS / 70% and POPC 50% POPS / 50% POPC). The total net charge of the buffer was maintained by adjusting Na^+ concentrations.

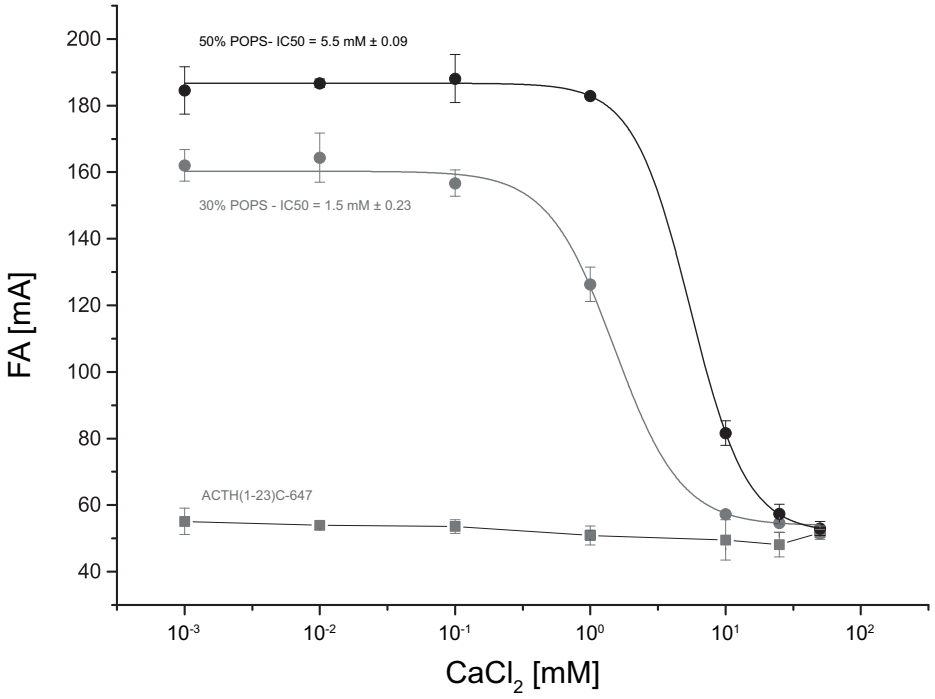

Figure 5.29: High calcium concentrations inhibit ACTH interaction with NDs. FA values and fits for the interaction of 100 nM ACTH(1-23)C-647 with 500 nM nanodiscs comprised of 50% POPS (black) and 30% POPS (gray), respectively, in presence of increasing $CaCl_2$ concentrations but stable net charge at 28 °C are displayed as indicated. The FA values decrease with increasing $CaCl_2$ concentrations when 0.1 mM / 1 mM calcium is exceeded and reach the baseline at concentrations higher than 25 mM / 50 mM for NDs comprised of 30% / 50% POPS. FA values recorded for ACTH in the presence of increasing $CaCl_2$ concentrations without NDs do not show an increase and therefore no interaction was observed for ACTH and Ca^{2+} in this assay. An half maximal inhibitory concentration (IC_{50}) of 5.5 ± 0.09 mM or 1.5 ± 0.23 mM was calculated for NDs comprised of 50% or 30% POPS, respectively.

While calcium alone does not alter fluorescence polarization of ACTH(1-23)C-647, a signal increase can be observed in presence of NDs with negative charge and a calcium concentration lower than 25 mM (50% POPS / 50% POPC) or 10 mM (30% POPS / 70% POPC). The binding curve of ACTH and NDs with 50% negatively charged lipids stays at up to 1 mM Ca^{2+} while NDs with only 30% negative charge are already effected at ∼ 0.5 mM Ca^{2+}. These findings are in line with the previous results showing that the strength of peptide binding to NDs is charge driven and less calcium is required to interrupt the weaker binding to NDs with less negative charge. To avoid interruption of the hormone-lipid interaction, due to an increased positive charge shielding the negative head groups, the titration was performed maintaining the total net charge of the buffer. This was achieved by decreasing the Na^+ concentration two-fold when increasing the Ca^{2+} concentration.

Furthermore the kinetic of calcium-induced ACTH release from nanodisc was studied (figure 5.30). Calcium chloride (10 mM) was added to ACTH(1-23)C-647 and Atto 647 interacting with 30% POPS / 70% or 50% POPS / 50% POPC ND in 20 mM HEPES, 50 mM NaCl buffer (figure 5.30). Time-dependent FA values at different ND ratios were recorded for 90 min measuring every 15 minutes.

A decrease of FA can be observed with ACTH(1-23)C-647 for all nanodisc concentrations directly after addition of 10 mM calcium chloride. By contrast unspecific interaction of free dye (Atto 647) was not influenced by the addition of calcium (figure 5.30). This shows on the one hand that the decrease of FA upon addition of 10 mM $CaCl_2$ is specific for the hormone-lipid interaction (not for the dye). On the other hand the data shows that the decrease is not by to a destructive effect of Ca^{2+} on the NDs, which would also be visible for free dye. Therefore we suggest that Ca^{2+} does have a modulating effect on the interaction of ACTH with negative charged lipids. This could be through competitive (steric) or electrostatic shielding effects of Ca^{2+} on the negative charged lipids or by interaction of the peptide with Ca^{2+}.

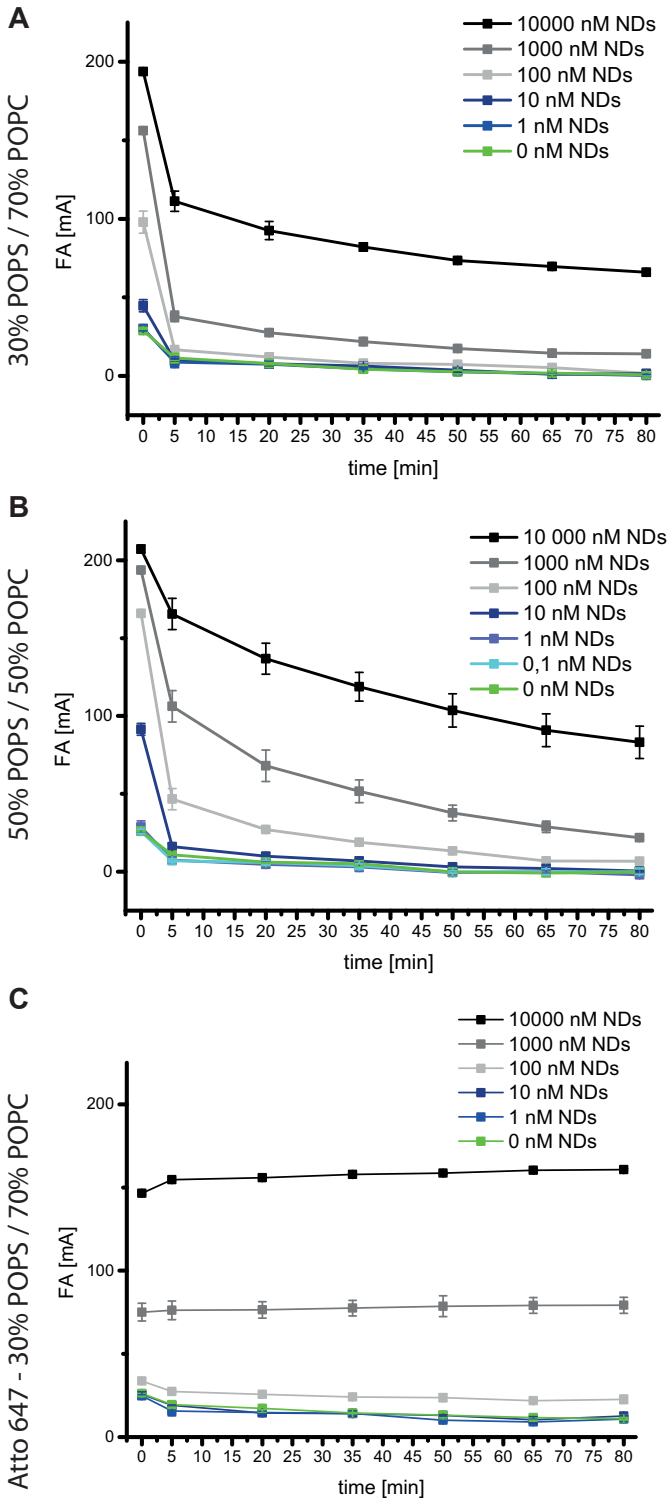

Figure 5.30: Time-dependent, calcium mediated release of ACTH from NDs. Hormone-membrane interaction is disrupted upon addition of 10 mM $CaCl_2$. FA vales and fits are displayed as indicated for 40 nM ACTH(1-23)C-647 with 1 nM to 10 µM NDs of **(A)** 30% POPS / 70% and 10 µM to 0.1 nM **(B)** 50% POPS / 50% POPC lipid content at 28 °C. **(C)** Calcium does not influence unspecific interaction of free dye (Atto 647) with NDs (30% POPS / 70% POPS).

The effect of calcium on the charge driven interaction of ACTH and ND was also studied by NMR (figures 5.31, 5.33, 5.34). These experiments were performed to gain residue specific information on ACTH in presence of Ca^{2+} and / or nanodiscs and to further exclude effects of the dye.

Interaction of ^{15}N ACTH and nanodiscs with varying negative charge was studied by NMR in presence of an increasing $CaCl_2$ concentrations (figure 5.31). NaCl concentrations were adjusted to $CaCl_2$ concentrations to maintain the total net charge of the buffer. NDs comprised a lipid content of 100% POPC, 30% POPS / 70% POPC or 50% POPS / 50% POPC. Figure 5.31 part **(A)** and **(B)** show overlays of ^{1}H- ^{15}N HSQC spectral segments (zoom) of ACTH (black), with NDs (red) and with NDs and Ca^{2+} (green / yellow) as well as ACTH in presence of 10 mM $CaCl_2$ (blue). For the complete spectra see supplement 2.1.1.

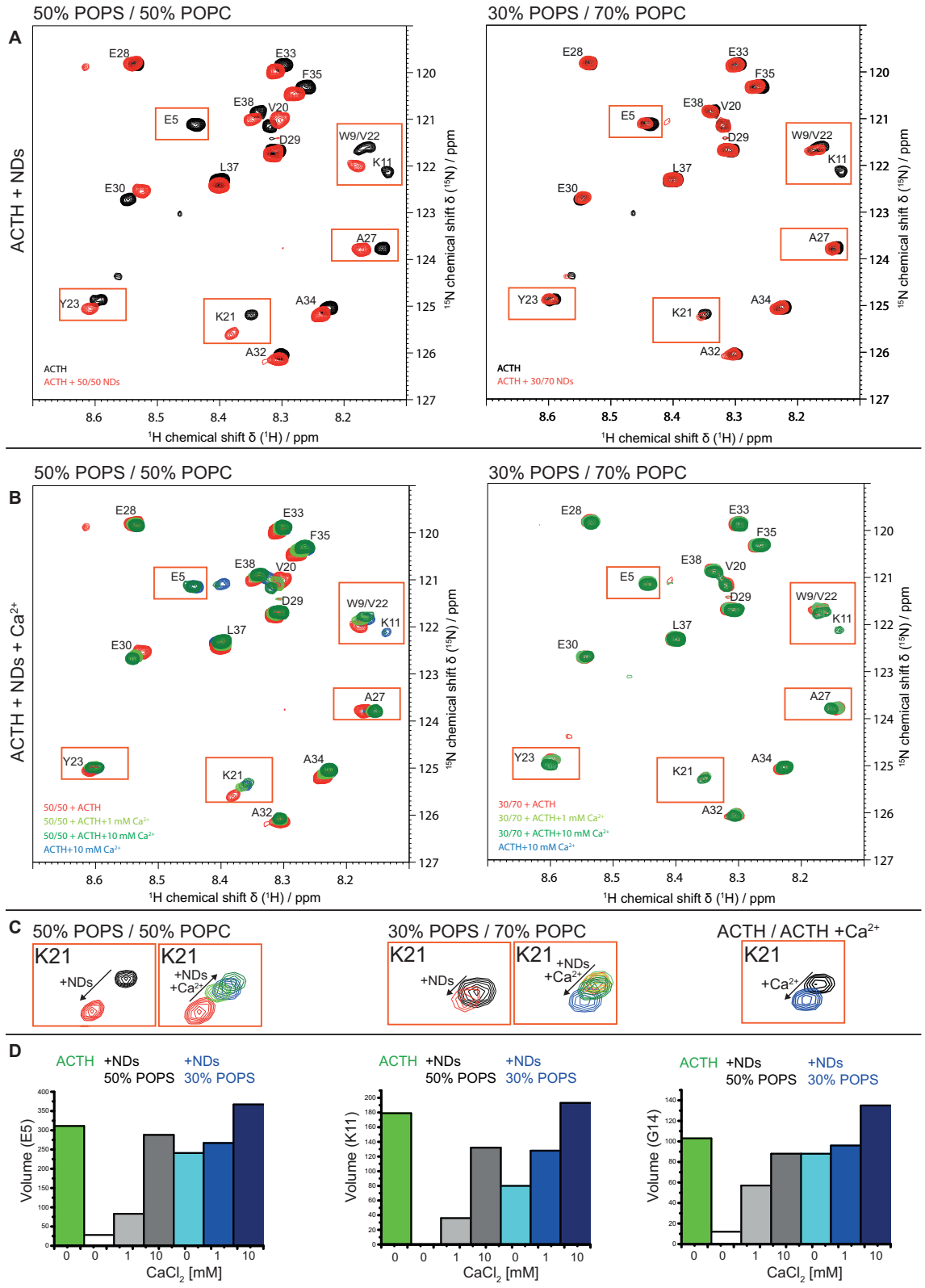

Figure 5.31: Calcium interrupts interaction of ACTH with charged NDs. Overlay of ^{1}H- ^{15}N HSQC spectra of 30 µM ^{15}N ACTH **(A)** alone (black) and with 30 µM NDs (red) and **(B)** with increasing concentrations of calcium (0 mM, 1 mM and 10 mM $CaCl_2$) as well as 30 µM ^{15}N ACTH wit 10 mM $CaCl_2$ (colors indicated in the figure legends) at 10 °C. **(C)** Zoom into K21 chemical shift perturbations in presence of NDs, ND + 0-10 mM $CaCl_2$ or only 10 mM $CaCl_2$ and **(D)** variations in peak volumes of E5, K11, G14 show ACTH-ND interaction (50% POPS / 50% POPC, 30% POPS / 70% POPC) and its disruption in presence of Ca^{2+}.

The data in figure 5.31 shows that several amide groups of ACTH are affected by the presence of NDs. This effect can be seen by chemical shift and volume differences when comparing the free and lipid-bound peptide (red boxes in figure 5.31, **(A)**) and it is more pronounced for NDs with higher content of negatively charged lipids. In this context, a drastic decrease in peak intensity (peak bleaching), e.g. E5 or K11, can be indicative of a slow exchange process (in the NMR time scale), therefore, strong binding. On the other hand, shifting of the amide resonances - e.g. K21, A27, A32, E33, F35 or A34 - points to a fast exchange process.
Spectra displayed above (figure 5.31) and in figure 5.33 show only a zoom of the amide region, for spectra of the complete amide region see supplement 8.1 figures 8.10, 8.11 and 8.12. In light of this data, we propose a model (figure 5.32) in which the N-terminal part of ACTH (roughly residues 1 to 14) shows a strong binding (slow and / or intermediate exchange) to the lipids. The remaining residues show a lower affinity (fast exchange) which at the same time is driven by the amount of negatively charged lipids available in the NDs. In case of NDs containing 50% POPS a fast exchange is observed for the remaining residues (figure 5.32, **(A)**), while for those containing 30% POPS this interaction mode is only observed up to residue 27, i.e. the *C-terminus* is not involved in lipid binding (figure 5.32, **(B)**).

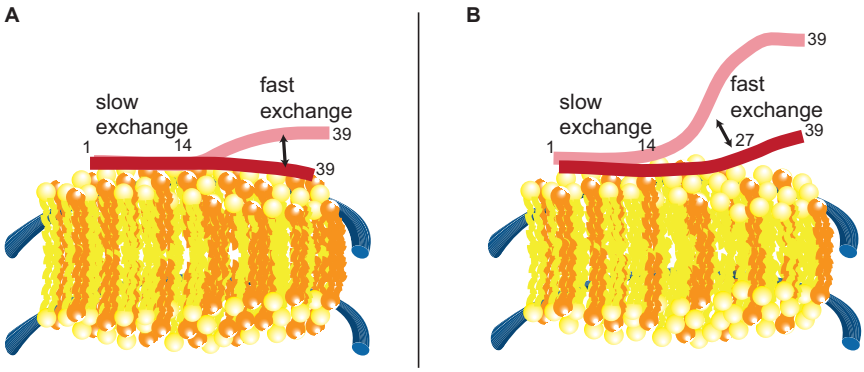

Figure 5.32: Interaction modes of ACTH. The *N-terminus* of ACTH (roughly 1 to 14) shows a strong binding to negative lipids (slow exchange). This is indicated by the disappearance (peak bleaching) of peptide residue peaks in their lipid-bound form. The remaining residues show a weaker (fast exchange) or no binding, indicated by differences in chemical shifts of free and bound peptide, depending on the amount of negatively charged lipids present in the NDs. In the presence of NDs containing 50% POPS a fast exchange is seen for residues around 14-39 (**(A)**, while in the presence of NDs containing 30% POPS this interaction is roughly limited to the residues 14-27 **(B)**.

Upon calcium addition (figure 5.31, **(B)** and **(C)**) we see that the peaks that were shifted due to the interaction with the lipids (red) gradually return to their initial positions in the presence of 10 mM calcium (blue). Also, peaks that disappeared due to the lipid-interaction (e.g. E5, K11) reappear upon calcium addition. Furthermore, we also see that the peak volumes, which initially decrease due to the interaction with the NDs, progressively return to the values close to those they had in the free ACTH state (figure 5.31, **(D)**). Note that peak volumes of free ACTH do not change significantly upon addition of calcium (see supplement 8.1, 8.14). This data indicates that calcium releases ACTH from its lipid-bound form.

From these experiments and the FA calcium titration we know that binding of ACTH to NDs and its release by calcium are dependent on the amount of negatively charged lipids present. This implies that the calcium-mediated release of ACTH is caused by a competition of the divalent cations with the peptide for binding sites at anionic lipids.

A direct effect of Ca^{2+} on protein-membrane interactions (with anionic lipids) was already reported for α-synuclein, a protein (14.46 kDa) related to the pathology of Parkinson's disease (PD). As observed for ACTH, also α-synuclein was shown to be released from its lipid-bound form by addition of calcium [108]. In their study, the authors suggest that the normal function of α-synuclein is membrane-mediated and that a calcium-mediated release can lead to its pathological dysfunction.

ACTH was furthermore studied in the presence of NDs containing solely neutral charged lipids (POPC) with and without 10 mM $CaCl_2$ (figure 5.33).

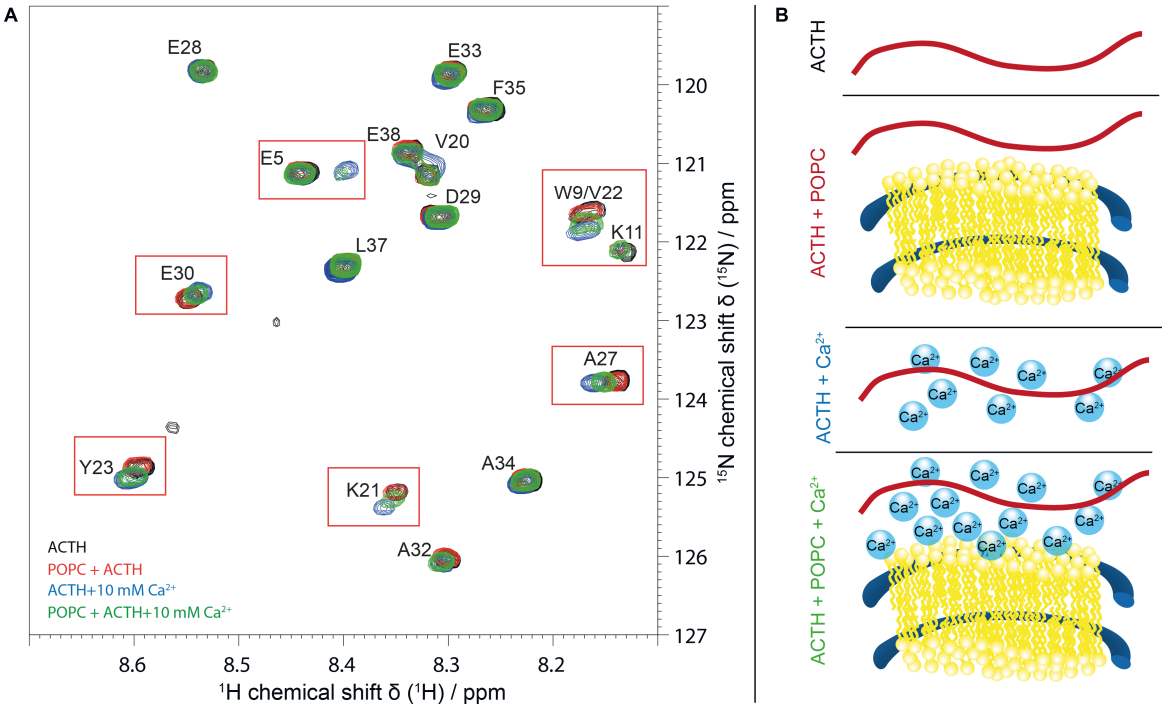

Figure 5.33: ACTH does not interact with neutral charged NDs but with Ca^{2+}. **(A)** Overlay of ^{1}H-, ^{15}N-HSQC spectra and **(B)** schemes of 30 µM ^{15}N ACTH alone (black), with 10 mM Ca^{2+} (blue) and in presence of 30 µM NDs with neutral charge (100% POPC) with 10 mM and without Ca^{2+} (green / red) at 10 °C. While no interaction can be observed for ACTH with neutral charged POPC lipids, several peaks shift in the presence of calcium (indicated with red boxes).

Comparing free ACTH without (black) and with calcium (blue) in figure 5.33, peak shifts can be observed, implying that calcium does have an impact on ACTH free in solution. The data suggests an interaction of ACTH with calcium at the core of the peptide (position 21-27) behind its tetrabasic region (position 15-18).
The presence of neutral charged NDs with 100% POPC does not lead to detectable chemical shift perturbations, i.e. no interaction is found for ACTH with these NDs. Addition of 10 mM $CaCl_2$ to the mix of 40 µM ACTH and 30 µM NDs leads to a transition of the peaks towards the calcium-interacting form of ACTH observed with 10 mM calcium without NDs.
Although the same concentration of calcium chloride was added to the sample with NDs, some peaks do not completely shift back to the state of ACTH with Ca^{2+}. This implies that the overall accessible calcium concentration decreased due to interaction of Ca^{2+} with 100% POPC NDs.

When comparing ^{1}H-, ^{15}N-HSQC spectra of ACTH with 10 mM Ca^{2+} and ACTH with different types of NDs (100% POPC, 30% POPS / 70% POPC and 50% POPS / 50% POPC) after addition of 10 mM calcium (figure 5.34), differences are observed between ACTH with and without NDs, indicating a comparable decrease of the accessible Ca^{2+} concentration. This is noteworthy because it implies that calcium binding by NDs is not predominantly dependent on the amount of charged lipids of the bilayers, although lipid binding and the release of ACTH by calcium was shown to be mainly charge driven. Therefore, the observed effect, of decreased accessible calcium, by NDs seems to be mainly dependent on other property than charge.
Binding of Ca^{2+} to PS^{-} lipids was found to be involving carboxylic and phosphate portions of the headgroups, incorporating the ion into the hydrophilic region of the lipid bilayer [110]. Calcium was also shown to neutralize charge fractions of POPS and POPC NDs [111]. As such, it is likely that the interaction with phosphate head groups or charge-independent binding of calcium to phospholipids drives the reduction of accessible ion concentration in solution.

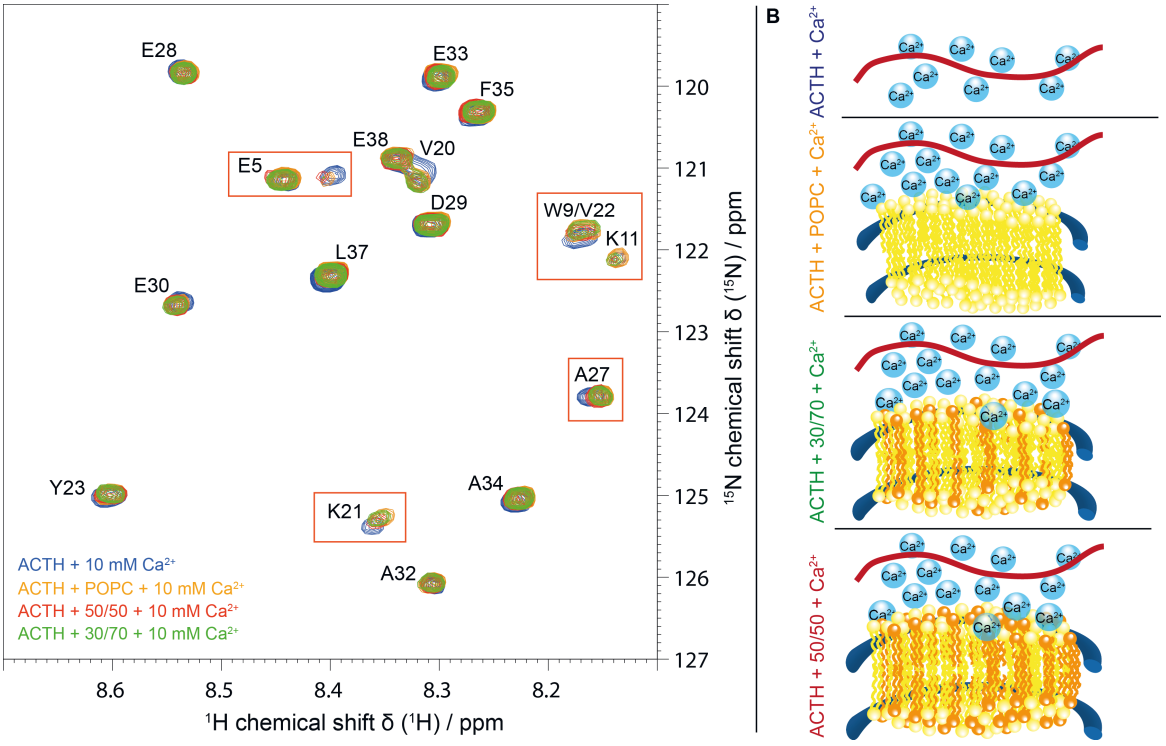

Figure 5.34: Calcium interaction with NDs. Overlay of ^{1}H-, ^{15}N-HSQC spectra showing ACTH with 10 mM Ca^{2+} (blue) and with 100% POPC, 30% POPS / 70% POPC and 50% POPS / 50% POPC NDs with 10 mM Ca^{2+} (red, yellow, green). ACTH released from its lipid-bound form by addition of 10 mM Ca^{2+} shows small shifts compared to ACTH with 10 mM Ca^{2+}, indicating interaction of Ca^{2+} and NDs. No shifts are observed between NDs with an increasing content of negatively charged lipids, implying that all NDs bind the same amount of Ca^{2+}.

The modulating effect of calcium on peptide-lipid interaction enables ligand binding assays in presence of biological membranes.
Binding of ACTH(1-23)C-647 to whole, MC4R overexpressing HEK 293-F cells (Supplement: figure 8.24), as well as in a membrane preparation of Tnao38 insect cells (Supplement: figure 8.23) was tested by FA. For both setups calcium does lead to a decrease of FA values, thus, in the light of our recent findings, indicating that the hormone is released from its interaction with the cell membranes (Supplement: chapter 8, section 8.4).
Although addition of calcium dramatically reduced the hormone's interaction with biological membranes, no specific binding to its receptor MC4R could be detected in these measurements.
In the experiment with HEK 293-F cells this could be caused by too low concentrations of receptor available for ligand binding on the cell surface. This is not expected to be the case for the setup using a membrane preparation of Tnao38 cells which provides highly concentrated membrane fractions carrying the receptor. Nevertheless, the harsh sample preparation process could have lead to a decreased ligand binding activity of MC4R.

In addition, the binding mode of ACTH(1-23)C-647 to MC4R may be different from that found for the hormone-lipid interaction (figure 5.32). Although the residues 1-20 have been described to be important for the MC2R mediated corticotropic activity of ACTH [52], activation of MC4R by ACTH may be restricted to binding of the residues corresponding to α-MSH (ACTH(1-13)). If a large part of the peptide's *C-terminus* would not be involved in the receptor binding, it could remain very flexible leading to a decrease of FA values, due to a rapid movement of the fluorophore.
Future experiments need to verify whether the use of a shorter peptide conjugate (e.g. α-MSH-647) leads to an increase in FA values, or if sample preparation can be further optimized to avoid loss of receptor activity.

At the beginning of this section binding of ACTH to DDM micelles was described to differ from the hormone-membrane interaction. Unlike the only N-terminal interaction of ACTH and NDs a N- and C-terminal interaction was observed for DDM micelles. The influence of calcium on this type of interaction was therefore studied by FA using ACTH(1-23)C-647 but also α-MSH-Rhodamine as ligands (figure 5.35).

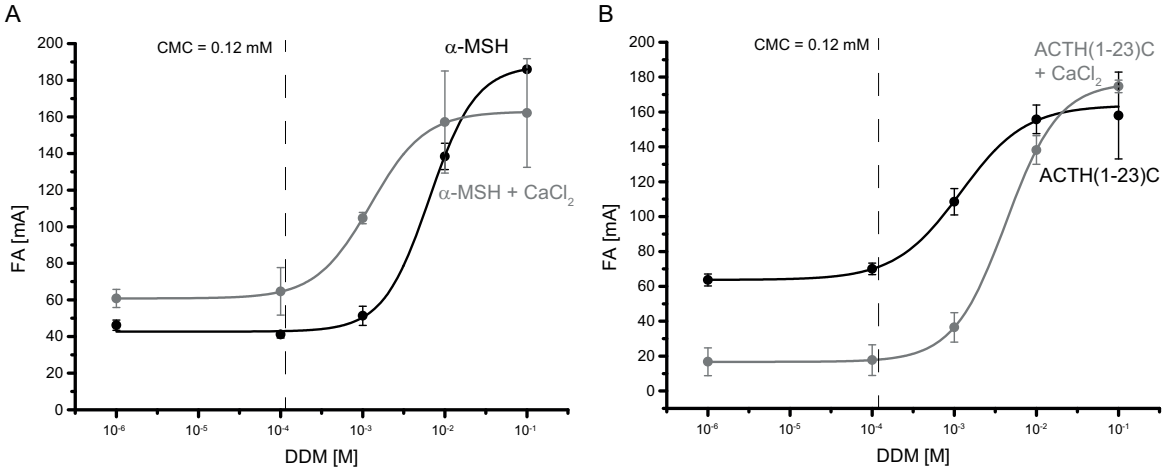

Figure 5.35: Calcium does not influence hormone interaction with DDM micelles. Interaction of ACTH and α-MSH with DDM is not disturbed by addition of 10 mM $CaCl_2$. Minor variations in FA curves are possibly due to changes in the critical micellar concentration (CMC) of detergents by salts.

Addition of calcium does not essentially vary interaction of the hormones with DDM micelles. Minor differences can be caused by the influence of salts on the critical micellar concentration (CMC) of detergents in general.
As interaction of ACTH with NDs was shown to be charge driven, interaction with DDM micelles needs to be driven by another force. Our data shows that the unspecific interaction of these melanocortins with NDs and DDM are of a different type, as the peptide sequence found to interact as well as the effects of calcium differ for lipid and detergent interaction, respectively.

Overall these findings suggest that hormone-membrane interaction could be a spatial mechanism to control ligand accessibility by altering physiological conditions such as ion concentrations or membrane lipid composition. In this way accessibility of neuropeptides due to membrane release could possibly be targeted towards post-synaptic membranes by calcium gradients in the synaptic cleft. Restriction of ligand movement to a two-dimensional (2D) scale on the membrane surface could furthermore provide high ligand concentrations close to the targeted receptor.
With respect to a probable regulative mechanism of Ca^{2+} on distinct protein and peptide-membrane interactions, deficiencies in the regulation of calcium concentrations during physiological processes can have a larger extend than known to date.

Stimulation of cortisol synthesis by ACTH was shown to be strongly dependent on the extracellular calcium concentration and its influx [112]. Effects of ACTH were decreased by extracellular addition of a chelating agent and could be recovered by extracellular addition of Ca^{2+}. Furthermore Davies et al. were able to show that inhibition of calcium influx into the cytosol inhibits the stimulation of cortisol synthesis by ACTH. They hypothesized a role of calcium either in the cAMP-dependent response to ACTH - possibly linked by calmodulin - or in a second cAMP-independent pathway responding to ACTH. Our data suggests that the role of hormone-membrane interactions and its modulation by Ca^{2+} should be considered in the pathology of diseases related to ACTH signaling dysfunctions.

5.4 HIV-1 Vpr - Zinc Promoted Solubility

Cell-free expression is a technique suitable to express cytotoxic but also aggregation prone proteins in high yields. It is an open system allowing to add agents that provide protein solubility. Alternatively harvesting of precipitated protein for refolding can be easily performed, separating the precipitate from the soluble proteins of the (*E.coli*) cell extract comprising translational and transcriptional machinery. Therefore expression of HIV type 1 viral protein R was tested in a continuous exchange cell-free expression (CECF) setup using different plasmids. Constructs varied by vectors, codon optimization and fusion tags for protein purification. The following experiments were performed based on the hypothesis that Vpr is a zinc binding protein, due to its conserved zinc binding motif as reported for Vpx [90]. This motif comprises three histidines ($pK_s \approx 6.4$ - only one imine deprotonated / $pK_s \approx 14$ - bot nitrogen atoms deprotonated) and one cysteine ($pK_s \approx 8.5$), stably coordinating Zn^{2+} in a tetrahedral coordination geometry.

5.4.1 Vpr Expression with Zinc

To test the impact of zinc on the solubility of Vpr during expression, zinc acetate was added to several cell-free expression reactions. Expression of WT Vpr with zinc acetate ranging in concentrations from 1-20 µM is shown in figure 5.36. A negative control (0 µM zinc acetate) was used to determine whether solubility is facilitated only by addition of zinc.

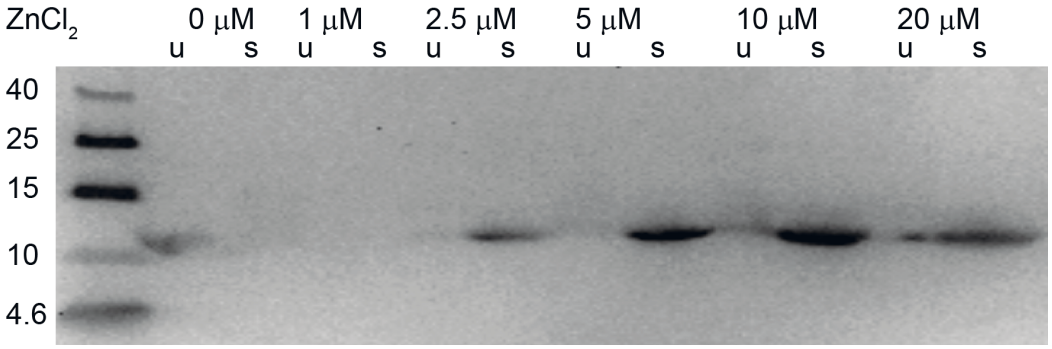

Figure 5.36: Vpr solubility increases with zinc concentration. Western Blot of cell-free expressed HIV-1 Vpr WT with increasing zinc acetate concentrations (0 to 20 µM). Vpr was specificaly detected by using the HIV-1 Vpr antibody vN-20 (Santa Cruz) as a primary antibody.

Bands coresponding to HIV-1 Vpr were specifically detected with a primary antibody (vN20, Santa Cruz). While Vpr remains in the unsoluble fraction (u) without addition of zinc, the protein is shifted to the soluble fraction at zinc concentrations of 2.5 to 20 µM zinc acetate. Protein concentration also seems to increase with the concentration of zinc. This implies that coordination of zinc promotes solubility of Vpr during expression and possibly even increases protein yield.

To test if soluble Vpr expressed with zinc is active, interaction with a well known interaction partner was tested in a pull down assay (figure 5.37). Therefore HIV-1 p6 with a N-terminal His-tag was bound to a Ni-NTA sepharose gravity flow column. Unbound p6 was washed off the column before applying CECF supernatant containing soluble Vpr. Interaction of p6 with Vpr can be observed by co-elution of both proteins after several washing steps to remove proteins with low binding affinities.

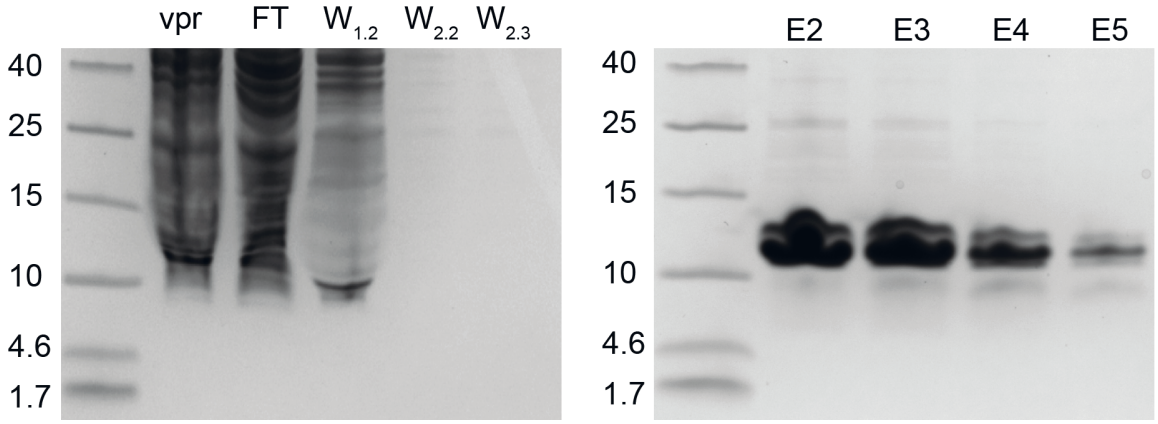

Figure 5.37: HIV-1 Vpr interacts with HIV-1 p6. A double band at 12 kDa can be observed in the elution fractions using 150 mM imidazole. This implies that Vpr co-elutes with 6xHis-p6 bound to a Ni-NTA column.

In figure 5.37 a double band at $\sim$ 12 kDa implies that HIV-1 p6 co-elutes with Vpr. To verify if the protein bands seen in the CBB stain above contain Vpr a Western Blot was performed (figure 5.38).

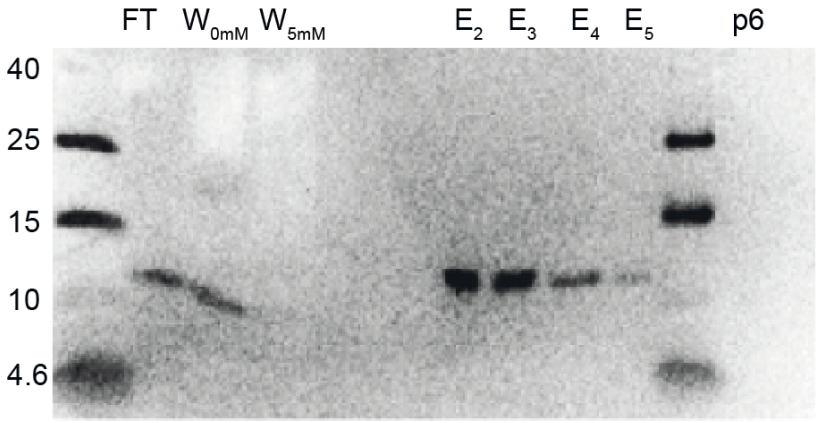

Figure 5.38: Coelution of HIV-1 Vpr and HIV-1 p6 in Western Blot. Strong signals of Vpr are visible in elution fractions E2-E3. Less intense signals can be found in the flow through (FT), each second washing fraction with 0 mM and 50 mM imidazole as well as in elution fractions E4-E5. No unspecific signal is produced by p6 as seen in the last lane.

The data shows that only few protein was lost in the flow through (FT) and the first washing step after applying HIV-1 Vpr. Vpr could be detected mainly in the elution fractions E2-E5 proving the co-elution of Vpr and p6. As a negative control purified 6xHis-p6 was applied to the blot not showing any signal. Therefore detected bands clearly belong to Vpr and can not be caused by unspecific interaction with p6. This interaction strongly suggests that soluble Vpr expressed with zinc is in an active form. Purification of soluble Vpr thus would be providing the possibility to study protein-protein interactions under physiological and well defined conditions *in vitro*.

5.4.2 Vpr Expression without Zinc

A precipitate based CECF setup without addition of zinc was also tested for expression of codon optimized wilde type Vpr. Here the protein was expected to remain unsoluble which should enable a separation from the strong soluble background given in cell-free expression. After the unsoluble protein was fractionated by centrifugation it was washed in a NaPi buffer without zinc. The protein was again centrifuged and precipitated Vpr was resuspended with NaPi buffer containing 50 µM zinc chloride. Finally the unsolube fraction was separated from the supernatant and resuspended in the same volume (figure 5.39).

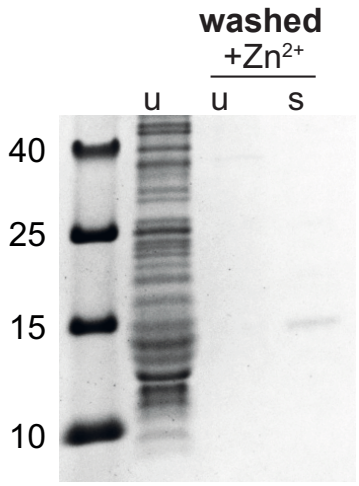

Figure 5.39: Vpr resolubilization with zinc. CBB Tricine-PAGE of resolubilized HIV-1 Vpr wilde type with zinc chloride. Unsoluble Vpr (u) was washed in zinc free buffer before resuspension with 50 µM $ZnCl_2$ (washed u / s $+Zn^{2+}$). Unsoluble and soluble fractions were separated by centrifugation before resuspension of pellets in the same volume as the supernatant.

Addition of zinc chloride to the buffer promotes solubility of Vpr. Moreover, a reduced background of soluble *E.coli* proteins can be observed after washing. Resolubilization of Vpr therefore can be used to gain very pure protein without the need of any chromatographic step possibly leading to protein loss. Activity of resolubilized Vpr could not be confirmed. Only a low signal in the flow through (FT) of a pull-down assay with HIV-1 p6 was detected in a western blot. Nevertheless, signals in this experiment were found to be at the detection limit. A repetition of this experiment with higher protein concentrations is therefore desirable. The exchange of the psCodon-vector used in this experiment to a pIVEX vector, which is optimized for rapid translation systems (RTS), could offer a better yield of WT Vpr in cell-free expression.

5.4.3 Optimization of the Vpr Expression Construct

Different strategies of optimizing the Vpr expression construct were chosen to enable affinity purification and also increase protein yield.

Two constructs kindly provided by the lab of Prof. Dr. Loidl-Stahlhofen (WHS, Gelsenkirchen) were used in a first test expression. While codon optimized wilde type Vpr provided on a psCodon vector showed moderate protein yields (see figures 5.36, 5.39) no expression was detected for not codon optimized pET-Vpr.

As protein yields were low compared to other proteins expressed in control reactions (e.g. pIVEX-bR, pIVEX-GFP), the expression vector was optimized to pIVEX. Within this optimization a N-terminal Strep-tag I followed by a TEV recognition site was added to Vpr.

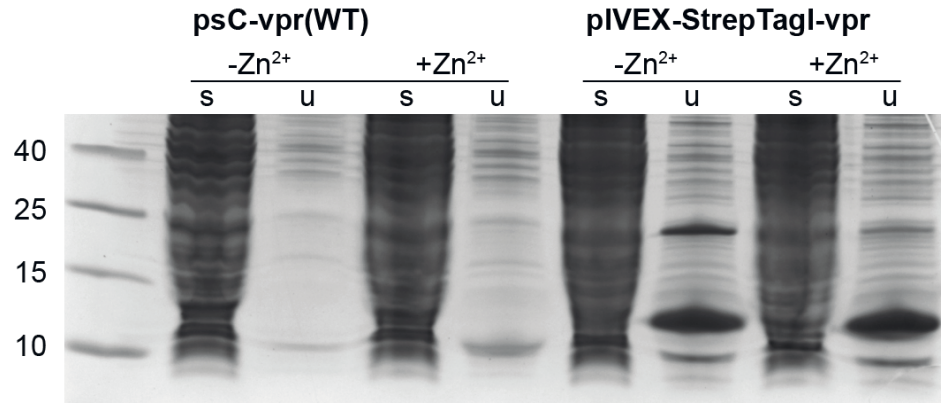

Figure 5.40: Expression pIVEX-Strep-tag I Vpr leads to increased yields. CBB Tricine-PAGE of HIV-1 Vpr WT and Strep-tag I Vpr with and without zinc chloride. Protein yields are higher when Vpr is expressed with a Strep-tag I using pIVEX instead of expressing the Vpr WT using the psCodon vector.

The CBB stained SDS-PAGE of WT and Strep-tag I Vpr shows a stronger expression of the new construct when compared to the wilde type. Addition of zinc to the CECF mixture did not lead to solubility of the peptides, nor for Strep-tag I Vpr neither for the wilde type - as in contrast to previous experiments (figure 5.36). For further details on the reproducibility of the soluble expression of Vpr with zinc see section 5.4.4.

5.4.4 Reproducibility

Data obtained on psCodon-Vpr WT expression with zinc, as shown in figure 5.36, was not reproducible. After several experiments showing solubility of Vpr when expressed with zinc, no soluble Vpr could be obtained by the same protocol anymore. Varying zinc salts and concentrations did not overcome this problem.

Latest data produced under my supervision by Maria Dalhaus showed promising effects on the solubility of a Strep-tag II Vpr construct when no DTT was added to the cell free expression mixtures (figure 5.41). Concentration of DTT in CECF is normally set to 2 mM. This high amount of reducing agent could be disturbing the binding of zinc by the unique cysteine of Vpr. Although the thiol group of cysteine needs to be reduced to be available for coordination of zinc together with three other histidines, high levels of reducing agents could possibly break this bond again. On the other hand,

DTT was shown to be forming stable coordination complexes with metal ions, such as Zn^{2+}. Therefore, a high excess of DTT will lead to a decrease of zinc accessible for coordination by Vpr.

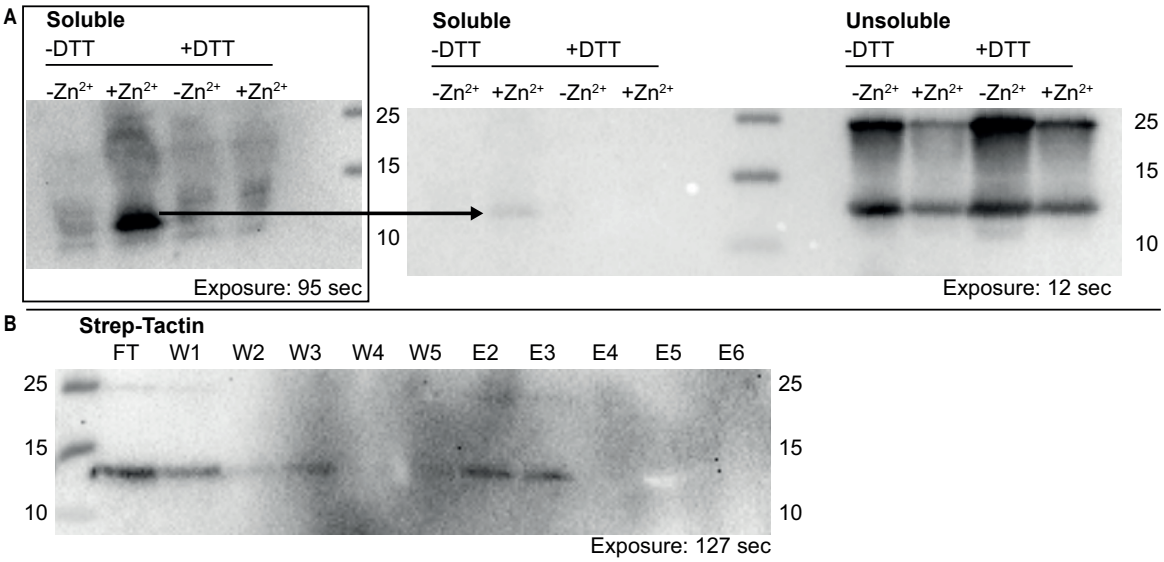

Figure 5.41: Purification of soluble Strep-tag II Vpr. Western blots of **(A)** Strep-tag II Vpr expression with and without 50 µM zinc acetate in presence and without addition of reducing agent (DTT) and **(B)** of Strep-Tactin affinity chromatography of soluble expressed Strep-tag II Vpr. Detection was performed with the HIV-1 Vpr antibody vN-20 from Santa Cruz as a primary antibody.

Strep tagged Vpr expressed without addition of DTT but in presence of 50 µM zinc acetate is mostly unsoluble (figure 5.41 **(A)**). However, soluble protein was also present and used to perform a first purification test by Strep-Tactin affinity chromatography (figure 5.41 **(B)**). Strep-tag II Vpr monomers are found in the elution fractions but protein loss in FT and washing fractions can be observed. Further optimization of this step will be necessary to gain higher yields of pure and soluble zinc coordinating Vpr.

6

Conclusions and Outlook

6.1 Hormone-Receptor Interactions

The aim of this work was to establish the expression of MC4R and its ligand ACTH for use in ligand binding assays and NMR experiments. As reported above, we were able to produce and purify (isotope labeled) ACTH (full-length and truncations) in the mg-range, using the *E. coli* BL21 expression system. Expression of MC4R construct with a N-terminal prolactin (signal peptide) and FLAG-tag together with a C-terminal 6-fold His-tag (SF-MC4R-6xHis) HEK 293(-F) cells was optimized by the use of a more moderate promoter (chicken β-actin (CBA) instead of cytomegalovirus (CMV) promoter). Down stream activation of MC4R expressed in human cells was successful using commercial ligands, as well as *E.coli* expressed peptide and the newly designed peptide conjugate ACTH(1-23)C-Atto 647.
NMR experiments revealed a random coiled structure of the melanocortins ACTH and α-MSH with several secondary amino acid conformations when free in solution. Moreover truncations (1-23, 1-28) as well as addition of a C-terminal cysteine to ACTH and ACTH(1-23) were shown to not essentially alter structural features of these ligands.
Charge driven membrane interaction could be described to be a special feature of the hormones studied (ACTH, α-MSH). These experiments also revealed, that ACTH(1-23)C-Atto 647, designed for fluorescence anisotropy (FA)-based ligand binding assays, is suitable for its purpose in a N-terminal binding mode with strong interaction up to position 14 and weaker or no binding of the remaining residues. Hormone-lipid interaction could furthermore be shown to differ from hormone interaction with anionic detergent micelles (DDM).
With respect to the role of calcium at the synaptic cleft but also in cells all over the body the effect of $CaCl_2$ on hormone-membrane interaction was studied. By addition of 1 to 10 mM calcium chloride we were able to reduce the interaction of hormones with negative charged lipids. These findings do not only provide a convenient way for optimized sample preparation in hormone-receptor studies , but do also imply a possible physiological role of hormone-membrane interaction. NMR and FA are shown

to be suitable methods to gain more knowledge about this yet not well understood feature of certain peptides.
Our protocols and data will form the base of future work to reveal the structure and dynamics of MC4R-ligand interaction. Spectra recorded of free ligands will serve as references for NMR studies of the GPCR in its ligand-bound form. In addition FA-based binding assays can be applied to screen the impact of different ions on the hormone-lipid interaction. By this optimized ligand binding conditions and further knowledge on their possible role in hormone signaling can be provided. The modified ligand ACTH(1-23)C-Atto 647, which was shown to activate MC4R G-protein signaling, will be applied in fluorescence-based (FI / FA) ligand binding assays to establish receptor purification protocols.

Key findings

- Expression of different MC4R constructs was established in HEK 293-F cells
- Expression of SF-MC4R-6xHis on a pHL-IRES vector increases protein yields
- Signal(Prolactin)-FLAG-tag-MC4R-6xHis was shown to be active
- An expression and purification protocol for ACTH in *E. coli* was established
- ACTH and α-MSH are unfolded when free in solution
- ACTH(1-23)C-Atto 647 is suitable for FA ligand binding assays
- ACTH and α-MSH do interact with anionic lipids in NDs
- ACTH-lipid interaction differs from ACTH-detergent micelle interaction
- Recombinantly expressed and modified ligands were shown to maintain their receptor activation abilities
- Calcium disturbs ACTH-lipid interaction, suggesting a heretofore unknown way of hormone signaling modulation

6.2 HIV-1 Vpr

We were able to establish cell-free expression of the cytotoxic protein HIV-1 Vpr. Furthermore its expression yields were optimized by the use of a pIVEX vector. An impact of zinc on the solubility of HIV-1 Vpr was shown when introduced during cell-free expression as well as upon suspension after precipitate based expression. This data confirms that HIV-1 Vpr is able to coordinate zinc as it was postulated by Schwefel et al. [90]. Activity of soluble expressed Vpr could be successfully tested in a pull-down assay with the Vpr interaction partner HIV-1 p6. Purification of HIV-1 Vpr was achieved in a precipitate based expression setup with subsequent washing steps before addition of zinc chloride to promote protein solubility. Although effects of zinc on the solubility of Vpr were not reproducible after a large set of experiments new data implies a possible role of the excess of reducing agent present during CECF on the coordination of zinc by Vpr. A first purification of soluble Vpr was tested successfully but needs to be further optimized to increase binding to strep-tactin purification resin.

Overall cell-free expression was shown to be suitable for expression of HIV-1 Vpr providing soluble protein upon addition of zinc. It is a promising tool to gain protein yields sufficient for NMR experiments to study the zinc coordinating structure of Vpr.

Key findings

- HIV-1 vpr can be expressed with CECF
- Zinc does have a positive impact on the solubility of Vpr
- Vpr soluble expressed in the presence of zinc is actively binding HIV-1 p6
- Soluble Strep-tag II Vpr (expressed with zinc) was found to bind to Strep-Tactin

7

Publications

Melanocortin Signaling: Modulation through Membrane Interaction and Calcium.

Authors: Schriek S., Viegas A., Viennet T., Etzkorn M.

Manuscript based on the data represented in section 5.3.2 (Hormone-Membrane Interaction) in preparation.

Co-authorships under maiden name Arens:

Selective Protein Hyperpolarization in Cell Lysates Using Targeted Dynamic Nuclear Polarization.

Authors: Viennet T., Viegas A., Kuepper A., Arens S., Gelev V., Petrov O., Grossmann T.N., Heise H., Etzkorn M.

Journal: Angewandte Chemie (International Edition in Englisch),
2016 August 26; 55(36):10746-50. doi: 10.1002/anie.201603205.
Epub 2016 Jun 28 [113]

Abstract: Nuclear magnetic resonance (NMR) spectroscopy has the intrinsic capabilities to investigate proteins in native environments. In general, however, NMR relies on non-natural protein purity and concentration to increase the desired signal over the background. We here report on the efficient and specific hyperpolarization of low amounts of a target protein in a large isotope-labeled background by combining dynamic nuclear polarization (DNP) and the selectivity of protein interactions. Using a biradical-labeled ligand, we were able to direct the hyperpolarization to the protein of interest, maintaining comparable signal enhancement with about 400-fold less radicals than conventionally used. We could selectively filter out our target protein directly from crude cell lysate obtained from only 8 mL of fully isotope-enriched cell culture. Our approach offers effective means to study proteins with atomic resolution in increasingly native concentrations and environments.

The use of amphipols for NMR structural characterization of 7-TM proteins.

Authors: Elter S., Raschle T., Arens S., Viegas A., Gelev V. Etzkorn M., Wagner G.
Journal: The Journal of Membrane Biology,
2014 October, 247(0): 957964.
Published online 2014 May 25. doi: 10.1007/s00232-014-9669-5 [114]

Abstract: While amphipols have been proven useful for refolding of seven transmembrane helical (7-TM) proteins including G-protein coupled receptors (GPCRs) and it could be shown that an amphipol environment is in principle suitable for NMR structural studies of the embedded protein, high-resolution NMR insights into amphipol refolded and isotopically labelled GPCRs are still very limited. Here we report on recent progress towards NMR structural studies of the melanocortin-2 and -4 receptor, two class A GPCRs which so far have not been reported to be incorporated into an amphipol environment. Making use of the established 7-TM protein bacteriorhodopsin (BR) we initially tested and optimized amphipol refolding conditions. Most promising conditions were transferred to the refolding of the two melanocortin receptors. Analytical scale refolding experiments on the melanocortin-2 receptor show very similar behavior to results obtained on BR. Using cell-free protein expression we could generate sufficient amounts of isotopically labeled bacteriorhodopsin as well as melanocortin-2 and -4 receptors for an initial NMR analysis. Upscaling of the amphipol refolding protocol to protein amounts needed for NMR structural studies was, however, not straight forward and impeded detailed NMR insights for the two GPCRs. While well resolved and dispersed NMR spectra could only be obtained for bacteriorhodopsin, a comparison of NMR data recorded on the melanocortin-4 receptor in SDS and in an amphipol environment indicates that amphipol refolding induces larger structural modifications in the receptor.

8

Supplement

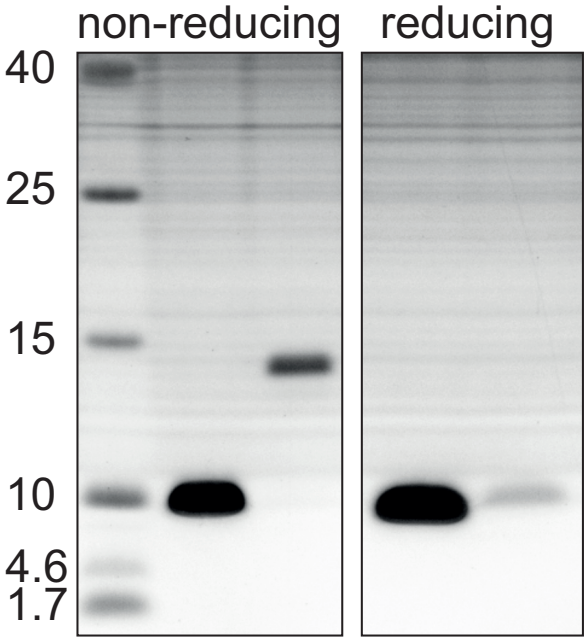

Figure 8.1: RP-HPLC separated ACTH(1-39)C monomers and dimers. SDS-PAGE analysis of ACTH(1-39)C purified without DTT in reducing and non-reducing sample buffer.

8.1 NMR

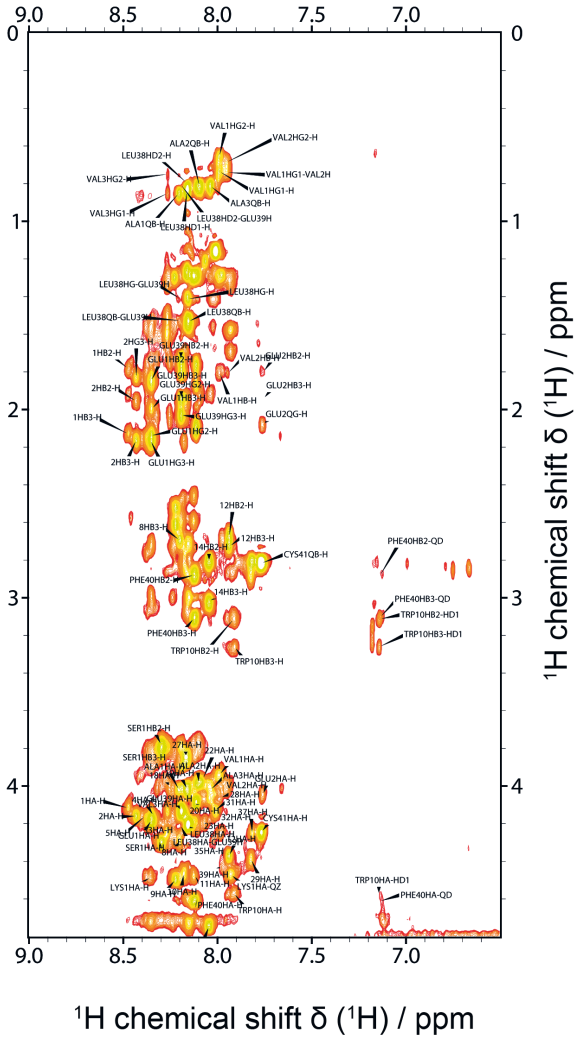

Figure 8.2: ACTH(1-39)C after centrifugal concentration. HSQC of ACTH(1-39)C after protein concentration with a centrifugal concentrator. The narrow peak dispersion indicates that the peptide is mainly unfolded.

Table 8.1: Acquisition parameters of NMR experiments.

Spectra	Complex points			Spectral width (Hz)			NS
	^{1}H	^{15}N	^{13}C	^{1}H	^{15}N	^{13}C	
^{15}N,$^{1}H-HSQC$	2048	256	-	13	30	-	32
^{13}C,$^{1}H-HSQC$	2048	-	256	13	-	165	32
HNCO	2048	40	128	13	30	22	8
HN(CA)CO	2048	40	128	13	30	22	16
CBCA(CO)NH	2048	40	128	13	30	75	16
HNCACB	2048	40	128	13	30	75	16
	^{1}H	^{13}C	^{13}C	^{1}H	^{13}C	^{13}C	
(H)CCH-TOCSY	2048	64	128	13	75	75	16
	^{1}H	^{15}N	^{1}H	^{1}H	^{15}N	^{1}H	
$^{15}N-TOCSY-HSQC$	2048	40	128	13	30	13	16
$^{15}N-NOESY-HSQC$	2048	40	128	13	30	13	16

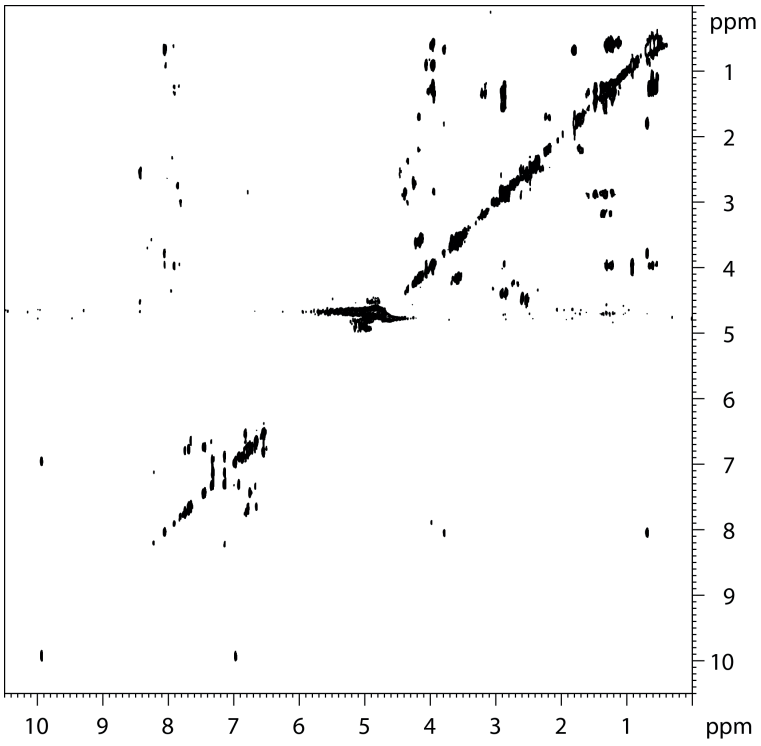

Figure 8.3: TOCSY spectrum of MC4R 1-26. A TOCSY spectrum of 836 µM MC4R(1-26), the receptors *N-terminus*, which was shown to maintain the receptors basal activity [49], was recorded. The synthesized peptide was ordered N-terminal acetylated and as a C-terminal amide (Peptide and Elephants GmbH).

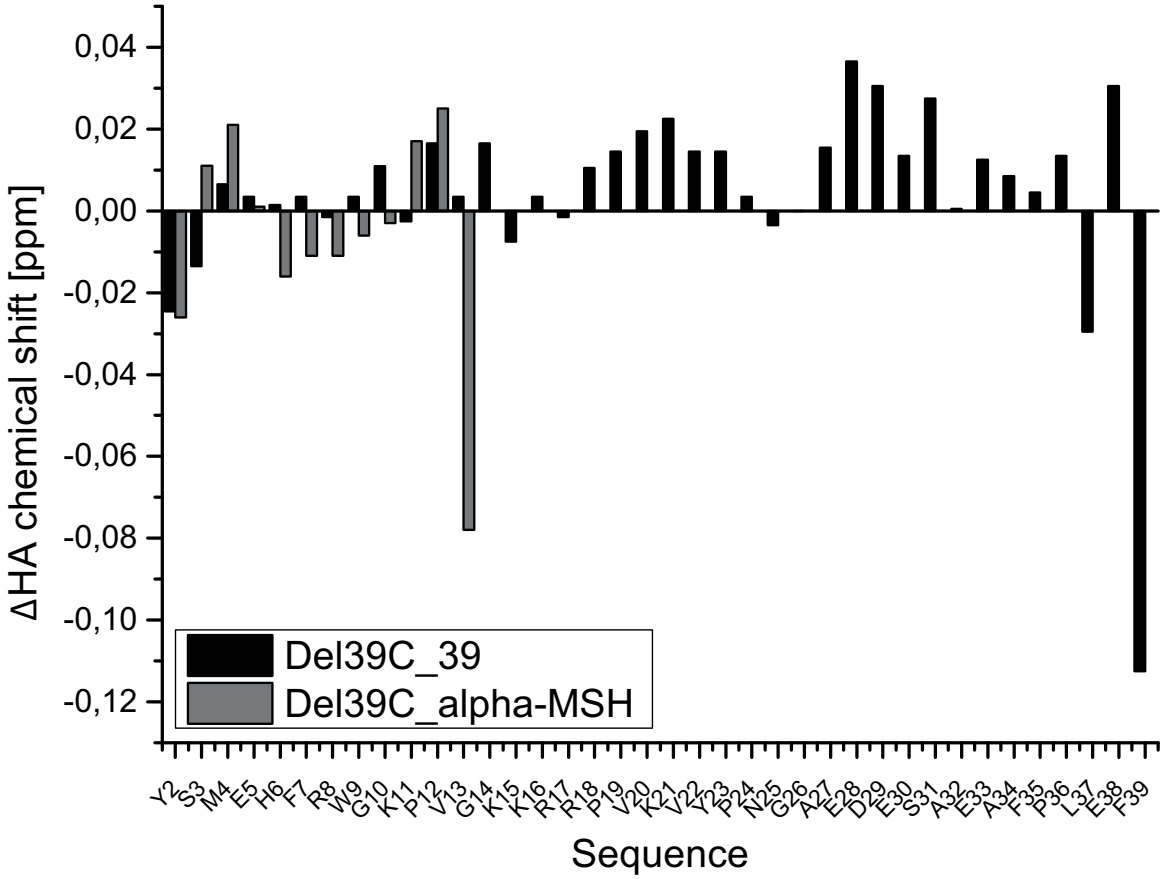

Figure 8.4: Comparison of ACTH(1-39)/Cys and α-MSH chemical shifts. Overlay of Δ HA chemical shifts of ACTH(1-39) and acetylated α-MSH (Peptides and Elephants) to ACTH(1-39)C.

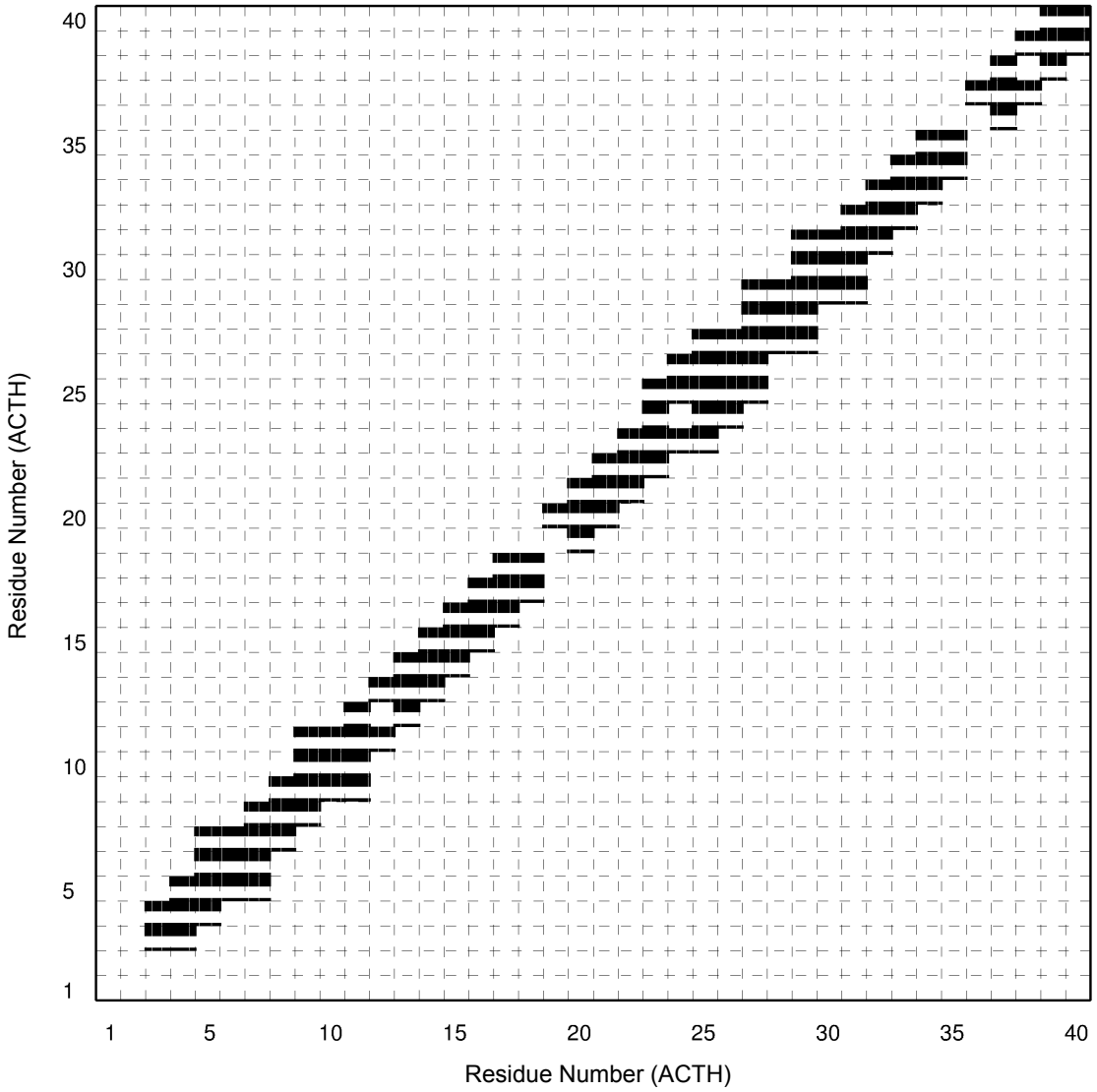

Figure 8.5: Interresidue NOE contact scheme. Connections indicate ^{1}H-^{1}H-interresidue NOE cross peaks. Only neighbouring contacs but no long-range interactions, indicative for a tertiary structure, are visible.

ResID	N	H	CA	CB	CO	HA
S1						
Y2			58,19	38,93	175,90	4,66
S3	118,31	8,51	58,29	63,73	174,64	4,43
M4	122,47	8,49	55,85	32,64	176,71	4,46
E5	121,10	8,42	57,21	30,06	176,49	4,14
H6	119,04	8,28	56,09	29,91	174,91	4,50
F7	120,86	8,14	57,92	39,45	175,73	4,55
R8	122,45	8,27	56,28	30,76	175,87	4,19
W9	121,55	8,20	57,21	29,27	176,81	4,70
G10	109,84	8,36	44,99		173,48	3,91
K11	121,88	8,16	54,10	32,61	174,41	4,59
P12			62,91	31,98	177,03	4,44
V13	121,00	8,41	62,37	32,95	176,83	4,13
G14	112,74	8,59	45,09		173,95	3,96
K15	121,35	8,41	56,05	33,11	176,71	4,34
K16	122,84	8,49	56,23	33,05	176,47	4,32
R17	123,26	8,56	55,86	30,92	176,06	4,34
R18	124,28	8,59	53,95	30,10	174,21	4,61
P19			62,98	31,98	176,65	4,47
V20	120,84	8,37	62,30	32,73	175,94	4,10
K21	125,49	8,40	56,05	33,40	175,43	4,29
V22	121,97	8,21	61,81	33,08	175,54	4,14
Y23	125,11	8,64	55,97	38,26	174,63	4,84
P24			63,21	31,99	176,92	4,43
N25	117,46	8,64	53,25	38,57	175,96	4,74
G26	109,71	8,49	45,33		173,88	4,00
A27	123,73	8,20	52,34	19,37	177,52	4,34
E28	119,74	8,56	56,51	30,33	176,25	4,24
D29	120,91	8,33	54,03	41,21	176,49	4,57
E30	122,46	8,55	56,86	30,00	176,75	4,30
S31	116,91	8,51	58,78	63,89	174,54	4,39
A32	126,01	8,32	52,64	19,26	177,78	4,32
E33	119,86	8,33	56,44	30,21	175,90	4,19
A34	125,02	8,25	52,26	19,42	177,00	4,24
F35	120,35	8,30	55,55	38,99	173,74	4,87
P36			63,02	32,08	176,83	4,42
L37	122,41	8,42	55,34	42,31	177,46	4,34
E38	120,93	8,40	56,49	30,44	175,93	4,24
F39	120,79	8,36	57,52	39,58	174,82	4,73
C40	124,57	7,97	59,53	29,09	178,53	4,38

Figure 8.6: ACTH(1-39)C chemical shifts. Chemical shifts of ACTH(1-39)C.

#	RES	ATOM	Chemical Shift			#	RES	ATOM	Chemical Shift		
			ACTH	ACTH(1-39)C	α-MSH				ACTH	ACTH(1-39)C	α-MSH
1	SER	H			8,36	9	TRP	HB2	3,25	3,23	3,28
1	SER	HA			4,40	9	TRP	HB3	3,40	3,38	3,41
1	SER	HB2			3,79	9	TRP	HD1	7,28	7,26	7,30
1	SER	HB3			3,79	9	TRP	HE1	10,24	10,24	10,24
2	TYR	H	8,43		8,35	9	TRP	HE3	7,65	7,62	
2	TYR	HA	4,64	4,66	4,64	9	TRP	HZ2	7,47	7,46	
2	TYR	HB2	2,67	3,02	2,97	9	TRP	HZ3	7,16	7,17	
2	TYR	HB3	2,76	3,02	3,08	9	TRP	HH2	7,23		
3	SER	H	8,51	8,51	8,38	10	GLY	H	8,36	8,36	8,30
3	SER	HA	4,42	4,43	4,45	10	GLY	HA2	3,94	3,91	3,87
3	SER	HB2	3,83	3,82	3,85	10	GLY	HA3	3,91	3,91	3,96
3	SER	HB3	3,91	3,91	3,94	11	LYS	H	8,17	8,16	8,14
4	MET	H	8,49	8,49	8,52	11	LYS	HA	4,59	4,59	4,61
4	MET	HA	4,46	4,46	4,48	11	LYS	HB2	1,82	1,83	1,83
4	MET	HB2	2,02	2,02	2,03	11	LYS	HB3	1,82	1,83	1,83
4	MET	HB3	2,12	2,11	2,13	11	LYS	HG2	1,45	1,45	1,47
4	MET	HG2	2,54	2,53	2,55	11	LYS	HG3	1,45	1,45	1,47
4	MET	HG3	2,61	2,61	2,63	11	LYS	HD2	1,72	1,70	1,72
5	GLU	H	8,42	8,42	8,44	11	LYS	HD3	1,72	1,70	1,72
5	GLU	HA	4,15	4,14	4,15	11	LYS	HE2	3,01	3,00	3,02
5	GLU	HB2	1,88	1,86	1,89	11	LYS	HE3	3,01	3,00	3,02
5	GLU	HB3	2,15	2,13	1,89	11	LYS	HZ			6,87
5	GLU	HG2	2,21	2,21	2,15	12	PRO	HA	4,46	4,44	4,47
5	GLU	HG3	2,21	2,21	2,22	12	PRO	HB2	1,89	1,88	2,07
6	HIS	H	8,30	8,28	8,24	12	PRO	HB3	2,26	2,27	2,30
6	HIS	HA	4,50	4,50	4,49	12	PRO	HG2	2,00	2,04	
6	HIS	HB2	2,99	2,98	3,02	12	PRO	HG3	2,05	2,04	
6	HIS	HB3	3,04	3,04	3,02	12	PRO	HD2	3,63	3,63	3,65
7	PHE	H	8,14	8,14	8,11	12	PRO	HD3	3,83	3,82	3,84
7	PHE	HA	4,56	4,55	4,54	12	PRO	HG2			1,92
7	PHE	HB2	2,94	2,95	2,99	12	PRO	HG3			2,03
7	PHE	HB3	2,94	2,95	2,99	13	VAL	H	8,43	8,41	8,40
7	PHE	HD1	7,12	7,12		13	VAL	HA	4,13	4,13	4,05
7	PHE	HD2	7,12	7,12		13	VAL	HB	2,08	2,08	2,07
7	PHE	HZ	6,82			13	VAL	QQG	0,98	0,97	1,00
6	PHE	HE1	7,26			14	GLY	H	8,60	8,59	
7	PHE	HE2	7,26			14	GLY	HA2	3,96	3,96	
8	ARG	H	8,26	8,27	8,22	14	GLY	HA3	4,00	3,96	
8	ARG	HA	4,19	4,19	4,18	15	LYS	H	8,42	8,41	
8	ARG	HB2	1,55	1,55	1,56	15	LYS	HA	4,33	4,34	
8	ARG	HB3	1,55	1,55	1,56	15	LYS	HB2	1,75	1,83	
8	ARG	HG2	1,26	1,26	1,26	15	LYS	HB3	1,84	1,83	
8	ARG	HG3	1,31	1,31	1,32	15	LYS	HG2	1,45	1,45	
8	ARG	HD2	3,02	3,02	3,03	15	LYS	HG3	1,45	1,45	
8	ARG	HD3	3,02	3,02	3,03	15	LYS	HD2	1,70	1,69	
8	ARG	HE	7,18		7,16	15	LYS	HD3	1,70	1,69	
9	TRP	H	8,19	8,20	8,15	15	LYS	HE2	3,01	2,86	
9	TRP	HA	4,70	4,70	4,69	15	LYS	HE3	3,01	3,00	

Figure 8.7: Table.1: Comparison of ACTH(1-39)/Cys and α-MSH chemical shifts. Overlay of Δ HA chemical shifts of ACTH(1-39) (Peptides and Elephants) and acetylated α-MSH to ACTH(1-39)C.

#	RES	ATOM	Chemical Shift			#	RES	ATOM	Chemical Shift		
			ACTH	ACTH(1-39)C	α-MSH				ACTH	ACTH(1-39)C	α-MSH
16	LYS	H	8,50	8,49		21	LYS	HD2	1,61	1,61	
16	LYS	HA	4,32	4,32		21	LYS	HD3	1,70	1,69	
16	LYS	HB2	1,78	1,75		21	LYS	HE2	2,87		
16	LYS	HB3	1,82	1,81		21	LYS	HE3	2,87		
16	LYS	HG2	1,48	1,46		22	VAL	H	8,21	8,21	
16	LYS	HG3	1,48	1,46		22	VAL	HA	4,15	4,14	
16	LYS	HD2	1,71	1,69		22	VAL	HB	1,93	1,91	
16	LYS	HD3	1,71	1,69		22	VAL	QG1	0,82	0,84	
16	LYS	HE2	3,01	2,97		22	VAL	QG2	0,88	0,87	
16	LYS	HE3	3,01	2,97		23	TYR	H	8,63	8,64	
17	ARG	H	8,57	8,56		23	TYR	HA	4,85	4,84	
17	ARG	HA	4,34	4,34		23	TYR	HB2	2,84	2,83	
17	ARG	HB2	1,76	1,76		23	TYR	HB3	3,12	3,08	
17	ARG	HB3	1,84	1,76		23	TYR	HD1	7,16	7,16	
17	ARG	HG2	1,62	1,63		23	TYR	HD2	7,26	7,16	
17	ARG	HG3	1,65	1,63		23	TYR	HE1		7,25	
17	ARG	HD2	3,18	3,19		23	TYR	HE2		7,25	
17	ARG	HD3	3,18	3,19		24	PRO	HA	4,43	4,43	
17	ARG	HE	7,33			24	PRO	HB2	1,99	1,98	
18	ARG	H	8,60	8,59		24	PRO	HB3	2,32	2,31	
18	ARG	HA	4,62	4,61		24	PRO	HG2	2,04	2,03	
18	ARG	HB2	1,76	1,78		24	PRO	HG3	2,04	2,03	
18	ARG	HB3	1,86	1,78		24	PRO	HD2	3,82	3,82	
18	ARG	HE	7,36			24	PRO	HD3	3,82	3,82	
18	ARG	HG2	1,71	1,68		25	ASN	H	8,61	8,64	
18	ARG	HG3	1,71	1,68		25	ASN	HA	4,74	4,74	
18	ARG	HD2	3,20	3,19		25	ASN	HB2	2,91	2,86	
18	ARG	HD3	3,20	3,19		25	ASN	HB3	2,91	2,91	
19	PRO	HA	4,49	4,47		25	ASN	HD21	7,75	7,75	
19	PRO	HB2		2,27		25	ASN	HD22	7,02	7,03	
19	PRO	HB3		2,27		26	GLY	H	8,49	8,49	
19	PRO	HG2	2,00	1,99		26	GLY	HA2	3,91	3,91	
19	PRO	HG3	1,90	1,99		26	GLY	HA3	4,10	4,10	
19	PRO	HD2	3,65	3,63		27	ALA	H	8,18	8,20	
19	PRO	HD3	3,84	3,82		27	ALA	HA	4,36	4,34	
19	PRO		2,29			27	ALA	QB	1,42	1,42	
20	VAL	H	8,38	8,37		28	GLU	H	8,57	8,56	
20	VAL	HA	4,12	4,10		28	GLU	HA	4,28	4,24	
20	VAL	HB	2,06	2,03		28	GLU	HB2	1,94	1,93	
20	VAL	QQG		0,95		28	GLU	HB3	2,05	2,03	
20	VAL	QG1	0,97			28	GLU	HG2	2,28	2,27	
20	VAL	QG2	0,95			28	GLU	HG3	2,28	2,27	
21	LYS	H	8,39	8,40		29	ASP	H	8,34	8,33	
21	LYS	HA	4,31	4,29		29	ASP	HA	4,60	4,57	
21	LYS	HB2	1,65	1,65		29	ASP	HB2	2,57	2,58	
21	LYS	HB3	1,65	1,65		29	ASP	HB3	2,72	2,73	
21	LYS	HG2	1,16	1,15		30	GLU	H	8,56	8,55	
21	LYS	HG3	1,28	1,27		30	GLU	HA	4,31	4,30	

Figure 8.8: Table 2. Comparison of ACTH(1-39)/Cys and α-MSH chemical shifts. Overlay of Δ HA chemical shifts of ACTH(1-39) (Peptides and Elephants) and acetylated α-MSH to ACTH(1-39)C.

#	RES	ATOM	Chemical Shift			#	RES	ATOM	Chemical Shift		
			ACTH	ACTH(1-39)C	α-MSH				ACTH	ACTH(1-39)C	α-MSH
30	GLU	HB2	1,97	1,97		39	PHE	H	8,30	8,36	
30	GLU	HB3	2,14	2,13		39	PHE	HA	4,62	4,73	
30	GLU	HG2	2,26	2,29		39	PHE	HB2	3,00	3,00	
30	GLU	HG3	2,31	2,29		39	PHE	HB3	3,20	3,24	
31	SER	H	8,51	8,51		39	PHE	HD1	7,27	7,26	
31	SER	HA	4,42	4,39		39	PHE	HD2	7,27	7,26	
31	SER	HB2	3,94	3,93		39	PHE	H	7,98		
31	SER	HB3	3,94	3,93		40	CYS	H		7,97	
32	ALA	H	8,33	8,32		40	CYS	HA		4,38	
32	ALA	HA	4,32	4,32		40	CYS	HB2		2,94	
32	ALA	QB	1,42	1,40		40	CYS	HB3		2,94	
33	GLU	H	8,33	8,33							
33	GLU	HA	4,21	4,19							
33	GLU	HB2	1,90	1,91							
33	GLU	HB3	1,99	1,91							
33	GLU	HG2	2,21	2,22							
33	GLU	HG3	2,25	2,22							
34	ALA	H	8,25	8,25							
34	ALA	HA	4,25	4,24							
34	ALA	QB	1,29	1,27							
35	PHE	H	8,28	8,30							
35	PHE	HA	4,87	4,87							
35	PHE	HB2	2,94	2,93							
35	PHE	HB3	3,16	3,15							
35	PHE	HD1	7,29	7,29							
35	PHE	HD2	7,29	7,29							
35	PHE	HE1	7,35								
35	PHE	HE2	7,35								
36	PRO	HA	4,43	4,42							
36	PRO	HB2	1,89	1,89							
36	PRO	HB3	1,99	1,98							
36	PRO	HG2	1,94	1,94							
36	PRO	HG3	2,28	2,26							
36	PRO	HD2	3,50	3,51							
36	PRO	HD3	3,73	3,73							
37	LEU	H	8,46	8,42							
37	LEU	HA	4,31	4,34							
37	LEU	HB2	1,55	1,53							
37	LEU	HB3	1,66	1,66							
37	LEU	HG	1,69	1,69							
37	LEU	QD1	0,98	0,97							
37	LEU	QD2	0,93	0,92							
38	GLU	H	8,39	8,40							
38	GLU	HA	4,27	4,24							
38	GLU	HB2	1,94	1,87							
38	GLU	HB3	2,07	2,05							
37	GLU	HG2	2,32								
38	GLU	HG3	2,32								

Figure 8.9: Table 3. Comparison of ACTH(1-39)/Cys and α-MSH chemical shifts. Overlay of Δ HA chemical shifts of ACTH(1-39) (Peptides and Elephants) and acetylated α-MSH to ACTH(1-39)C.

8.1.1 ACTH Membrane-Interaction in Presence of Calcium

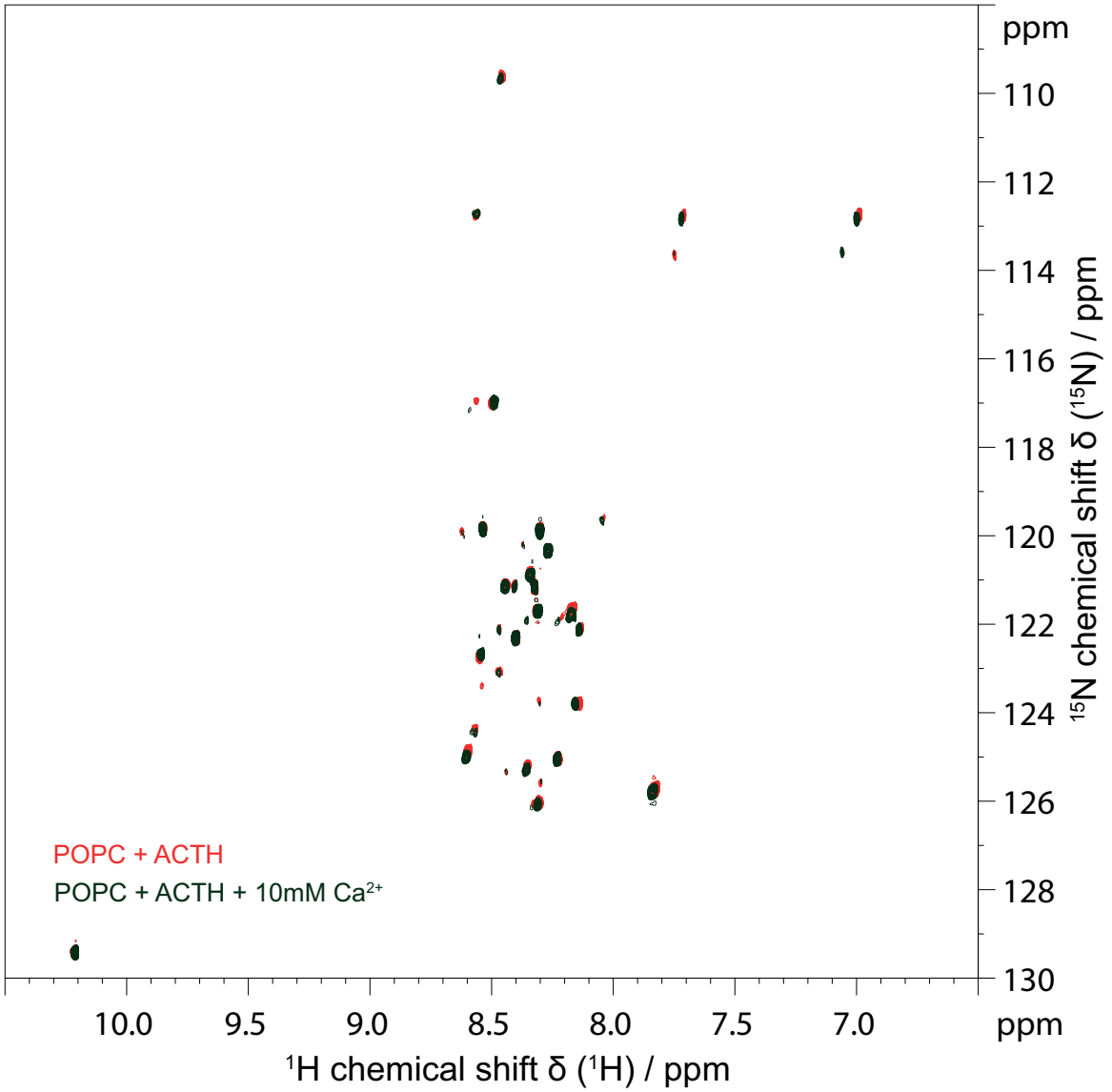

Figure 8.10: ACTH in presence of 100% POPC NDs. Overlay of ^{1}H-, ^{15}N-HSQC spectra showing 30 µM ACTH with 30 µM 100% POPC NDs without (red) and with 10 mM Ca^{2+} (green) at 10 °C.

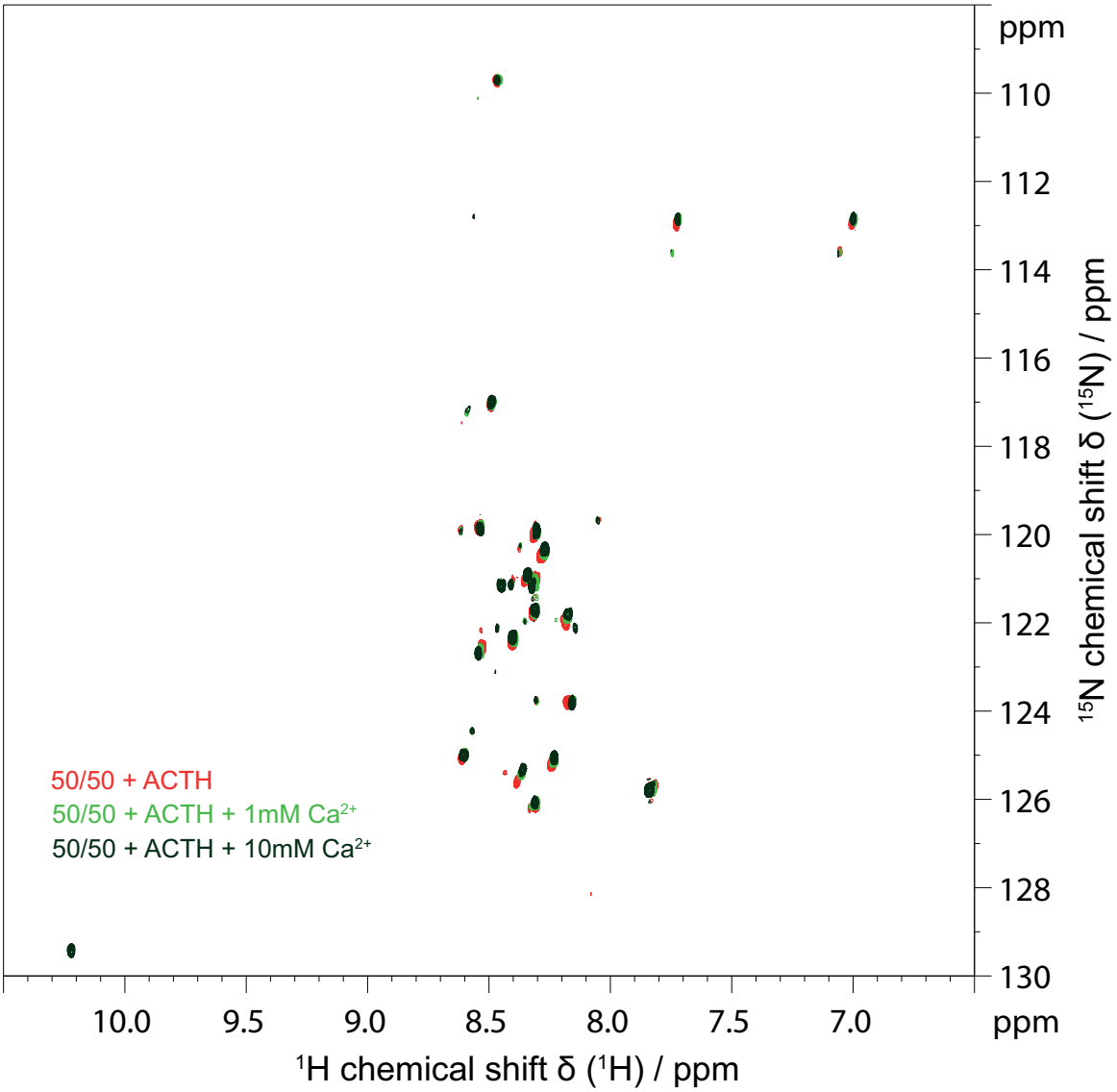

Figure 8.11: ACTH in presence of 50% POPS NDs. Overlay of ^{1}H-, ^{15}N-HSQC spectra showing 30 µM ACTH with 30 µM 50% POPS NDs without (red) and with 1 mM / 10 mM Ca^{2+} (green) at 10 °C.

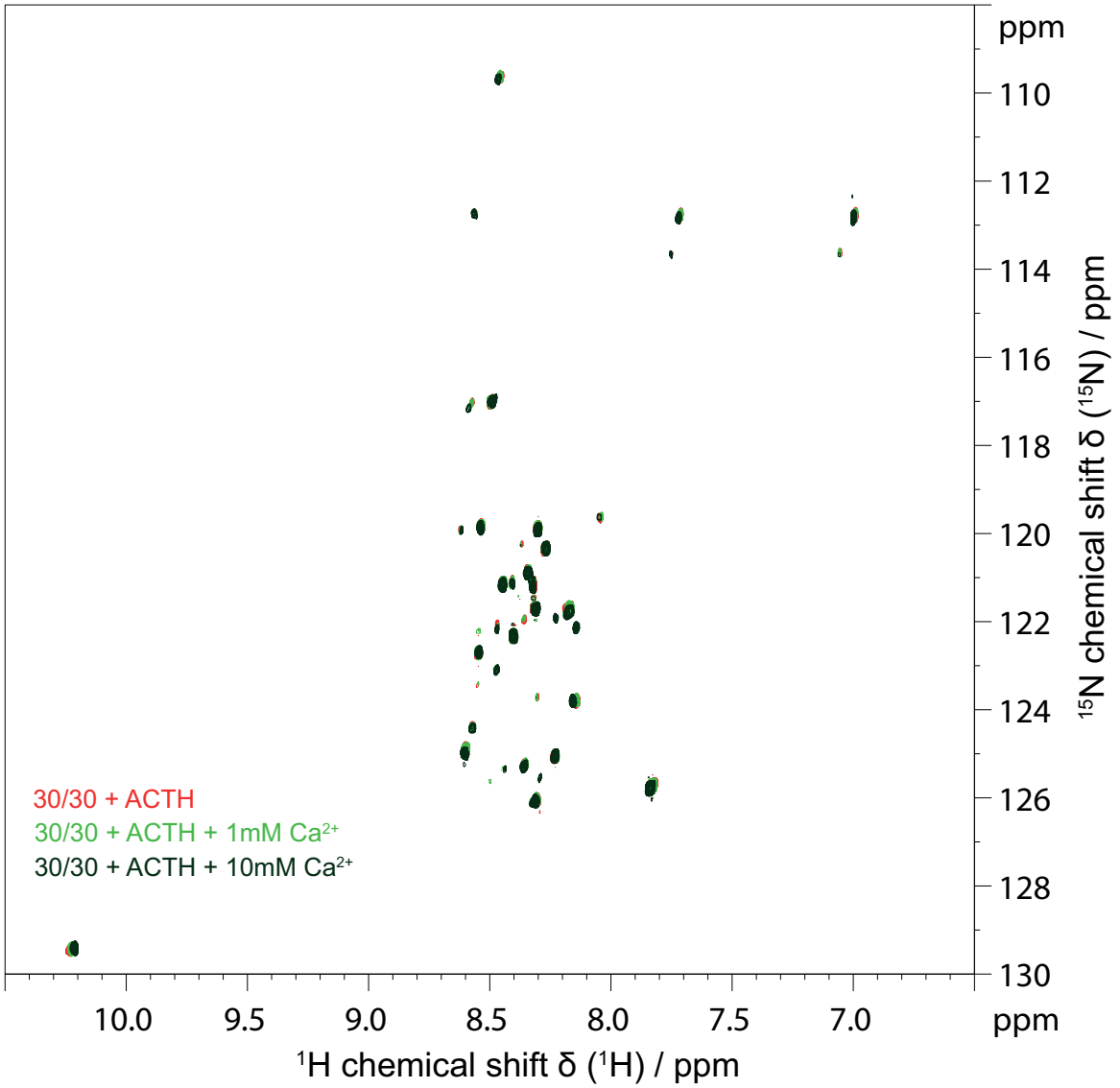

Figure 8.12: ACTH in presence of 30% POPS NDs. Overlay of ^{1}H-, ^{15}N-HSQC spectra showing 30 µM ACTH with 30 µM 30% POPS NDs without (red) and with 1 mM / 10 mM Ca^{2+} (green) at 10 °C.

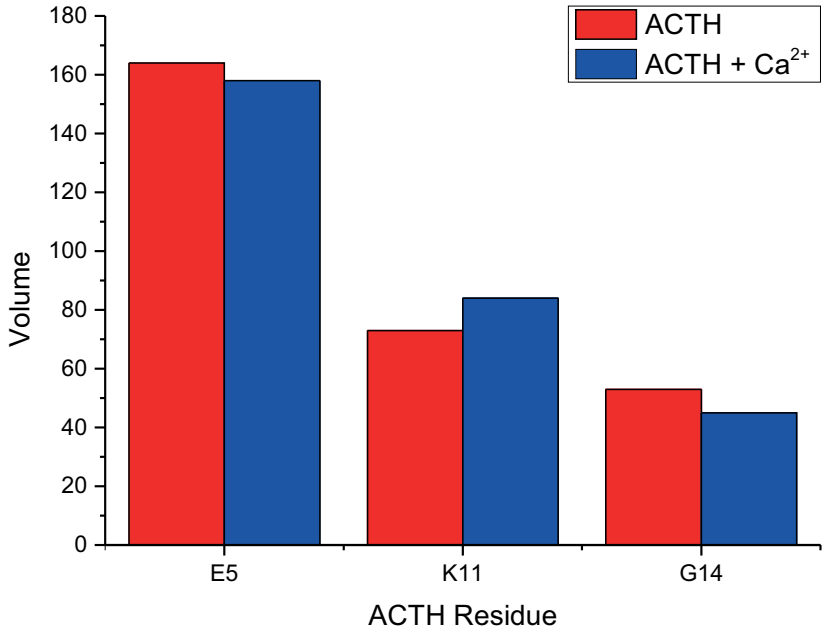

Figure 8.13: Peak volume of ACTH residues is not influenced by calcium. Peak volumes of ACTH residues E5, K11, G14 without (red) and with 10 mM Ca^{2+} (blue) do not essentially differ.

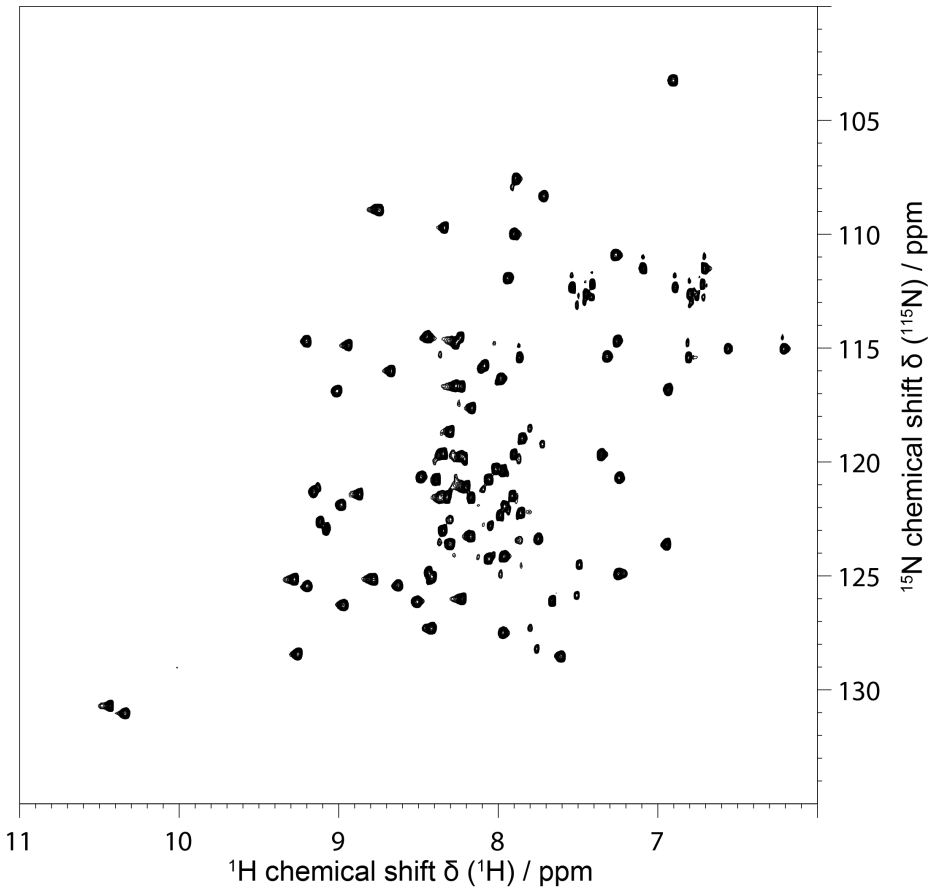

Figure 8.14: HSQC of 6xHis-GB1. HSQC spectrum of 1.3 mM 6xHis-GB1 fusion tag in 50 mM NaPi pH 7.0 with 150 mM NaCl after TEV protease cleavage, purified by SEC.

8.2 Mass Spectrometry

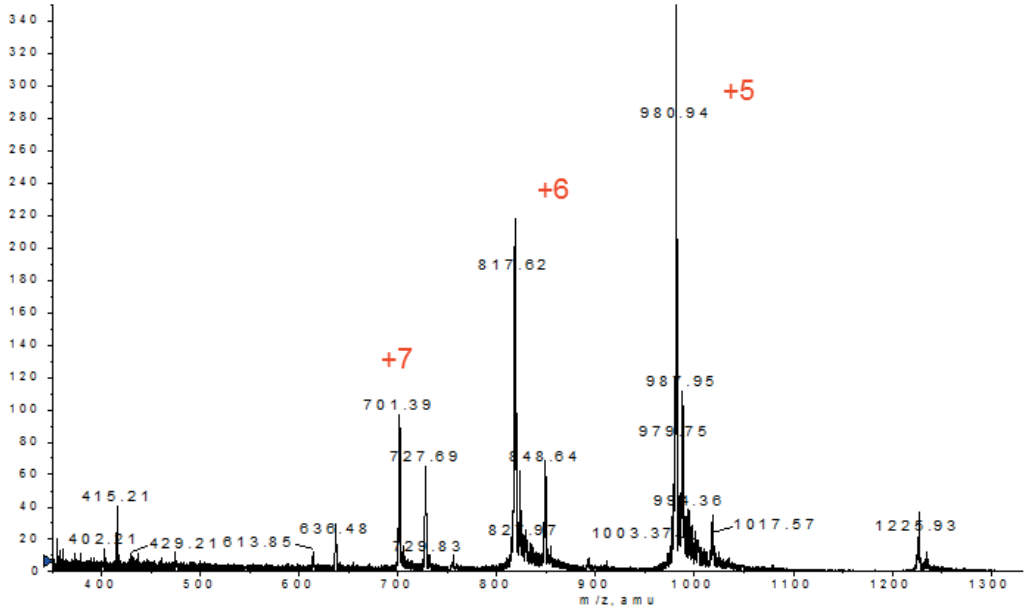

Figure 8.15: Molecular mass of ^{13}C, ^{15}N ACTH(1-39)C was confirmed by MS. ESI MS reveals that peptides with a mass compatible to that of ^{13}C, ^{15}N labeled ACTH(1-39)C could be purified from one SEC peak using RP-HPLC.

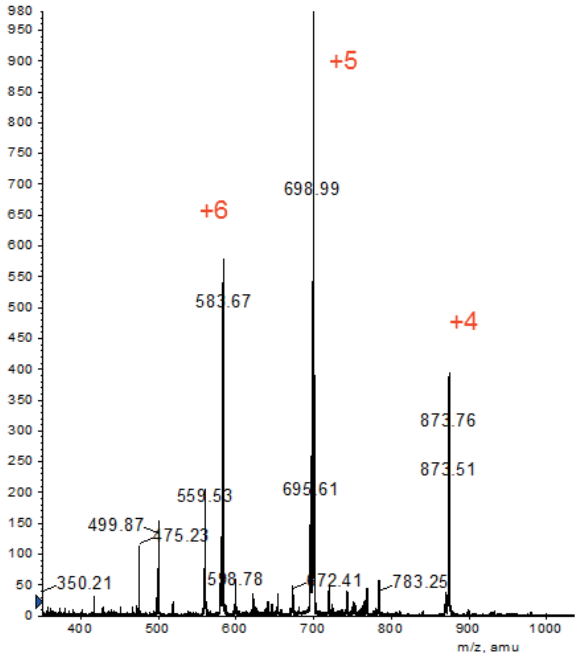

Figure 8.16: ^{13}C, ^{15}N labeled truncated peptide ACTH(1-28) ESI mass spectrometry reveals that a peptides of approximately a mass according to 28 ACTH(1-28) was purified from ACTH(1-39)C expression by SEC.

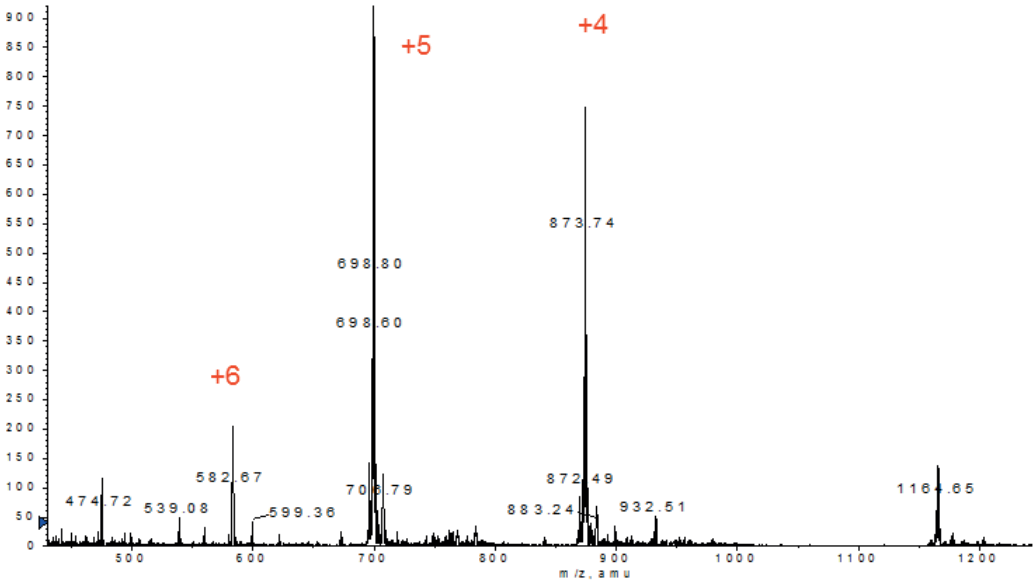

Figure 8.17: ACTH(1-39) gained from ^{13}C, ^{15}N ACTH(1-39)C SEC peak. ESI MS reveals that peptides with a mass compatible to that of ^{13}C, ^{15}N labeled ACTH(1-39) could be purified from ACTH(1-39)C expression via SEC and RP-HPLC.

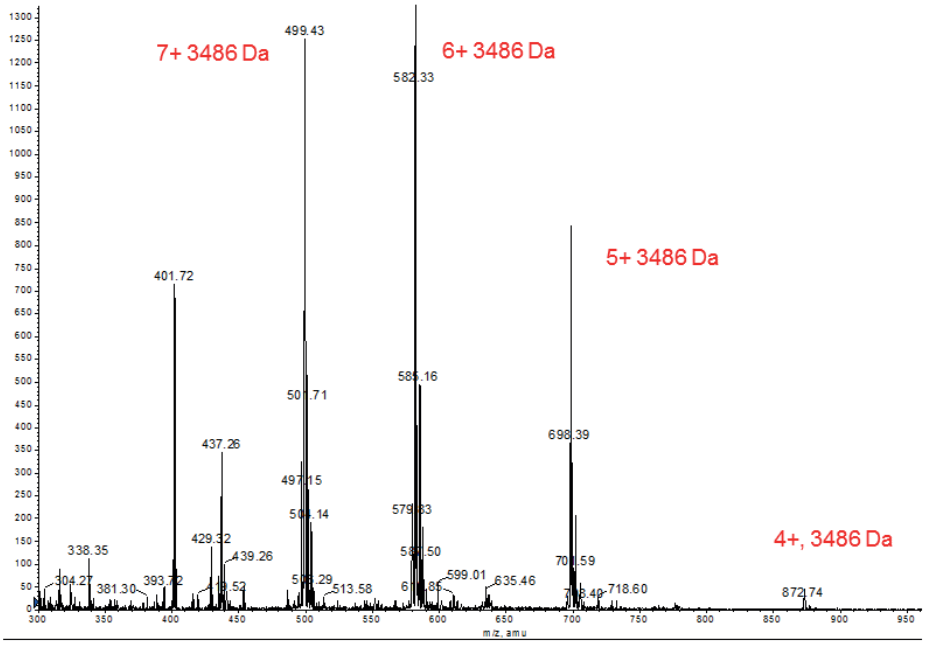

Figure 8.18: Mass Spectrometry data of ACTH(1-23)C-Totapol conjugate. ESI MS determined molecule size according to the ACTH(1-23)C-Totapol conjugate.

8.3 cAMP-based Bioassay

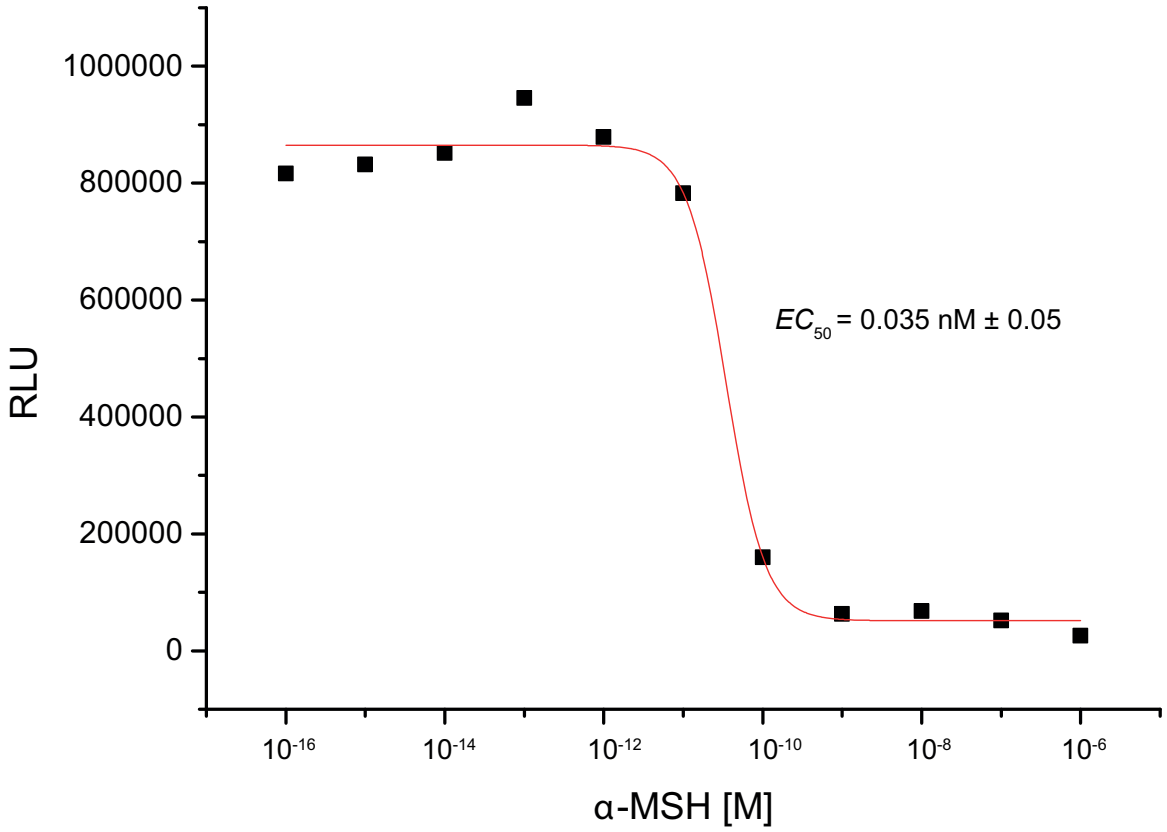

Figure 8.19: Activation of MC4R by α-MSH. Down stream activation of MC4R was recorded in a cAMP-bioassay after incubation of SF-MC4R-6xHis transfected HEK 293-F cells (24,000 / well) with an increasing concentration of α-MSH (Tocris). An EC_{50} = 0.035 ± 0.007 nM was calculated. RLU values for the described conditions are displayed as black squares, the corresponding curve fit is shown as a red curve.

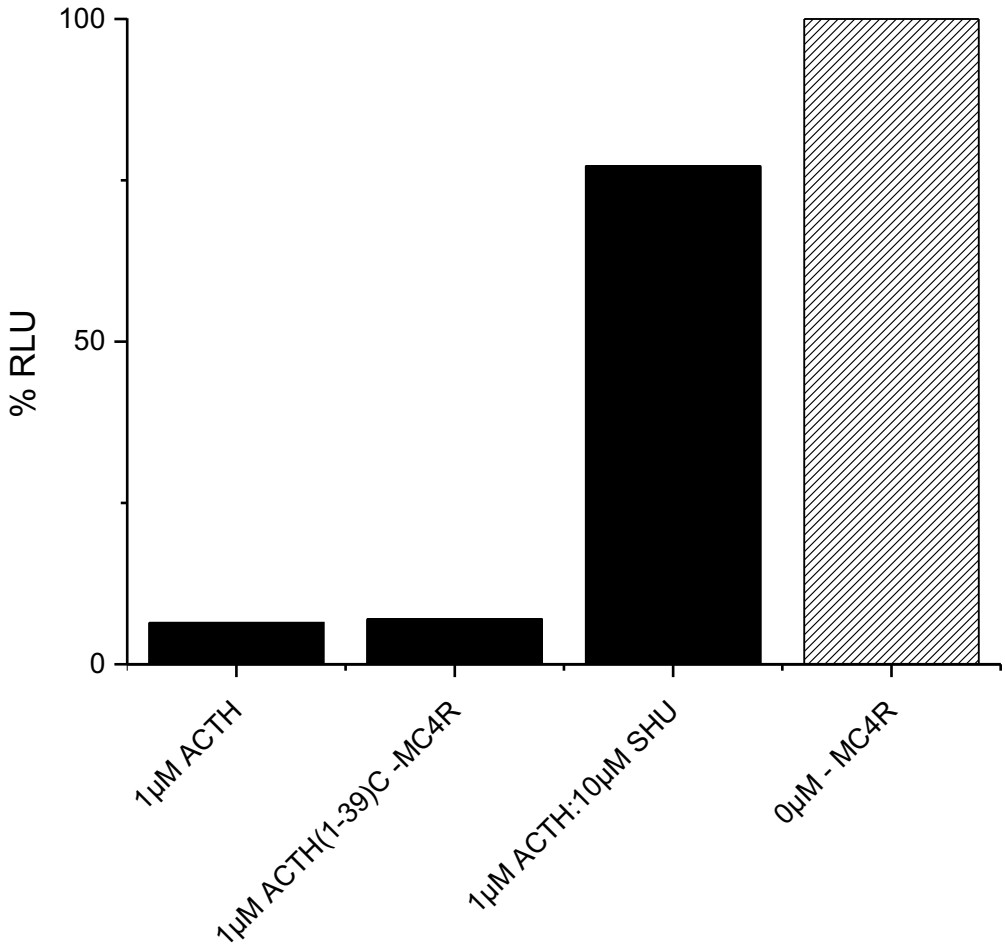

Figure 8.20: Competitive cAMP assay. MC4R activation by 1 µM ACTH (Ana Spec) alone and in presence of a 10-fold excess (10 µM) SHU 9119 (synthetic antagonist). Untreated (no ligand) SF-MC4R-6xHis expressing cells are depicted as hatched bars. Receptor activity is displayed by the decrease of relative luminescence (RLU) in % (100% = MC4R expressing cells without ligand (Ctrl.)). SHU 9119 decreases ACTH mediated MC4R activation.

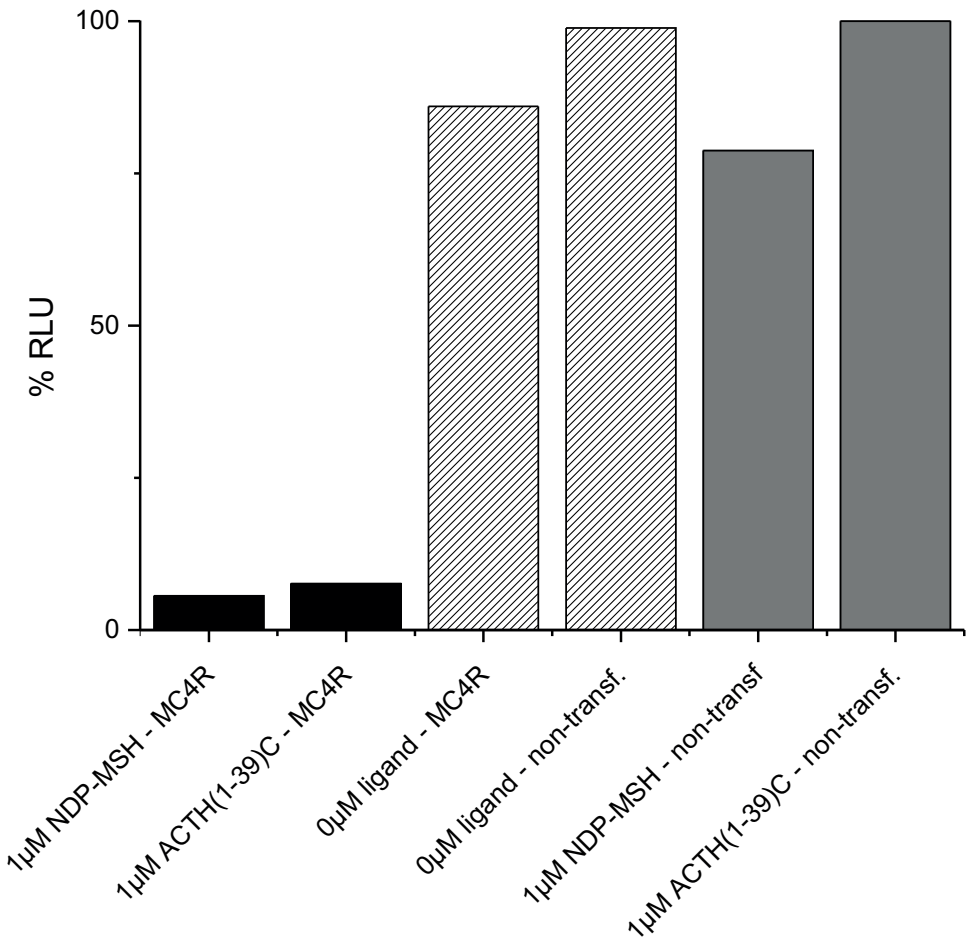

Figure 8.21: Specificity of cAMP assay. Non-transfected (gray) and SF-MC4R expressing (black) HEK 293-F cells were incubated with 1 µM ACTH or NDP-α-MSH to exclude an unspecific ligand mediated luminescence decrease without receptor activation. Untreated (no ligand) non-transfected and SF-MC4R-6xHis expressing cells are depicted as hatched bars. Receptor activity is displayed by the decrease of relative luminescence (RLU) in % (100% = non-transfected cells with 0 µM ligand (Ctrl.)). No unspecific signal decrease is observed.

8.4 Fluorescence Anisotropy

A comparison of membrane interactions of ACTH(1-23)C-647 and the smaller ligand α-MSH-Rhodamine (Phoenix Peptides, INC.) - according to the first 13 amino acids of ACTH - is shown in figure 8.22. Binding was tested in a HEPES buffer using NDs with 50% negative charge (50% POPS / 50% POPC).

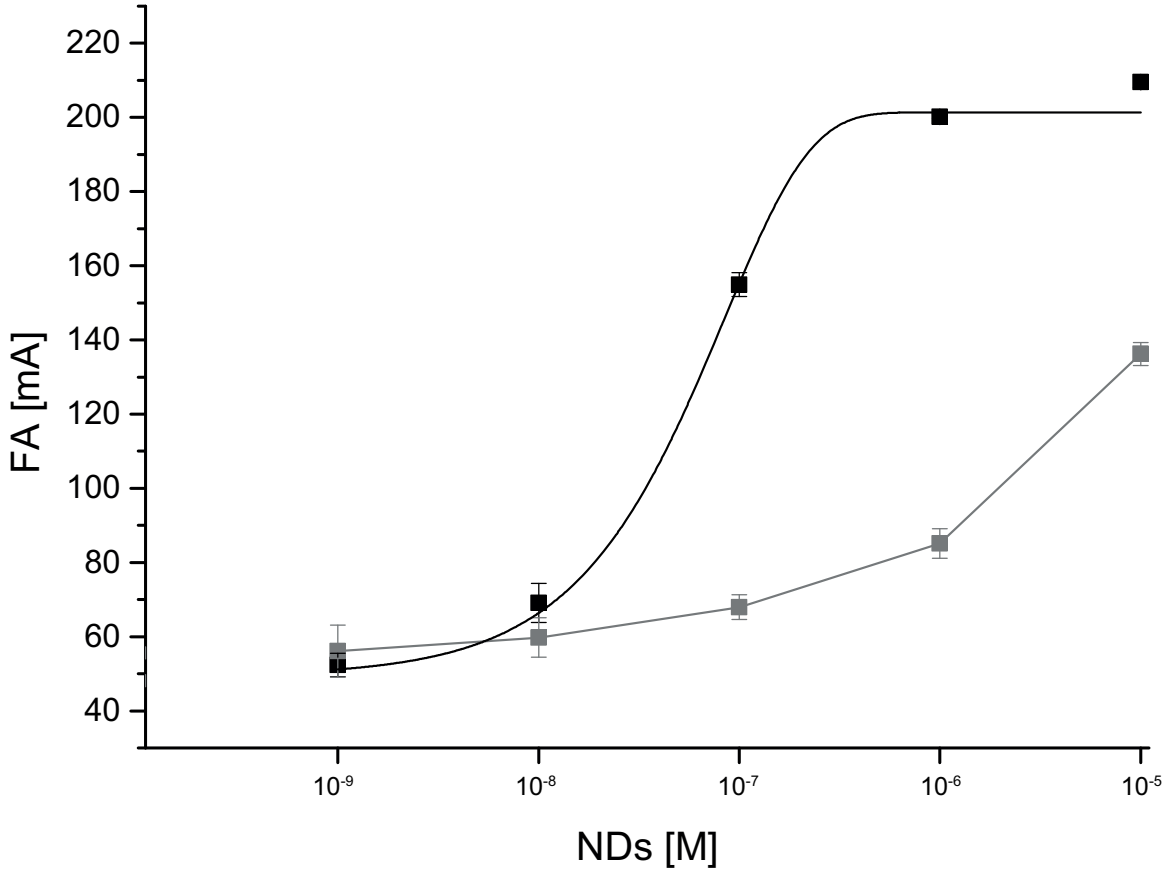

Figure 8.22: Binding affinity of α-MSH to NDs varies from ACTH(1-23)C. FA values and fits for the interaction of 100 nM ACTH(1-23)C-647 (black) or α-MSH-Rhodamine with (gray) in the presence of an increasing concentration of nanodiscs (50% POPS / 50% POPC) at 23 °C, respectively.

A lower binding affinity of α-MSH-Rhodamine to the NDs with respect to ACTH(1-23)C-647 could be observed. Differences could be due to the lower number of amino acids interacting but also due to the different dye attached to the C-terminus of the peptide, as well as its N-terminal acetylation.

To verify if specific hormone-receptor interaction can be observed in a membrane preparation of MC4R expressing insect cells ligand binding was not only studied with 10 mM $CaCl_2$ and without calcium but also in a competition assay in presence of 10 mM Ca^{2+}. Ligand binding was studied in presence of a decreasing concentration of membrane fragments. For competition a 20-fold excess of SHU9119 (Tocris) was applied to a serial dilution of membrane preparation before adding 40 nM of ACTH(1-23)C-647.

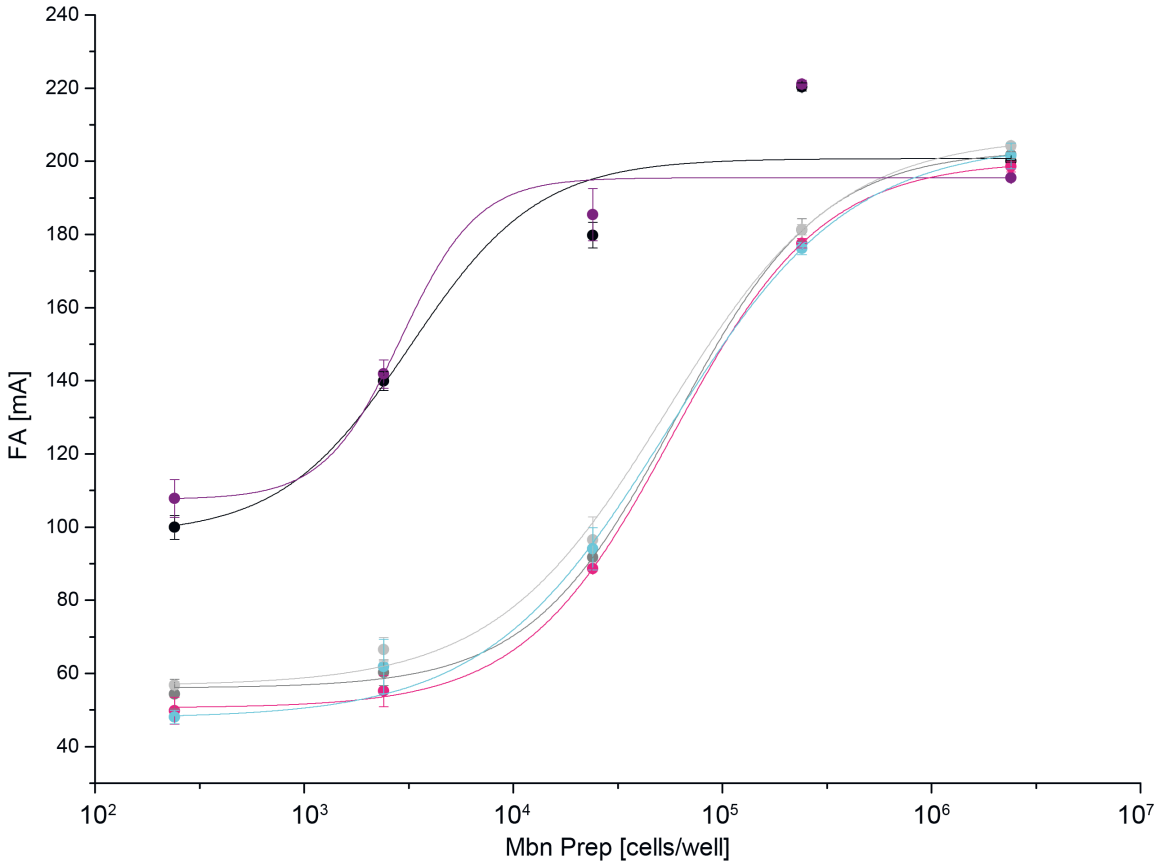

Figure 8.23: Calcium disrupts ACTH interaction with Tnao38 membrane. Binding of 40 nM ACTH(1-23)C-647 to a membrane preparation from Tnao38 insect cells expressing SF-MC4R-6xHis (MC4R) was measured at 28 °C. Membrane preparation was diluted in buffer either containing 0 mM or 10 mM $CaCl_2$. Additionally replacement of ACTH by a 20-fold excess of SHU 9119 (Tocris) was tested.

Differences in the binding curves with and without calcium show a strong reduction of unspecific interaction in presence of 10 mM calcium. Specific binding of ACTH can not be detected as there are no significant differences between curves with ACTH and calcium and ACTH competing with SHU9119 in presence of calcium. If there was specific hormone-receptor interaction ACTH(1-23)C-647 should not be able to bind in a 20-fold excess of the strong agonist SHU9119 an therefore differences should be visible when compared to 40 nM ACTH with 10 mM Ca^{2+}. Possibly the high concentration of calcium does inhibit the interaction of the receptor with its ligand. At the other hand 10 mM calcium was not sufficient to completely block unspecific interaction. Further optimization will be necessary to set up a FA based binding assay in presence of natural membranes. Nevertheless the use of calcium will be absolutely essential to avoid unspecific interaction of the peptides with membranes.

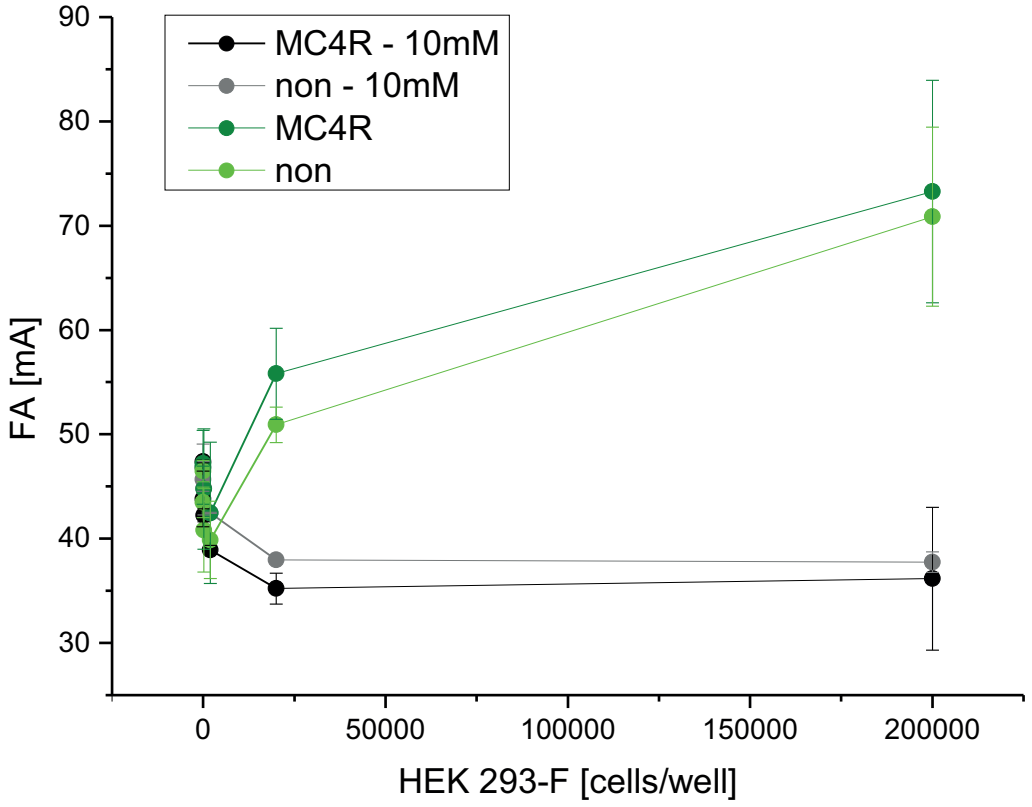

Figure 8.24: Calcium disrupts unspecific ACTH interaction with HEK 293F cells. Binding of 40 nM ACTH(1-23)C-647 to HEK 293F cells not transfected (non) and transfected with pHL-IRES-SF-MC4R-6xHis (MC4R) was observed at 30 °C without and in the presence of 10 mM $CaCl_2$ using FA. Cells were diluted in a 1:10 serial dilution starting at $2x10^5$ cells / well (SD n=2) before adding the ligand.

9

Acknowledgments

I would like to thank my doctorate supervisor Dr. Manuel Etzkorn for choosing me to be the first PhD candidate in his workgroup. I appreciate his steady support, patience and enthusiasm. I am especially grateful for the possibility to realize my own ideas in a second project.

Furthermore I would like to thank Prof. Dr. Georg Groth for mentoring me and Prof. Dr. Willbold for giving me the possibility to work in his institute. My sincerest thanks goes to my workgroup and lab colleagues for their support and for always being available for intense data discussion. Special thanks goes to Dr. Aldino Viegas who performed almost all NRM experiments including data processing and assignments. He helped me to learn how to read my data and his dedication for research was always motivating me. Further thanks goes to Thibault Viennet and Laetitia Heid for providing nanodiscs used in this work.
Realization of the HIV-1 Vpr project would not have been possible without Shantha Elter offering me to use her cell-free expression system and sharing her experience how to gain optimal plasmid and protein yields in this setup. Further thanks goes to Steffen Mielenbrink and Maria Dahlhaus who worked with me in the lab as undergraduate students and helped me to make considerable progress in my project, as well as Dr. Oliver Bannach and Michael Wörderhoff who helped me to record LSM data of fixated cells.

I would also like to thank Prof. Dr. Gerhard Wagner and Dr. James J. Yu (Department of Biological Chemistry and Molecular Pharmacology at Harvard Medical School, Boston, USA). Prof. Dr. Gerhard Wagner for giving me the great opportunity to work in his lab for one month. Dr. Yames J. Yu for teaching me how to cultivate HEK 293 cells for expression of recombinant proteins as well as for designing the pHLIRES-SF-MC4R-6xHis construct. I enjoyed my stay in the Wagner Lab especially due to the openess and kindness of the people working there. I would also like to acknowledge that Dr. Baran Ersoy (Harvard Medical School) provided different MC4R-expression vectors for my work.

Furthermore, I would like to thank my cooperation partners Prof. Dr. Loidl-Stahlhofen (University of Applied Sciences Gelsenkirchen) and Dr. Karen Hänel (Jülich Research Center) for for providing HIV-1 Vpr constructs and for chairing their expertise on this project with me.

My special thanks goes to Dipl.-Oecotroph. Monika Brummel (FH Münster) for sharing her broad knowledge on the topic of HIV-1 Vpr but also for beeing a friend for many years.

Further thanks goes to Prof. Dr. Reza Ahmadian (HHU Düsseldorf) and Marcel Falke (HHU Düsseldorf) for providing Tnao38 insect cells and to Dr. Vlado Gelev (Sofia University, Bulgaria) for providing maleimide-TOTAPOL.

I also acknowledge access to the Jülich-Düsseldorf Biomolecular NMR Center and thank the DFG for support through the Emmy Noether grant ET103/2-1 to Manuel Etzkorn.

Bibliography

[1] R. Fredriksson, M. C. Lagerstrom, L. G. Lundin, and H. B. Schioth. The g-protein-coupled receptors in the human genome form five main families. phylogenetic analysis, paralogon groups, and fingerprints. *Mol Pharmacol*, 63(6):1256–72, 2003.

[2] Kelly E Marrion N Peters JA Benson HE Faccenda E Pawson AJ Sharman JL Southan C Davies JA Alexander SPH, Davenport AP and CGTP Collaborators. The concise guide to pharmacology 2015/16: G protein-coupled receptors, 2015.

[3] T. Klabunde and G. Hessler. Drug design strategies for targeting g-protein-coupled receptors. *Chembiochem*, 3(10):928–44, 2002.

[4] J. P. Overington, B. Al-Lazikani, and A. L. Hopkins. How many drug targets are there? *Nat Rev Drug Discov*, 5(12):993–6, 2006.

[5] K. L. Pierce, R. T. Premont, and R. J. Lefkowitz. Seven-transmembrane receptors. *Nat Rev Mol Cell Biol*, 3(9):639–50, 2002.

[6] T. Kenakin. Inverse, protean, and ligand-selective agonism: matters of receptor conformation. *FASEB J*, 15(3):598–611, 2001.

[7] M. E. Cvijic, C. S. Sum, A. Alt, and L. Zhang. Gpcr profiling: from hits to leads and from genotype to phenotype. *Drug Discov Today Technol*, 18:30–7, 2015.

[8] T. Flock, C. N. Ravarani, D. Sun, A. J. Venkatakrishnan, M. Kayikci, C. G. Tate, D. B. Veprintsev, and M. M. Babu. Universal allosteric mechanism for galpha activation by gpcrs. *Nature*, 524(7564):173–9, 2015.

[9] M. Strathmann and M. I. Simon. G protein diversity: a distinct class of alpha subunits is present in vertebrates and invertebrates. *Proc Natl Acad Sci U S A*, 87(23):9113–7, 1990.

[10] M. P. Strathmann and M. I. Simon. G alpha 12 and g alpha 13 subunits define a fourth class of g protein alpha subunits. *Proc Natl Acad Sci U S A*, 88(13):5582–6, 1991.

[11] Y. Oka and S. I. Korsching. The fifth element in animal galpha protein evolution. *Commun Integr Biol*, 2(3):227–9, 2009.

[12] Y. Imoto, A. Yatani, J. P. Reeves, J. Codina, L. Birnbaumer, and A. M. Brown. Alpha-subunit of gs directly activates cardiac calcium channels in lipid bilayers. *Am J Physiol*, 255(4 Pt 2):H722–8, 1988.

[13] R. R. Mirotznik, X. Zheng, and E. F. Stanley. G-protein types involved in calcium channel inhibition at a presynaptic nerve terminal. *J Neurosci*, 20(20):7614–21, 2000.

[14] V. V. Gurevich and E. V. Gurevich. The structural basis of arrestin-mediated regulation of g-protein-coupled receptors. *Pharmacol Ther*, 110(3):465–502, 2006.

[15] K. Jalink and W. H. Moolenaar. G protein-coupled receptors: the inside story. *Bioessays*, 32(1):13–6, 2010.

[16] A. J. Venkatakrishnan, X. Deupi, G. Lebon, C. G. Tate, G. F. Schertler, and M. M. Babu. Molecular signatures of g-protein-coupled receptors. *Nature*, 494(7436):185–94, 2013.

[17] R. O. Dror, A. C. Pan, D. H. Arlow, D. W. Borhani, P. Maragakis, Y. Shan, H. Xu, and D. E. Shaw. Pathway and mechanism of drug binding to g-protein-coupled receptors. *Proc Natl Acad Sci U S A*, 108(32):13118–23, 2011.

[18] C. O'Connor, K. L. White, N. Doncescu, T. Didenko, B. L. Roth, G. Czaplicki, R. C. Stevens, K. Wuthrich, and A. Milon. Nmr structure and dynamics of the agonist dynorphin peptide bound to the human kappa opioid receptor. *Proc Natl Acad Sci U S A*, 112(38):11852–7, 2015.

[19] S. Luca, J. F. White, A. K. Sohal, D. V. Filippov, J. H. van Boom, R. Grisshammer, and M. Baldus. The conformation of neurotensin bound to its g protein-coupled receptor. *Proc Natl Acad Sci U S A*, 100(19):10706–11, 2003.

[20] F. Al-Obeidi, V. J. Hruby, A. M. Castrucci, and M. E. Hadley. Design of potent linear alpha-melanotropin 4-10 analogues modified in positions 5 and 10. *J Med Chem*, 32(1):174–9, 1989.

[21] F. Al-Obeidi, A. M. Castrucci, M. E. Hadley, and V. J. Hruby. Potent and prolonged acting cyclic lactam analogues of alpha-melanotropin: design based on molecular dynamics. *J Med Chem*, 32(12):2555–61, 1989.

[22] J. Oosterom, W. A. Nijenhuis, W. M. Schaaper, J. Slootstra, R. H. Meloen, W. H. Gispen, J. P. Burbach, and R. A. Adan. Conformation of the core sequence in melanocortin peptides directs selectivity for the melanocortin mc3 and mc4 receptors. *J Biol Chem*, 274(24):16853–60, 1999.

[23] J. J. Liu, R. Horst, V. Katritch, R. C. Stevens, and K. Wuthrich. Biased signaling pathways in beta2-adrenergic receptor characterized by 19f-nmr. *Science*, 335(6072):1106–10, 2012.

[24] A. Breit, T. R. Buch, I. Boekhoff, H. J. Solinski, E. Damm, and T. Gudermann. Alternative g protein coupling and biased agonism: new insights into melanocortin-4 receptor signalling. *Mol Cell Endocrinol*, 331(2):232–40, 2011.

[25] P. S. Chae, S. G. Rasmussen, R. R. Rana, K. Gotfryd, R. Chandra, M. A. Goren, A. C. Kruse, S. Nurva, C. J. Loland, Y. Pierre, D. Drew, J. L. Popot, D. Picot, B. G. Fox, L. Guan, U. Gether, B. Byrne, B. Kobilka, and S. H. Gellman. Maltose-neopentyl glycol (mng) amphiphiles for solubilization, stabilization and crystallization of membrane proteins. *Nat Methods*, 7(12):1003–8, 2010.

[26] M. J. Serrano-Vega, F. Magnani, Y. Shibata, and C. G. Tate. Conformational thermostabilization of the beta1-adrenergic receptor in a detergent-resistant form. *Proc Natl Acad Sci U S A*, 105(3):877–82, 2008.

[27] K. Palczewski, T. Kumasaka, T. Hori, C. A. Behnke, H. Motoshima, B. A. Fox, I. Le Trong, D. C. Teller, T. Okada, R. E. Stenkamp, M. Yamamoto, and M. Miyano. Crystal structure of rhodopsin: A g protein-coupled receptor. *Science*, 289(5480):739–45, 2000.

[28] C. K. Engel, L. Chen, and G. G. Prive. Insertion of carrier proteins into hydrophilic loops of the escherichia coli lactose permease. *Biochim Biophys Acta*, 1564(1):38–46, 2002.

[29] D. M. Rosenbaum, V. Cherezov, M. A. Hanson, S. G. Rasmussen, F. S. Thian, T. S. Kobilka, H. J. Choi, X. J. Yao, W. I. Weis, R. C. Stevens, and B. K. Kobilka. Gpcr engineering yields high-resolution structural insights into beta2-adrenergic receptor function. *Science*, 318(5854):1266–73, 2007.

[30] E. Chun, A. A. Thompson, W. Liu, C. B. Roth, M. T. Griffith, V. Katritch, J. Kunken, F. Xu, V. Cherezov, M. A. Hanson, and R. C. Stevens. Fusion partner toolchest for the stabilization and crystallization of g protein-coupled receptors. *Structure*, 20(6):967–76, 2012.

[31] J. F. White, N. Noinaj, Y. Shibata, J. Love, B. Kloss, F. Xu, J. Gvozdenovic-Jeremic, P. Shah, J. Shiloach, C. G. Tate, and R. Grisshammer. Structure of the agonist-bound neurotensin receptor. *Nature*, 490(7421):508–13, 2012.

[32] B. E. Krumm and R. Grisshammer. Peptide ligand recognition by g protein-coupled receptors. *Front Pharmacol*, 6:48, 2015.

[33] G. Skretas and G. Georgiou. Engineering g protein-coupled receptor expression in bacteria. *Proc Natl Acad Sci U S A*, 105(39):14747–8, 2008.

[34] M. Salzmann, K. Pervushin, G. Wider, H. Senn, and K. Wuthrich. Trosy in triple-resonance experiments: new perspectives for sequential nmr assignment of large proteins. *Proc Natl Acad Sci U S A*, 95(23):13585–90, 1998.

[35] A. Sitarska, L. Skora, J. Klopp, S. Roest, C. Fernandez, B. Shrestha, and A. D. Gossert. Affordable uniform isotope labeling with (2)h, (13)c and (15)n in insect cells. *J Biomol NMR*, 62(2):191–7, 2015.

[36] C. G. Tate. Overexpression of mammalian integral membrane proteins for structural studies. *FEBS Lett*, 504(3):94–8, 2001.

[37] Y. Aponte, D. Atasoy, and S. M. Sternson. Agrp neurons are sufficient to orchestrate feeding behavior rapidly and without training. *Nat Neurosci*, 14(3):351–5, 2011.

[38] M. J. Krashes, S. Koda, C. Ye, S. C. Rogan, A. C. Adams, D. S. Cusher, E. Maratos-Flier, B. L. Roth, and B. B. Lowell. Rapid, reversible activation of agrp neurons drives feeding behavior in mice. *J Clin Invest*, 121(4):1424–8, 2011.

[39] C. Zhan, J. Zhou, Q. Feng, J. E. Zhang, S. Lin, J. Bao, P. Wu, and M. Luo. Acute and long-term suppression of feeding behavior by pomc neurons in the brainstem and hypothalamus, respectively. *J Neurosci*, 33(8):3624–32, 2013.

[40] M. W. Schwartz, R. J. Seeley, S. C. Woods, D. S. Weigle, L. A. Campfield, P. Burn, and D. G. Baskin. Leptin increases hypothalamic pro-opiomelanocortin mrna expression in the rostral arcuate nucleus. *Diabetes*, 46(12):2119–23, 1997.

[41] L. E. Pritchard, A. V. Turnbull, and A. White. Pro-opiomelanocortin processing in the hypothalamus: impact on melanocortin signalling and obesity. *J Endocrinol*, 172(3):411–21, 2002.

[42] D. J. MacNeil, A. D. Howard, X. Guan, T. M. Fong, R. P. Nargund, M. A. Bednarek, M. T. Goulet, D. H. Weinberg, A. M. Strack, D. J. Marsh, H. Y. Chen, C. P. Shen, A. S. Chen, C. I. Rosenblum, T. MacNeil, M. Tota, E. D. MacIntyre, and L. H. Van der Ploeg. The role of melanocortins in body weight regulation: opportunities for the treatment of obesity. *Eur J Pharmacol*, 450(1):93–109, 2002.

[43] Y. X. Tao. The melanocortin-4 receptor: physiology, pharmacology, and pathophysiology. *Endocr Rev*, 31(4):506–43, 2010.

[44] L. H. Van der Ploeg, W. J. Martin, A. D. Howard, R. P. Nargund, C. P. Austin, X. Guan, J. Drisko, D. Cashen, I. Sebhat, A. A. Patchett, D. J. Figueroa, A. G. DiLella, B. M. Connolly, D. H. Weinberg, C. P. Tan, O. C. Palyha, S. S. Pong, T. MacNeil, C. Rosenblum, A. Vongs, R. Tang, H. Yu, A. W. Sailer, T. M. Fong, C. Huang, M. R. Tota, R. S. Chang, R. Stearns, C. Tamvakopoulos, G. Christ, D. L. Drazen, B. D. Spar, R. J. Nelson, and D. E. MacIntyre. A role for the melanocortin 4 receptor in sexual function. *Proc Natl Acad Sci U S A*, 99(17):11381–6, 2002.

[45] D. Huszar, C. A. Lynch, V. Fairchild-Huntress, J. H. Dunmore, Q. Fang, L. R. Berkemeier, W. Gu, R. A. Kesterson, B. A. Boston, R. D. Cone, F. J. Smith, L. A. Campfield, P. Burn, and F. Lee. Targeted disruption of the melanocortin-4 receptor results in obesity in mice. *Cell*, 88(1):131–41, 1997.

[46] G. S. Yeo, E. J. Lank, I. S. Farooqi, J. Keogh, B. G. Challis, and S. O'Rahilly. Mutations in the human melanocortin-4 receptor gene associated with severe familial obesity disrupts receptor function through multiple molecular mechanisms. *Hum Mol Genet*, 12(5):561–74, 2003.

[47] K. Midthjell, C. M. Lee, A. Langhammer, S. Krokstad, T. L. Holmen, K. Hveem, S. Colagiuri, and J. Holmen. Trends in overweight and obesity over 22 years in a large adult population: the hunt study, norway. *Clin Obes*, 3(1-2):12–20, 2013.

[48] C. L. Ogden, M. M. Lamb, M. D. Carroll, and K. M. Flegal. Obesity and socioeconomic status in adults: United states, 2005-2008. *NCHS Data Brief*, (50):1–8, 2010.

[49] B. A. Ersoy, L. Pardo, S. Zhang, D. A. Thompson, G. Millhauser, C. Govaerts, and C. Vaisse. Mechanism of n-terminal modulation of activity at the melanocortin-4 receptor gpcr. *Nat Chem Biol*, 8(8):725–30, 2012.

[50] H. B. Schioth, T. Haitina, M. K. Ling, A. Ringholm, R. Fredriksson, J. M. Cerda-Reverter, and J. Klovins. Evolutionary conservation of the structural, pharmacological, and genomic characteristics of the melanocortin receptor subtypes. *Peptides*, 26(10):1886–900, 2005.

[51] X. Gao and T. C. Wong. Nmr studies of adrenocorticotropin hormone peptides in sodium dodecylsulfate and dodecylphosphocholine micelles: proline isomerism and interactions of the peptides with micelles. *Biopolymers*, 58(1):20–32, 2001.

[52] R. Schwyzer. Acth: a short introductory review. *Ann N Y Acad Sci*, 297:3–26, 1977.

[53] P. G. Squire and T. Bewley. Adrenocorticotropins. xxxv. the optical rotatory dispersion of sheep adrenocorticotropic hormone in acidic and basic solutions. *Biochim Biophys Acta*, 109(1):234–40, 1965.

[54] M. Low, L. Kisfaludy, and S. Fermandjian. Proposed preferred conformation of acth. *Acta Biochim Biophys Acad Sci Hung*, 10(3):229–31, 1975.

[55] I. D. Pogozheva, B. X. Chai, A. L. Lomize, T. M. Fong, D. H. Weinberg, R. P. Nargund, M. W. Mulholland, I. Gantz, and H. I. Mosberg. Interactions of human melanocortin 4 receptor with nonpeptide and peptide agonists. *Biochemistry*, 44(34):11329–41, 2005.

[56] V. J. Hruby, S. D. Sharma, K. Toth, J. Y. Jaw, F. al Obeidi, T. K. Sawyer, and M. E. Hadley. Design, synthesis, and conformation of superpotent and prolonged acting melanotropins. *Ann N Y Acad Sci*, 680:51–63, 1993.

[57] B. Xu, E. H. Goulding, K. Zang, D. Cepoi, R. D. Cone, K. R. Jones, L. H. Tecott, and L. F. Reichardt. Brain-derived neurotrophic factor regulates energy balance downstream of melanocortin-4 receptor. *Nat Neurosci*, 6(7):736–42, 2003.

[58] J. R. Nicholson, J. C. Peter, A. C. Lecourt, Y. A. Barde, and K. G. Hofbauer. Melanocortin-4 receptor activation stimulates hypothalamic brain-derived neurotrophic factor release to regulate food intake, body temperature and cardiovascular function. *J Neuroendocrinol*, 19(12):974–82, 2007.

[59] M. G. Hohenadel, M. S. Thearle, B. A. Grice, H. Huang, M. H. Dai, Y. X. Tao, L. A. Hunter, G. I. Palaguachi, Z. Mou, R. C. Kim, M. M. Tsang, K. Haack, V. S. Voruganti, S. A. Cole, N. F. Butte, A. G. Comuzzie, Y. L. Muller, L. J. Baier, J. Krakoff, W. C. Knowler, J. A. Yanovski, and J. C. Han. Brain-derived neurotrophic factor in human subjects with function-altering melanocortin-4 receptor variants. *Int J Obes (Lond)*, 38(8):1068–74, 2014.

[60] K. Matsuda, K. Kojima, S. Shimakura, K. Wada, K. Maruyama, M. Uchiyama, S. Kikuyama, and S. Shioda. Corticotropin-releasing hormone mediates alpha-melanocyte-stimulating hormone-induced anorexigenic action in goldfish. *Peptides*, 29(11):1930–6, 2008.

[61] C. Fekete, G. Legradi, E. Mihaly, Q. H. Huang, J. B. Tatro, W. M. Rand, C. H. Emerson, and R. M. Lechan. alpha-melanocyte-stimulating hormone is contained in nerve terminals innervating thyrotropin-releasing hormone-synthesizing neurons in the hypothalamic paraventricular nucleus and prevents fasting-induced suppression of prothyrotropin-releasing hormone gene expression. *J Neurosci*, 20(4):1550–8, 2000.

[62] R. Hanada, M. Nakazato, S. Matsukura, N. Murakami, H. Yoshimatsu, and T. Sakata. Differential regulation of melanin-concentrating hormone and orexin genes in the agouti-related protein/melanocortin-4 receptor system. *Biochem Biophys Res Commun*, 268(1):88–91, 2000.

[63] G. van Meer, D. R. Voelker, and G. W. Feigenson. Membrane lipids: where they are and how they behave. *Nat Rev Mol Cell Biol*, 9(2):112–24, 2008.

[64] N. Tavoosi, R. L. Davis-Harrison, T. V. Pogorelov, Y. Z. Ohkubo, M. J. Arcario, M. C. Clay, C. M. Rienstra, E. Tajkhorshid, and J. H. Morrissey. Molecular determinants of phospholipid synergy in blood clotting. *J Biol Chem*, 286(26):23247–53, 2011.

[65] P. M. Sharp and B. H. Hahn. Origins of hiv and the aids pandemic. *Cold Spring Harb Perspect Med*, 1(1):a006841, 2011.

[66] M. L. Mzingwane and C. T. Tiemessen. Mechanisms of hiv persistence in hiv reservoirs. *Rev Med Virol*, 2017.

[67] C. T. Su, W. L. Ling, W. H. Lua, Y. X. Haw, and S. K. Gan. Structural analyses of 2015-updated drug-resistant mutations in hiv-1 protease: an implication of protease inhibitor cross-resistance. *BMC Bioinformatics*, 17(Suppl 19):500, 2016.

[68] WHO. *Global update on the health sector response to HIV, 2014*. World Health Organization, October 2014.

[69] UNAIDS. Global aids update 2016. Technical report, UNAIDS Joint United Nations Programm on HIV/AIDS, May, 2016 2016.

[70] V. Planelles, J. B. Jowett, Q. X. Li, Y. Xie, B. Hahn, and I. S. Chen. Vpr-induced cell cycle arrest is conserved among primate lentiviruses. *J Virol*, 70(4):2516–24, 1996.

[71] D. Lai, S. P. Singh, M. Cartas, R. Murali, V. S. Kalyanaraman, and A. Srinivasan. Extent of incorporation of hiv-1 vpr into the virus particles is flexible and can be modulated by expression level in cells. *FEBS Lett*, 469(2-3):191–5, 2000.

[72] C. A. Guenzel, C. Herate, and S. Benichou. Hiv-1 vpr-a still "enigmatic multitasker". *Front Microbiol*, 5:127, 2014.

[73] G. Li, M. Bukrinsky, and R. Y. Zhao. Hiv-1 viral protein r (vpr) and its interactions with host cell. *Curr HIV Res*, 7(2):178–83, 2009.

[74] M. Kogan and J. Rappaport. Hiv-1 accessory protein vpr: relevance in the pathogenesis of hiv and potential for therapeutic intervention. *Retrovirology*, 8:25, 2011.

[75] N. Laguette, C. Bregnard, P. Hue, J. Basbous, A. Yatim, M. Larroque, F. Kirchhoff, A. Constantinou, B. Sobhian, and M. Benkirane. Premature activation of the slx4 complex by vpr promotes g2/m arrest and escape from innate immune sensing. *Cell*, 156(1-2):134–45, 2014.

[76] V. S. Yedavalli, H. M. Shih, Y. P. Chiang, C. Y. Lu, L. Y. Chang, M. Y. Chen, C. Y. Chuang, A. I. Dayton, K. T. Jeang, and L. M. Huang. Human immunodeficiency virus type 1 vpr interacts with antiapoptotic mitochondrial protein hax-1. *J Virol*, 79(21):13735–46, 2005.

[77] R. M. Welsh, K. Bahl, and X. Z. Wang. Apoptosis and loss of virus-specific cd8+ t-cell memory. *Curr Opin Immunol*, 16(3):271–6, 2004.

[78] U. F. Greber and A. Fassati. Nuclear import of viral dna genomes. *Traffic*, 4(3):136–43, 2003.

[79] Y. Nitahara-Kasahara, M. Kamata, T. Yamamoto, X. Zhang, Y. Miyamoto, K. Muneta, S. Iijima, Y. Yoneda, Y. Tsunetsugu-Yokota, and Y. Aida. Novel nuclear import of vpr promoted by importin alpha is crucial for human immunodeficiency virus type 1 replication in macrophages. *J Virol*, 81(10):5284–93, 2007.

[80] Y. Jenkins, O. Pornillos, R. L. Rich, D. G. Myszka, W. I. Sundquist, and M. H. Malim. Biochemical analyses of the interactions between human immunodeficiency virus type 1 vpr and p6(gag). *J Virol*, 75(21):10537–42, 2001.

[81] L. A. Stark and R. T. Hay. Human immunodeficiency virus type 1 (hiv-1) viral protein r (vpr) interacts with lys-trna synthetase: implications for priming of hiv-1 reverse transcription. *J Virol*, 72(4):3037–44, 1998.

[82] Jeang Kuan-The. *Molecular Biology and Pathogenesis: Viral Mechanisms*. Elsevier Inc., 2007, 2nd edition, 1999.

[83] F. Bachand, X. J. Yao, M. Hrimech, N. Rougeau, and E. A. Cohen. Incorporation of vpr into human immunodeficiency virus type 1 requires a direct interaction with the p6 domain of the p55 gag precursor. *J Biol Chem*, 274(13):9083–91, 1999.

[84] F. Cornille, K. Wecker, A. Loffet, R. Genet, and B. Roques. Efficient solid-phase synthesis of vpr from hiv-1 using low quantities of uniformly 13c-, 15n-labeled amino acids for nmr structural studies. *J Pept Res*, 54(5):427–35, 1999.

[85] W. Schuler, K. Wecker, H. de Rocquigny, Y. Baudat, J. Sire, and B. P. Roques. Nmr structure of the (52-96) c-terminal domain of the hiv-1 regulatory protein vpr: molecular insights into its biological functions. *J Mol Biol*, 285(5):2105–17, 1999.

[86] K. Wecker and B. P. Roques. Nmr structure of the (1-51) n-terminal domain of the hiv-1 regulatory protein vpr. *Eur J Biochem*, 266(2):359–69, 1999.

[87] K. Wecker, N. Morellet, S. Bouaziz, and B. P. Roques. Nmr structure of the hiv-1 regulatory protein vpr in h2o/trifluoroethanol. comparison with the vpr n-terminal (1-51) and c-terminal (52-96) domains. *Eur J Biochem*, 269(15):3779–88, 2002.

[88] N. Morellet, S. Bouaziz, P. Petitjean, and B. P. Roques. Nmr structure of the hiv-1 regulatory protein vpr. *J Mol Biol*, 327(1):215–27, 2003.

[89] Y. Wu, X. Zhou, C. O. Barnes, M. DeLucia, A. E. Cohen, A. M. Gronenborn, J. Ahn, and G. Calero. The ddb1-dcaf1-vpr-ung2 crystal structure reveals how hiv-1 vpr steers human ung2 toward destruction. *Nat Struct Mol Biol*, 23(10):933–940, 2016.

[90] D. Schwefel, H. C. Groom, V. C. Boucherit, E. Christodoulou, P. A. Walker, J. P. Stoye, K. N. Bishop, and I. A. Taylor. Structural basis of lentiviral subversion of a cellular protein degradation pathway. *Nature*, 505(7482):234–8, 2014.

[91] Timothy D. W. Claridge. *High-resolution NMR techniques in organic chemistry*. Tetrahedron organic chemistry series. Elsevier, Amsterdam ; Boston, 2nd edition, 2009.

[92] W. A. Lea and A. Simeonov. Fluorescence polarization assays in small molecule screening. *Expert Opin Drug Discov*, 6(1):17–32, 2011.

[93] D. M. Jameson and J. A. Ross. Fluorescence polarization/anisotropy in diagnostics and imaging. *Chem Rev*, 110(5):2685–708, 2010.

[94] D. Schwarz, C. Klammt, A. Koglin, F. Lohr, B. Schneider, V. Dotsch, and F. Bernhard. Preparative scale cell-free expression systems: new tools for the large scale preparation of integral membrane proteins for functional and structural studies. *Methods*, 41(4):355–69, 2007.

[95] H. P. Erickson. Size and shape of protein molecules at the nanometer level determined by sedimentation, gel filtration, and electron microscopy. *Biol Proced Online*, 11:32–51, 2009.

[96] Simon Roe. *Protein Purification Techniques*. Oxford University Press, United States, 2nd edition, 2001.

[97] U. K. Laemmli. Cleavage of structural proteins during the assembly of the head of bacteriophage t4. *Nature*, 227(5259):680–5, 1970.

[98] H. Schagger and G. von Jagow. Tricine-sodium dodecyl sulfate-polyacrylamide gel electrophoresis for the separation of proteins in the range from 1 to 100 kda. *Anal Biochem*, 166(2):368–79, 1987.

[99] H. Schagger. Tricine-sds-page. *Nat Protoc*, 1(1):16–22, 2006.

[100] T. K. Ritchie, Y. V. Grinkova, T. H. Bayburt, I. G. Denisov, J. K. Zolnerciks, W. M. Atkins, and S. G. Sligar. Chapter 11 - reconstitution of membrane proteins in phospholipid bilayer nanodiscs. *Methods Enzymol*, 464:211–31, 2009.

[101] K. Wuthrich. Nmr studies of structure and function of biological macromolecules. *Biosci Rep*, 23(4):119–68, 2003.

[102] John Cavanagh. *Protein NMR spectroscopy : principles and practice*. Academic Press, Amsterdam ; Boston, 2nd edition, 2007.

[103] Keller Rochus. *The Computer Aided Resonance Assignment Tutorial*. The Swiss Federal Institute of Technology, Zürich, 2nd edition, 2004.

[104] M. C. Keightley, J. W. Funder, and P. J. Fuller. Molecular cloning and sequencing of a guinea-pig pro-opiomelanocortin cdna. *Mol Cell Endocrinol*, 82(1):89–98, 1991.

[105] Patrick Tarnow. Molekulare charakterisierung an der hypothalamischen appetitregulation beteiliger rezeptoren. Technical report, Humboldt-Universität zu Berlin, 2008.

[106] Y. Kofuku, T. Ueda, J. Okude, Y. Shiraishi, K. Kondo, M. Maeda, H. Tsujishita, and I. Shimada. Efficacy of the beta(2)-adrenergic receptor is determined by conformational equilibrium in the transmembrane region. *Nat Commun*, 3:1045, 2012.

[107] X. Gao and T. C. Wong. Studies of the binding and structure of adrenocorticotropin peptides in membrane mimics by nmr spectroscopy and pulsed-field gradient diffusion. *Biophys J*, 74(4):1871–88, 1998.

[108] Z. Zhang, C. Dai, J. Bai, G. Xu, M. Liu, and C. Li. Ca(2+) modulating alpha-synuclein membrane transient interactions revealed by solution nmr spectroscopy. *Biochim Biophys Acta*, 1838(3):853–8, 2014.

[109] C. Ghaddhab, J. M. Vuissoz, and J. Deladoey. From bioinactive acth to acth antagonist: The clinical perspective. *Front Endocrinol (Lausanne)*, 8:17, 2017.

[110] A. Martin-Molina, C. Rodriguez-Beas, and J. Faraudo. Effect of calcium and magnesium on phosphatidylserine membranes: experiments and all-atomic simulations. *Biophys J*, 102(9):2095–103, 2012.

[111] C. Her, D. I. Filoti, M. A. McLean, S. G. Sligar, J. B. Alexander Ross, H. Steele, and T. M. Laue. The charge properties of phospholipid nanodiscs. *Biophys J*, 111(5):989–98, 2016.

[112] E. Davies, C. J. Kenyon, and R. Fraser. The role of calcium ions in the mechanism of acth stimulation of cortisol synthesis. *Steroids*, 45(6):551–60, 1985.

[113] T. Viennet, A. Viegas, A. Kuepper, S. Arens, V. Gelev, O. Petrov, T. N. Grossmann, H. Heise, and M. Etzkorn. Selective protein hyperpolarization in cell lysates using targeted dynamic nuclear polarization. *Angew Chem Int Ed Engl*, 55(36):10746–50, 2016.

[114] S. Elter, T. Raschle, S. Arens, A. Viegas, V. Gelev, M. Etzkorn, and G. Wagner. The use of amphipols for nmr structural characterization of 7-tm proteins. *J Membr Biol*, 247(9-10):957–64, 2014.